

**IZMIR KATIP CELEBI UNIVERSITY  
GRADUATE SCHOOL OF NATURAL AND APPLIED  
SCIENCES**

**EXPERIMENTAL INVESTIGATION OF NEWTONIAN AND  
NON-NEWTONIAN FLUID FLOWS IN ROUGH PIPES AND  
MODELING USING COMPUTATIONAL FLUID DYNAMICS**

**PhD THESIS**

**Tevfik Denizhan MÜFTÜOĞLU**

**Department of Civil Engineering**

**Thesis Advisor: Prof. Dr. Mehmet SORGUN**

**APRIL 2021**

**IZMIR KATIP CELEBI UNIVERSITY  
GRADUATE SCHOOL OF NATURAL AND APPLIED  
SCIENCES**

**EXPERIMENTAL INVESTIGATION OF NEWTONIAN AND  
NON-NEWTONIAN FLUID FLOWS IN ROUGH PIPES AND  
MODELING USING COMPUTATIONAL FLUID DYNAMICS**

**PhD THESIS**

**Tevfik Denizhan MÜFTÜOĞLU  
(D160226001)  
ORCID ID 0000-0001-5836-3689**

**Department of Civil Engineering**

**Thesis Advisor: Prof. Dr. Mehmet SORGUN**

**APRIL 2021**

**İZMİR KÂTİP ÇELEBİ ÜNİVERSİTESİ**  
**FEN BİLİMLERİ ENSTİTÜSÜ**

**NEWTONYEN VE NEWTONYEN OLMAYAN AKIŞKANIN**  
**PÜRÜZLÜ BORUDAKİ AKIŞININ DENEYSEL OLARAK**  
**İNCELENMESİ VE HESAPLAMALI AKIŞKANLAR DİNAMİĞİ**  
**KULLANILARAK MODELLENMESİ**

**DOKTORA TEZİ**

**Tevfik Denizhan MÜFTÜOĞLU**

**(D160226001)**

**ORCID ID 0000-0001-5836-3689**

**İnşaat Mühendisliği Ana Bilim Dalı**

**Tez Danışmanı: Prof. Dr. Mehmet SORGUN**

**NİSAN 2021**

**Tevik Denizhan MÜFTÜOĞLU**, a **PhD** student of **IKCU Graduate School of Natural And Applied Sciences**, successfully defended the thesis entitled “**EXPERIMENTAL INVESTIGATION OF NEWTONIAN AND NON-NEWTONIAN FLUID FLOWS IN ROUGH PIPES AND MODELING USING COMPUTATIONAL FLUID DYNAMICS**”, which he prepared after fulfilling the requirements specified in the associated legislations, before the jury whose signatures are below.

**Thesis Advisor :**

**Prof. Dr. Mehmet SORGUN** .....  
İzmir Kâtip Çelebi University

**Jury Members :**

**Prof. Dr. Mehmet Ali YURDUSEV** .....  
Manisa Celal Bayar University

**Assoc. Prof. Dr. Gökçen BOMBAR** .....  
İzmir Kâtip Çelebi University

**Assoc. Prof. Dr. Mustafa DOĞAN** .....  
Dokuz Eylül University

**Assoc. Prof. Dr. Ayşegül ÖZGENÇ AKSOY** .....  
Dokuz Eylül University

**Date of Defense : 30.04.2021**

*To my family*

## **FOREWORD**

In this Ph.D. thesis, I aimed to present a detailed investigation of Newtonian and non-Newtonian fluid flows in rough pipes under different fluid temperature conditions. This thesis is based on the extensive experimental study that I have performed in the fluid mechanics and hydraulics laboratory of İzmir Katip Çelebi University, under the supervision of Prof. Dr. Mehmet SORGUN. I have proposed new correlations to predict pressure losses of Newtonian and non-Newtonian fluids that flow through rough pipes considering the different fluid temperatures. I also have developed a mathematical model in accordance with the results that I have obtained from the experimental study.

I believe that the following thesis brings a new standpoint on some engineering aspects according to the remarkable findings from the performed analyses.

I would like to thank my advisor, Prof. Dr. Mehmet SORGUN, for his guidance, motivation, and willingness to share the valuable experience he has throughout my education.

This thesis was supported by İzmir Kâtip Çelebi University, Scientific Research and Project Coordinatorship, under grant no 2018-TDR-FEBE-0042.

I also would like to give my sincere gratitude to my family, my relatives, and people who always encourage me under all circumstances, not only for the journey of my academic life but also for my whole life.

I dedicate this presented Ph.D. thesis to my caring mother Meral MÜFTÜOĞLU who never withholds her love and support from me, and to my kindhearted father Mehmet Emin MÜFTÜOĞLU that I know he would have been so proud of me.

April 2021

Tevfik Denizhan MÜFTÜOĞLU  
(Civil Engineer, M.Sc.)

# TABLE OF CONTENTS

	<u>Page</u>
<b>FOREWORD</b> .....	<b>vi</b>
<b>TABLE OF CONTENTS</b> .....	<b>vii</b>
<b>LIST OF TABLES</b> .....	<b>ix</b>
<b>LIST OF FIGURES</b> .....	<b>x</b>
<b>ABBREVIATIONS AND NOMENCLATURE</b> .....	<b>xiii</b>
<b>ABSTRACT</b> .....	<b>xv</b>
<b>ÖZET</b> .....	<b>xvii</b>
<b>1. INTRODUCTION</b> .....	<b>1</b>
1.1 Literature Review .....	3
1.1.1 Newtonian fluid flow in smooth pipes.....	4
1.1.2 Newtonian fluid flow in rough pipes .....	5
1.1.3 Non-Newtonian fluid flow in smooth pipes.....	16
1.1.4 Non-Newtonian fluid flow in rough pipes .....	18
1.2 Aim of the Study .....	21
<b>2. THEORY</b> .....	<b>22</b>
2.1 Geometry of the Model and Main Equations of Turbulent Pipe Flow .....	22
2.1.1 Mixing length model.....	24
2.2 Fluid Behavior Classification.....	27
2.2.1 Newtonian model.....	28
2.2.2 Power-Law model.....	28
2.2.3 Bingham Plastic model .....	29
2.2.4 Herschel-Bulkley model .....	29
<b>3. EXPERIMENTAL STUDY</b> .....	<b>31</b>
3.1 Experimental Setup .....	32
3.2 Experiment Procedures.....	39
<b>4. MATHEMATICAL MODEL TO PREDICT PRESSURE LOSS OF TURBULENT NEWTONIAN FLUID FLOW IN ROUGH PIPES CONSIDERING FLUID TEMPERATURE EFFECTS</b> .....	<b>41</b>
4.1 Explicit Solution of the Governing Equation.....	41
4.1.1 Finite difference method .....	41
4.2 Flow Chart of the Computer Program .....	43
<b>5. RESULTS AND DISCUSSION</b> .....	<b>46</b>
5.1 Determination of Pipe Roughness Values for Galvanized Pipes .....	46
5.2 A New Friction Factor Formula for Water Flow through Rough Pipes with Fluid Temperature Effects .....	49
5.3 A New Friction Factor Formula for non-Newtonian Fluid Flow through Rough Pipes .....	59
5.4 Comparison of the Pressure Gradients between The Developed Mathematical Model and Experimental Study.....	71

5.4.1	Comparisons for 40 mm pipe diameter.....	71
5.4.2	Comparisons for 50 mm pipe diameter.....	73
5.4.3	Comparisons for 80 mm pipe diameter.....	76
5.4.4	Comparisons for 90 mm pipe diameter.....	78
<b>6.</b>	<b>CONCLUSIONS .....</b>	<b>83</b>
	<b>REFERENCES .....</b>	<b>87</b>
	<b>CURRICULUM VITAE.....</b>	<b>93</b>



## LIST OF TABLES

	<u>Page</u>
<b>Table 3.1</b> Specifications of the experiments.....	32
<b>Table 5.1</b> Proposed pipe roughness values for galvanized pipes (Sorgun and Muftuoglu .....	49
<b>Table 5.2</b> Performance of the developed friction factor equation in terms of error metrics .....	52
<b>Table 5.3</b> F test results.....	56
<b>Table 5.4</b> Comparison of rheological models and the parameters for F-2 fluid.....	63
<b>Table 5.5</b> Comparison of rheological models and the parameters for F-3 fluid.....	63
<b>Table 5.6</b> Performance of developed friction factor equaiton .....	70

## LIST OF FIGURES

	<u>Page</u>
<b>Figure 1.1</b> Moody diagram.....	8
<b>Figure 2.1</b> Schematic drawing of the experimentally investigated pipe flow .....	22
<b>Figure 2.2</b> Non-Newtonian fluid classification based on the shear stress and shear rate relation.....	27
<b>Figure 3.1</b> Schematic drawing of the flow loop (plan view).....	33
<b>Figure 3.2</b> Izmir Katip Celebi University Civil Engineering (IKCU-CE) Flow Loop and galvanized pipes with different diameters (a. 40 mm, b. 50 mm, c. 80 mm, d. 90 mm).....	34
<b>Figure 3.3</b> Storage tank and mixer.....	35
<b>Figure 3.4</b> Mixing attachments of the mixer .....	35
<b>Figure 3.5</b> Temperature control panel.....	36
<b>Figure 3.6</b> Heating resistor .....	36
<b>Figure 3.7</b> Centrifugal pump .....	37
<b>Figure 3.8</b> Electromagnetic flowmeter.....	37
<b>Figure 3.9</b> Pressure transmitters .....	38
<b>Figure 3.10</b> Data acquisition device.....	38
<b>Figure 3.11</b> Power supply.....	39
<b>Figure 3.12</b> Real-time data readings .....	39
<b>Figure 5.1</b> Experimental and Colebrook friction factor comparisons for 40 mm pipe diameter and room temperature.....	47
<b>Figure 5.2</b> Experimental and Colebrook friction factor comparisons for 50 mm pipe diameter and room temperature.....	47
<b>Figure 5.3</b> Experimental and Colebrook friction factor comparisons for 80 mm pipe diameter and room temperature.....	48
<b>Figure 5.4</b> Experimental and Colebrook friction factor comparisons for 90 mm pipe diameter and room temperature.....	48
<b>Figure 5.5</b> Experimental and calculated friction factor comparisons using Eq. 5.5 ..	51
<b>Figure 5.6</b> Proposed friction factor comparisons with Blasius and Taler formulas for smooth pipes.....	52
<b>Figure 5.7</b> Proposed friction factor comparisons with experimental data and Colebrook formula for rough pipes .....	53
<b>Figure 5.8</b> Proposed friction factor comparisons with experimental data at 40 <sup>0</sup> C and Colebrook formula for rough pipes .....	54
<b>Figure 5.9</b> The relation between the friction factor and $\pi_1$ (Reynolds Number) for 80 mm Pipe diameter and room temperature .....	55
<b>Figure 5.10</b> The relation between the friction factor and $\pi_2$ (Relative Roughness)..	55

<b>Figure 5.11</b> The relation between the friction factor and friction and $\pi_3$ (Prandtl Number) .....	56
<b>Figure 5.12</b> Calculated and experimental data comparisons for low pressure gradient values .....	58
<b>Figure 5.13</b> Calculated and experimental data comparisons for high pressure gradient values .....	59
<b>Figure 5.14</b> Shear stress and shear rate relation of F-2 fluid for Power-Law model.	60
<b>Figure 5.15</b> Shear stress and shear rate relation of F-2 fluid for Bingham Plastic model.....	60
<b>Figure 5.16</b> Shear stress and shear rate relation of F-2 fluid for Herschel-Bulkley model.....	61
<b>Figure 5.17</b> Shear stress and shear rate relation of F-3 fluid for Power-Law model.	61
<b>Figure 5.18</b> Shear stress and shear rate relation of F-3 fluid for Bingham Plastic model.....	62
<b>Figure 5.19</b> Shear stress and shear rate relation of F-3 fluid for Herschel-Bulkley model.....	62
<b>Figure 5.20</b> Measured and estimated pressure gradient comparisons for F-2 and 50 mm pipe diameter .....	65
<b>Figure 5.21</b> Measured and estimated pressure gradient comparisons for F-2 and 80 mm pipe diameter .....	66
<b>Figure 5.22</b> Measured and estimated pressure gradient comparisons for F-2 and 90 mm pipe diameter .....	66
<b>Figure 5.23</b> Measured and estimated pressure gradient comparisons for F-3 and 90 mm pipe diameter .....	67
<b>Figure 5.24</b> Measured and estimated pressure gradient comparisons for F-3 and 80 mm pipe diameter .....	67
<b>Figure 5.25</b> Measured and estimated pressure gradient comparisons for F-3 and 50 mm pipe diameter .....	68
<b>Figure 5.26</b> Obtained friction factor values for $\varepsilon/D = 0.000875$ .....	68
<b>Figure 5.27</b> Obtained friction factor values for $\varepsilon/D = 0.0012$ .....	69
<b>Figure 5.28</b> Obtained friction factor values for $\varepsilon/D = 0.001337$ .....	69
<b>Figure 5.29</b> Comparison of measured friction factors with estimated friction factors for F-2 and F-3 fluids using the proposed correlation, and Reed and Pilehvari correlation.....	70
<b>Figure 5.30</b> Measured and predicted pressure gradient comparisons for 40 mm pipe diameter and 20 °C fluid temperature.....	71
<b>Figure 5.31</b> Measured and predicted pressure gradient comparisons for 40 mm pipe diameter and 40 °C fluid temperature.....	72
<b>Figure 5.32</b> Measured and predicted pressure gradient comparisons for 40 mm pipe diameter and 50 °C fluid temperature.....	72
<b>Figure 5.33</b> Measured and predicted pressure gradient comparisons for 40 mm pipe diameter and 60 °C fluid temperature.....	73
<b>Figure 5.34</b> Measured and predicted pressure gradient comparisons for 50 mm pipe diameter and 20 °C fluid temperature.....	74
<b>Figure 5.35</b> Measured and predicted pressure gradient comparisons for 50 mm pipe diameter and 40 °C fluid temperature.....	74
<b>Figure 5.36</b> Measured and predicted pressure gradient comparisons for 50 mm pipe diameter and 50 °C fluid temperature.....	75

<b>Figure 5.37</b> Measured and predicted pressure gradient comparisons for 50 mm pipe diameter and 60 °C fluid temperature .....	75
<b>Figure 5.38</b> Measured and predicted pressure gradient comparisons for 80 mm pipe diameter and 20 °C fluid temperature .....	76
<b>Figure 5.39</b> Measured and predicted pressure gradient comparisons for 80 mm pipe diameter and 40 °C fluid temperature .....	77
<b>Figure 5.40</b> Measured and predicted pressure gradient comparisons for 80 mm pipe diameter and 50 °C fluid temperature .....	77
<b>Figure 5.41</b> Measured and predicted pressure gradient comparisons for 80 mm pipe diameter and 60 °C fluid temperature .....	78
<b>Figure 5.42</b> Measured and predicted pressure gradient comparisons for 90 mm pipe diameter and 20 °C fluid temperature .....	79
<b>Figure 5.43</b> Measured and predicted pressure gradient comparisons for 90 mm pipe diameter and 40 °C fluid temperature .....	79
<b>Figure 5.44</b> Measured and predicted pressure gradient comparisons for 90 mm pipe diameter and 50 °C fluid temperature .....	80
<b>Figure 5.45</b> Measured and predicted pressure gradient comparisons for 90 mm pipe diameter and 60 °C fluid temperature .....	80
<b>Figure 5.46</b> Measured and predicted pressure gradient comparisons for low pressure gradient values and for all fluid temperatures .....	81
<b>Figure 5.47</b> Measured and predicted pressure gradient comparisons for high pressure gradient values and for all fluid temperatures .....	82

## ABBREVIATIONS AND NOMENCLATURE

<b>CMC</b>	: Carboxymethyl Cellulose
<b>D</b>	: Diameter [ $L$ ]
<b>g</b>	: Gravitational Acceleration [ $LT^{-2}$ ]
<b><math>g_c</math></b>	: Conversion Factor
<b><math>l_m</math></b>	: Mixing Length
<b>V</b>	: Average Velocity [ $LT^{-1}$ ]
<b>t</b>	: Time [ $T$ ]
<b>f</b>	: Darcy Friction Factor
<b><math>f'</math></b>	: F Value (F Test)
<b><math>f'_{cr}</math></b>	: Critical F Value (F Test)
<b><math>f_f</math></b>	: Fanning Friction Factor
<b><math>k'</math></b>	: Number of Independent Variables in Model (F Test)
<b>K</b>	: Consistency Index [ $L^{-1}MT^{n-2}$ ]
<b>m</b>	: Flow Behavior Index of Herschel-Bulkley Fluid
<b>n</b>	: Flow Behavior Index of Power-Law Fluid
<b><math>n'</math></b>	: Number of Total Data (F Test)
<b>N</b>	: Generalized Flow Behavior Index of Herschel-Bulkley Fluid
<b><math>N_{Reg}</math></b>	: Generalized Reynolds Number
<b>P</b>	: Pressure [ $ML^{-1}T^{-2}$ ]
<b>Pr</b>	: Prandtl Number
<b>R</b>	: Radius [ $L$ ]
<b>Re</b>	: Reynolds Number
<b>SSE</b>	: Sum of Squares Error (F Test)
<b>SSR</b>	: Sum of Squares due to Regression (F Test)
<b>Q</b>	: Flow Rate [ $L^3T^{-1}$ ]

$y$	: Distance from Wall of the Pipe to Centerline of the Pipe [ $L$ ]
$Y_{mean}$	: Mean of Experimental Data (F Test)
$Y_{i,exp}$	: Each Experimental Data (F Test)
$Y_{i,pre}$	: Predicted Data with Regression (F Test)
$\nu'_1$	: Numerator Degrees of Freedom (F Test)
$\nu'_2$	: Denominator Degrees of Freedom (F Test)
$u, v, w$	: Velocity Components [ $LT^{-1}$ ]
$\bar{u}, \bar{v}, \bar{w}$	: Mean Velocity Components [ $LT^{-1}$ ]
$u', v', w'$	: Fluctuation Velocity Components [ $LT^{-1}$ ]
$\varepsilon$	: Roughness Height [ $L$ ]
$\varepsilon/D$	: Relative Roughness
$\rho$	: Density of the Fluid [ $ML^{-3}$ ]
$\pi$	: Dimensionless Group
$\mu$	: Dynamic Viscosity [ $ML^{-1}T^{-1}$ ]
$\nu$	: Kinematic Viscosity [ $L^2T^{-1}$ ]
$\nu_t$	: Turbulent Kinematic Viscosity [ $L^2T^{-1}$ ]
$\tau$	: Shear Stress [ $ML^{-1}T^{-2}$ ]
$\tau_{ij}$	: Stress Tensor [ $ML^{-1}T^{-2}$ ]
$\tau_y$	: Yield Stress or Point [ $ML^{-1}T^{-2}$ ]
$\tau_w$	: Wall Shear Stress [ $ML^{-1}T^{-2}$ ]
$\gamma$	: Shear Rate [ $T^{-1}$ ]

# **EXPERIMENTAL INVESTIGATION OF NEWTONIAN AND NON-NEWTONIAN FLUID FLOWS IN ROUGH PIPES AND MODELING USING COMPUTATIONAL FLUID DYNAMICS**

## **ABSTRACT**

Estimation of pressure losses for pipe flows has great importance in engineering applications. Determining pumping requirements and proper selection of pump systems for efficient transportation of fluids are dependent on accurately estimated pressure losses.

In this study, the flow behaviors of Newtonian and non-Newtonian fluid flows in galvanized rough pipes are investigated experimentally and numerically with three different fluids (water and two polymeric solutions with different concentrations and viscous characteristics) for various flow rates, pipe diameters, and fluid temperature conditions. For this purpose, a comprehensive experimental study is performed in the Civil Engineering Flow Loop of İzmir Kâtip Çelebi University. Water and non-Newtonian fluid experiments for fluid temperatures ranged from 20°C to 60°C, for Reynolds numbers ranged from  $3.2 \times 10^3$  to  $8.6 \times 10^4$ , and for four relative roughness values are performed. During the experimental study, flowrates, pressure losses, and fluid temperatures are recorded.

Firstly, experimental friction factors and Colebrook friction factors are compared to determine if pipe roughness heights vary for pipe diameters. Different pipe roughness height values are obtained for each galvanized pipe used in the experimental study.

A dimensional analysis is performed to determine which dimensionless parameters influence the pressure loss of fully developed turbulent Newtonian fluid flow in rough pipes considering the room and various temperature conditions of the fluid. It is obtained that these dimensionless parameters are Reynolds number, relative roughness, and Prandtl Number. Under the guidance of data which are collected from the experimental study, a new friction factor equation for Newtonian fluid flows in rough pipes based on the relative roughness, Reynolds Number and Prandtl Number is proposed.

Estimating the pressure drop of non-Newtonian fluid flows is also an important issue. For this reason, friction factor correlations for Non-Newtonian fluid flows in pipes are analyzed. Rheological model investigations for Non-Newtonian fluids are performed in detail by conducting an extensive experimental study. Using the experimental study, for the fully developed turbulent flows of the non-Newtonian fluids through rough pipes, a new friction factor correlation as a function of generalized Reynolds number and relative roughness is proposed.

Moreover, a mathematical model is developed for the modeling of Newtonian fluids that flow through rough pipes in turbulent regime considering fluid temperature conditions. For this purpose, the Navier-Stokes equations in cylindrical coordinates are solved by using finite difference methods including fluid temperature effects, and the related computational process is performed by developing a code in MATLAB software. The appeared closure problem from the turbulence modeling is solved by using the mixing length theory. Krogstad's damping function which is proposed to extend van Driest's damping function is used to determine turbulent boundary layers on rough surfaces. The accuracy of the proposed mathematical model is analyzed by validating the model results with experimental data. According to the error values between the results of the model and the experimental study, it is obtained that the proposed mathematical model shows satisfactory agreement with the experimental study. The proposed mathematical model can be used to predict the pressure drop of turbulent Newtonian fluid flows in rough pipes for different fluid temperatures.

**Keywords:** Civil engineering, fluid mechanics, pipe flow, turbulence, rough pipe, friction factor, pressure loss, Newtonian fluid, non-Newtonian fluid, temperature, computational modeling



# NEWTONYEN VE NEWTONYEN OLMAYAN AKIŞKANIN PÜRÜZLÜ BORUDAKİ AKIŞININ DENEYSEL OLARAK İNCELENMESİ VE HESAPLAMALI AKIŞKANLAR DİNAMİĞİ KULLANILARAK MODELLENMESİ

## ÖZET

Boru akışlarındaki basınç kayıpların tahmini, mühendislik uygulamalarında büyük önem taşımaktadır. Akışkanların verimli bir şekilde taşınımı için pompalama gereksinimlerinin belirlenmesi ve doğru pompa sistemlerinin seçimi basınç kaybının hassas bir şekilde tahminine dayalıdır.

Bu çalışmada, Newtonyen ve Newtonyen olmayan akışkanların pürüzlü galvanizli borulardaki akışları üç farklı akışkanla (su ve bunun yanında farklı kontrastasyon ve viskoz karakteristiğine sahip iki polimerik solüsyon), çeşitli debiler ve akışkan sıcaklık koşulları için, farklı çaplara sahip galvanizli borularda deneysel ve sayısal olarak incelenmiştir. Bu inceleme için, İzmir Kâtip Çelebi Üniversitesi İnşaat Mühendisliği Akış Düzeneği'nde kapsamlı deneysel çalışmalar gerçekleştirilmiştir. Hem su hem de Newtonyen olmayan akışkan deneyleri, 20°C ile 60°C aralığındaki akışkan sıcaklıkları,  $3.2 \times 10^3$  ile  $8.6 \times 10^4$  arasında değişen Reynolds sayıları ve dört farklı göreceli pürüzlülük değerleri için gerçekleştirilmiştir. Deneysel çalışma boyunca, debiler, basınç kayıpları ve akışkan sıcaklıkları kaydedilmiştir.

Öncelikle, boru pürüzlülüğünün boru çapına göre değişip değişmediğini incelemek için, deneysel sürtünme faktörleri ve Colebrook sürtünme faktörleri karşılaştırılmıştır. Deneysel çalışmada kullanılan her bir galvanizli boru için farklı pürüzlülük yüksekliği değerleri elde edilmiştir.

Newtonyen akışkanın oda sıcaklığı ve çeşitli sıcaklıklara sahip olduğu durumlar göz önüne alınarak tam gelişmiş türbülanslı akımında basınç kayıplarını hangi boyutsuz parametrelerin etkilediğini belirlemek amacıyla bir boyut analizi gerçekleştirilmiş ve bu boyutsuz parametrelerin Reynolds sayısı, göreceli pürüzlülük ve Prandtl sayısı olduğu belirlenmiştir. Deneysel çalışmadan elde edilen veriler rehberliğinde, göreceli pürüzlülüğe, Reynolds sayısına ve Prandtl sayısına bağlı bir sürtünme faktörü denklemi önerilmiştir.

Newtonyen olmayan akışkanların basınç kayıplarının tahmini de önemli bir konudur. Bu yüzden, Newtonyen olmayan akışkanların boru içi akımlarının sürtünme faktörü denklemleri analiz edilmiştir. Detaylı bir deneysel çalışma yapılarak, Newtonyen olmayan akışkanların reolojik incelemeleri gerçekleştirilmiştir. Deneysel çalışmadan elde edilen verilere göre, akışkanların sahip olduğu oda sıcaklığı ve diğer

sıcaklıkların etkisi altında, pürüzlü borulardaki Newtonyen olmayan akışkanların tam gelişmiş tübülanslı akışları için, genelleştirilmiş Reynolds sayısı ve göreceli pürüzlülüğün bir fonksiyonu olarak yeni bir sürtünme faktörü korelasyonu önerilmiştir.

Ayrıca, Newtonyen akışkanın, akışkan sıcaklığı etkileri altındaki pürüzlü borulardaki tübülanslı akımını modellemek için matematiksel bir model geliştirilmiştir. Bunun için, silindirik koordinatlardaki Navier-Stokes denklemleri sonlu farklar yöntemiyle akışkan sıcaklığı etkileri dahil edilerek çözülmüştür ve ilgili hesaplama süreçleri MATLAB programında bir kod geliştirilerek gerçekleştirilmiştir. Tübülans modellemesi sırasında ortaya çıkan kapatma problemi, karışım uzunluğu teoremi kullanılarak çözülmüştür. Pürüzlü yüzeyler üzerindeki tübülans sınır tabakaları, Krogstad tarafından van Driest sönümlenme fonksiyonunun genişletildiği bir sönümlenme fonksiyonuyla belirlenmiştir. Önerilen matematiksel modelin hassasiyeti, model sonuçlarının deney sonuçlarıyla doğrulanmasıyla analiz edilmiştir. Model ve deney sonuçlarının arasındaki hata değerlerine bakıldığında, önerilen matematiksel modelin deneysel çalışmayla yeterli bir uyum içinde olduğu gözlemlenmiştir. Önerilen matematiksel model, Newtonyen akışkanların, pürüzlü borulardaki tübülanslı akımlarının farklı akışkan sıcaklıkları etkisi altında oluşan basınç kayıplarını tahmin etmede kullanılabilir.

**Anahtar Kelimeler:** İnşaat mühendisliği, akışkanlar mekaniği, boru akımı, tübülans, pürüzlü boru, sürtünme faktörü, basınç kaybı, Newtonyen akışkan, Newtonyen olmayan akışkan, sıcaklık, hesaplamalı modelleme

# 1. INTRODUCTION

Transportation of fluids through pipes has always been a great concern in many engineering areas such as civil, mechanical, chemical, petroleum, energy, food, etc. In these engineering areas, pipes and pumps are the fundamental elements of their applications.

Fluids can only move from top to bottom due to gravity or from higher pressure to lower pressure system. Other than these conditions, moving the fluid from one location to another can be achieved by adding the required energy. For this reason, pumping systems are used to add that energy to the fluids. Pumps operate in a hydraulic system to convert the electrical energy into hydraulic energy and that means they consume electricity. In a piping system, pumps take first place according to the electricity consumption among the other machines.

While the fluid flows through a pipe, it encounters frictional resistance, and due to this resistance, pressure loss occurs. This pressure loss may prevent fluid movement and affect the transportation of it through a pipe. In order to overcome the pressure loss that occurs in pipe flows, and to add the required energy as stated above, the properties of the pump which is used in a piping system have vital importance. Therefore, determining pump requirements and proper selection of pumps according to the frictional resistance, and the related pressure losses are important for proper transportation and energy efficiency.

The frictional pressure loss in a pipe flow is dependent on various effective parameters such as friction factor, length and diameter of the pipe, and flow velocity. For this reason, accurate determination of friction factor is as essential as other effective parameters to calculate the pressure losses. Any error or inadequate calculations of these parameters affect pressure loss and therefore significant incidents may occur.

Another important consideration for predicting frictional pressure losses is to understand the rheological behaviors of the fluids. Fluids are characterized according to their rheological behaviors under the applied shear stress on them and they are classified into two categories as Newtonian and non-Newtonian fluids. Flows of Newtonian fluids have been investigated for a long time since water shows Newtonian behavior. There are many applications of water flow in numerous engineering areas. On the other hand, investigations on non-Newtonian fluid flows have growing interest due to the improvement of techniques and increasing demand for the usage of non-Newtonian fluids in various engineering applications. For example, fracturing fluids are used in wells during drilling operations. These fluids show non-Newtonian behavior. There are rheological models to express the relation between shear stress and shear rate of non-Newtonian fluids. Therefore, to predict frictional pressure losses of non-Newtonian fluid flows these mathematical models have to be understood properly.

Moreover, fluid temperature is an important parameter for fluid flows in pipes. Numerous applications in engineering are temperature-dependent. In example, water from the geothermal area is transported by pipelines. Therefore, the fluid temperature has remarkable effects on the frictional pressure loss which makes it to be considered in detail.

In order to prevent overpredicting frictional pressure loss in terms of energy efficiency of selected pumps or miscalculating any other parameter, both theoretical and experimental investigations have to be combined. To achieve accurate results and develop precise models, the importance of the experimental study cannot be neglected. Therefore, in this thesis, an extensive experimental study is presented. The experiments are conducted at Izmir Katip Celebi University's Civil Engineering Flow Loop. The flow behaviors of fluid flows in rough pipes are investigated experimentally and numerically for different fluid types (Newtonian and non-Newtonian), various flow rates, pipe diameters, and fluid temperature conditions.

## 1.1 Literature Review

In the literature, there are lots of researches about the resistance of pipe flow to determine pressure loss. These researches interwind each other in many cases either due to joint studies or developments based on the preceding works. The most famous equation that is used in the engineering design of pipe flows is the Darcy-Weisbach equation.

Weisbach [1] proposed the following equation to express frictional resistance in terms of head loss ( $h_l$ ).

$$h_l = f \frac{L V^2}{D 2g} \quad (1.1)$$

where L represents pipe length, D represents the pipe diameter, V represents flow velocity, g represents gravitational acceleration and f represents the Darcy friction factor.

Darcy [2] introduced the surface roughness as an important parameter which is qualified by the pipe diameter, and it is linked to Darcy friction factor in Eq. 1.1. Therefore, this equation is today known as Darcy-Weisbach equation in the literature. The famous Darcy-Weisbach equation in terms of pressure loss is shown below.

$$\Delta P = f \frac{L \rho V^2}{D 2} \quad (1.2)$$

where L represents pipe length, D represents the pipe diameter, V represents flow velocity,  $\rho$  represents density of the fluid and f represents the Darcy friction factor.

A great amount of literature to determine frictional pressure loss in smooth and rough pipes can be found for Newtonian fluid both for laminar and turbulent flow situations. Also, there are various works available for non-Newtonian fluids in the literature.

As seen from Eq. 1.2., accurate determination of friction factor, f, carries great importance for obtaining pressure drop. For this reason, numerous researches are available in the literature for determining friction factor both for Newtonian and non-Newtonian fluid flows in smooth and rough pipes. The friction factor sometimes is

referred to as Darcy-Weisbach friction factor and sometimes as Fanning friction factor. The Darcy-Weisbach friction factor ( $f$ ) is four times the Fanning friction factor ( $f_F$ ).

When the fluid flows in the laminar regime, both for Newtonian and non-Newtonian fluids, it is already known that surface roughness does not affect the frictional pressure but if the fluid flows in the turbulent regime, then surface roughness is an effective parameter.

Some of the well-known studies for Newtonian and non-Newtonian fluid flows in smooth and rough pipes are presented. Also, if given, the range of validity for each equation is stated.

### **1.1.1 Newtonian fluid flow in smooth pipes**

Hagen [3] performed experiments with water that flowed through cylindrical brass tubes. He presented the linearity between the pressure gradient and the volume flow rate.

Poiseuille [4] independently investigated the relation between pressure gradient and volume flow rate of fluids in pipes. Poiseuille presented his study in which the flow in capillary glass tubes with varying diameters was investigated. From these researches, the well-known Hagen-Poiseuille law is established. In order to estimate the friction pressure for laminar Newtonian fluid flow in smooth pipes, the Hagen-Poiseuille equation can be used.

$$f = \frac{64}{Re} \quad (1.3)$$

where  $f$  is the Darcy friction factor and  $Re$  is the Reynolds Number. It is valid for the Reynolds number range of  $Re < 2100$ .

Blasius [5] was the first researcher who presented an empirical formula of friction factor for smooth pipes. His following explicit equation is valid for the Reynolds number range of  $3 \cdot 10^3 < Re < 10^5$ .

$$f = 0.3164Re^{-0.25} \quad (1.4)$$

Drew et al. [6] proposed a friction factor formula for Newtonian fluids in smooth pipes that flow in a fully developed turbulent regime. The proposed formula is valid for the Reynolds number range of  $4 \times 10^3 < Re < 3 \times 10^6$ .

$$f = 0.0014 + 0.125(Re)^{-0.32} \quad (1.5)$$

Prandtl [7] introduced a formula from the available experimental data. He proposed the following implicit friction factor equation for the turbulent flows in hydraulically smooth pipes. This formula is valid for  $4 \times 10^3 < Re$ .

$$\frac{1}{\sqrt{f}} = 2 \log(Re\sqrt{f}) - 0.8 \quad (1.6)$$

Filonienko [8] introduced the following friction factor equation. The presented equation is valid for the Reynolds number range of  $3 \times 10^4 < Re < 5 \times 10^7$ .

$$f = \frac{1}{(1.82 \log Re - 1.64)^2} \quad (1.7)$$

Allen and Eckert [9] presented their friction factor equation for turbulent flow in smooth tubes. The proposed equation is valid for the Reynolds number range of  $1.3 \times 10^4 < Re < 1.2 \times 10^5$ .

$$f = 0.00556 + \frac{0.432}{Re^{0.308}} \quad (1.8)$$

Taler [10] reviewed some of the well-known friction factor correlations in smooth tubes and introduced his own friction factor correlation. The proposed equation is valid for the Reynolds number range of  $3 \times 10^3 < Re < 10^7$ .

$$f = (1.2776 \log Re - 0.406)^{-2.246} \quad (1.9)$$

### **1.1.2 Newtonian fluid flow in rough pipes**

Darcy [2] presented a comprehensive study by performing experiments on pipes made of different materials which were glass, lead, cast iron, wrought iron, and asphalt-covered cast iron. The difference in materials provided different surfaces for pipes and therefore different roughness values. The lengths of pipes were 100 m except the glass one, and the diameters of them were from 1.2 to 50 cm. It was stated

that surface type, pipe diameter, and the inclination of the pipe affected the discharge. The performed experiments showed that for a constant relative roughness, the resistance factor had small variations according to the changes of Reynolds number. The inverse ratio between the friction factor and Reynolds number was noted as friction factor decreased while Reynolds number increased. Furthermore, Darcy stated that the decrement rate of friction factor got slower when the relative roughness increased. According to the performed study, for certain roughness values, the friction factor was found to be independent of the Reynolds number. On the other hand, the data of this study provided that when Reynolds number was constant, friction factor increased significantly with the relative roughness.

Mises [11], developed equations to state the relation between friction factor, relative roughness, and Reynolds number, under the guidance of Darcy's and Bazin's work. Mises proposed different equations which were valid for low and high Reynolds numbers. The relative roughness term was introduced for the first time by Mises. The following equation proposed by Mises is valid for large Reynolds number.

$$f = 0.0024 + \sqrt{2 \frac{\varepsilon}{D} + \frac{0.3}{\sqrt{Re}}} \quad (1.10)$$

And the following equation proposed by Mises is valid for the small Reynolds number near the critical value.

$$f = \left(0.0024 + \sqrt{2 \frac{\varepsilon}{D}}\right) \left(1 - \frac{1000}{Re}\right) + \frac{0.3}{\sqrt{Re}} \sqrt{1 - \frac{1000}{Re}} + \frac{8}{Re} \quad (1.11)$$

Schiller [12] performed experimental tests to investigate changes in friction factor with surface type and Reynolds number. According to the performed experiments, he obtained that critical Reynolds number and wall surface were independent of each other. Moreover, in his study, it was observed that as the surface was markedly roughened the quadratic law of friction took place when the turbulence formed up. Schiller obtained an increment of friction factor as the Reynolds number was increased but due to the lack of limits of apparatus at that time, he could not determine that whether the increment of friction factor for high Reynolds numbers could fall into the quadratic law of friction. Additionally, Schiller's results showed



that friction factor increased as the surface roughness increased for a constant value of Reynolds number.

Hopf [13] collected previous experimental studies on the investigation of the roughness concept and presented a detailed review from them. According to the previous studies, both for rough pipes and channels, he obtained two different roughnesses that were related to the resistance equations. The first roughness and square of the flow velocity were proportional to each other. It was noted that the resistance coefficient and Reynolds number were not dependent on each other. The resistance coefficient was linked to coarse roughness elements which had tight gaps in between. For this situation, the roughness phenomena could be represented by a simple roughness parameter which was relative roughness.

Fromm [14] and Fritsch [15] in their studies investigated the relationship between the resistance coefficient and roughness height by working on different pipes and channels that had the same absolute roughness but different hydraulic radii. They presented a proportional relation between friction factor and relative roughness.

Von Karman [16] presented his widely used friction factor equation for the fully rough regime. Since the equation is for the fully rough regime, Reynolds number does not present any effect.

$$1/\sqrt{f} = 2\log\left[\frac{3.7D}{\epsilon}\right] \quad (1.12)$$

Nikuradse [17] performed an extensive and systematic study that was focused on the effects of Reynolds number and relative roughness on velocity distribution and friction factor for pipe flows. Nikuradse glued sands with known grain size inside the wall of circular pipes very firmly. He varied the diameters of pipes and grain size to investigate the effect of relative roughness. By doing this, the relative roughness changed from 1/500 to 1/15. He worked with six different degrees of relative roughness and Reynolds ranged between 104 and 106. After his careful experiments, he stated that when the Reynolds number was small, the resistance factor was the same for both pipes regardless of being smooth or rough. It was noted that the roughening projections were kept completely in the laminar layer for the studied Reynolds number range. He observed that resistance factor increment was obtained

with Reynolds number increment. Nikuradse also stated in his work that when the Reynolds number was high, the resistance factor became independent of Reynolds number. Furthermore, Nikuradse developed a resistance factor equation and a general velocity distribution expression.

Colebrook [18] proposed an implicit equation, known as the famous Colebrook-White equation. This equation is commonly used for the turbulent flows through rough pipes. Darcy-Weisbach coefficient of the fluid flows is estimated by using Colebrook's equation. Colebrook's equation has implicit characteristics. Therefore, approximate solutions or iterations are necessary to arrive a solution. This equation was proposed as a combination of Prandtl and von Karman equations for transition and turbulent flows in rough pipes.

$$\frac{1}{\sqrt{f}} = -2.0 \log \left[ \frac{\epsilon}{3.7D} + \frac{2.51}{Re\sqrt{f}} \right] \quad (1.13)$$

Moody [19] plotted his famous Moody Diagram for the relation between the Darcy-Weisbach friction factor and Reynolds number considering the relative roughness,  $\epsilon/D$ , values. The main starting point of this chart was based on the inconvenience due to the iteration procedure of the Colebrook-White equation since it is an implicit equation. It was aimed to present a visual representation of the Colebrook function. Moody diagram is shown in Figure 1.1.

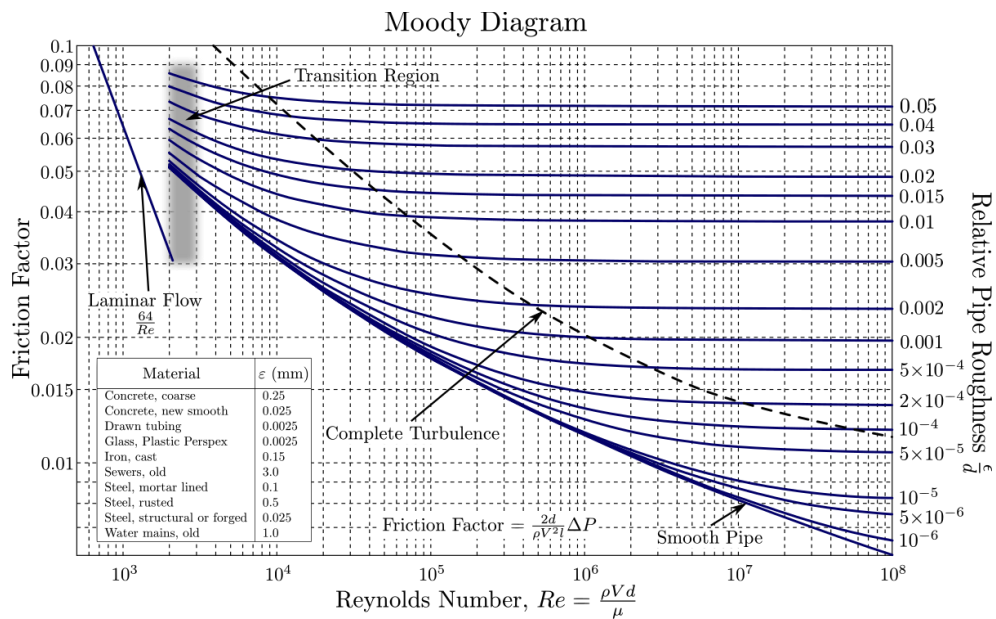


**Figure 1.1** Moody diagram

Nevertheless, Moody continued to study in search of a new friction factor equation that can eliminate the use of any chart or iteration procedure. Moody [20] presented an explicit friction factor equation to obtain  $f$ . The proposed equation is valid for the Reynolds number range of  $4000 \leq Re \leq 10^8$  and relative roughness range of  $0 \leq \frac{\varepsilon}{D} \leq 0.01$ .

$$f = 0.0055 \left( 1 + \left( 2 \times 10^4 \frac{\varepsilon}{D} + \frac{10^6}{Re} \right)^{1/3} \right) \quad (1.14)$$

In the literature, there are various studies that present approximations of the Colebrook-White equation. Some of the well-known studies and some approximations are presented.

Altshul [21]:

$$f = 0.11 \left( \frac{68}{Re} + \varepsilon \right)^{0.25} \quad (1.15)$$

valid for Reynolds number range of  $4000 \leq Re \leq 10^7$  and relative roughness range of  $0 \leq \frac{\varepsilon}{D} \leq 10^{-2}$ .

Wood [22]:

$$f = 0.094 \left( \frac{\varepsilon}{D} \right)^{0.225} + 0.53 \left( \frac{\varepsilon}{D} \right) + 88 \left( \frac{\varepsilon}{D} \right)^{0.44} Re^{1.62} \left( \frac{\varepsilon}{D} \right)^{0.134} \quad (1.16)$$

valid for Reynolds number range of  $4000 \leq Re \leq 5 \times 10^7$  and relative roughness range of  $0.00001 \leq \frac{\varepsilon}{D} \leq 0.04$ .

Powe and Townes [23] studied on the turbulence of fully developed rough pipe flows. They investigated the fluctuating velocities in all three coordinate directions and, they concluded that the flow was relatively independent of the solid boundary in the central region of the pipe. However, they obtained that the flow was dependent on solid boundary near the wall.

Eck [24]:

$$\frac{1}{\sqrt{f}} = -2 \log \left( \frac{\varepsilon}{3.715D} + \frac{15}{Re} \right) \quad (1.17)$$

Swamee and Jain [25]:

$$f = \frac{0.25}{\left[ \log\left(\frac{\varepsilon}{3.7D} + \frac{5.74}{Re^{0.9}}\right) \right]^2} \quad (1.18)$$

valid for Reynolds number range of  $5000 < Re < 10^8$  and relative roughness range of  $10^{-6} < \frac{\varepsilon}{D} < 10^{-2}$ .

Churchill [26]:

$$\frac{1}{\sqrt{f}} = -2 \log\left(\left(\frac{\varepsilon}{3.7D}\right) + \left(\frac{7}{Re}\right)^{0.9}\right) \quad (1.19)$$

valid for Reynolds number range of  $5000 < Re < 10^8$  and relative roughness range of  $0.000001 < \frac{\varepsilon}{D} < 0.05$ .

Cebeci and Chang [27] presented a classical numerical approach to turbulent flow over rough surfaces. In another study, they used algebraic eddy viscosity of their previous study [27] to represent the influence of the rough surface on the flow near the wall and dealt with the incompressible rough wall boundary layer flow [28].

Chen [29]:

$$\frac{1}{\sqrt{f}} = -2 \log\left(\frac{\varepsilon}{3.7065D} - \left(\frac{5.0452}{Re}\right) \log\left[\left(\frac{\varepsilon}{D}\right)^{1.1098} + \left(\frac{5.8506}{Re^{0.8981}}\right)\right]\right) \quad (1.20)$$

valid for Reynolds number range of  $4000 < Re < 4 \times 10^8$  and relative roughness range of  $10^{-7} \leq \left(\frac{\varepsilon}{D}\right) \leq 5 \times 10^{-2}$

Round [30]:

$$\frac{1}{\sqrt{f}} = -1.8 \log\left(\frac{Re}{0.135Re(\varepsilon/D)+6.5}\right) \quad (1.21)$$

valid for Reynolds number range of  $4000 \leq Re \leq 10^7$  and relative roughness range of  $0 \leq \left(\frac{\varepsilon}{D}\right) \leq 10^{-2}$

Barr [31]:

$$\frac{1}{\sqrt{f}} = -2 \log \left( \frac{\varepsilon}{3.7D} + \frac{4.518 \log\left(\frac{Re}{7}\right)}{Re \left(1 + \frac{Re^{0.52}}{29(\varepsilon/D)^{0.7}}\right)} \right) \quad (1.22)$$

valid for Reynolds number range of  $2300 \leq Re \leq 10^8$  and relative roughness range of  $0 \leq \left(\frac{\varepsilon}{D}\right) \leq 5 \times 10^{-2}$

Zigrang and Sylvester [32]:

$$\frac{1}{\sqrt{f}} = -2 \log \left( \frac{\varepsilon}{3.7D} - \frac{5.02}{Re} \log \left( \frac{\varepsilon}{3.7D} - \frac{5.02}{Re} \log \left( \frac{\varepsilon}{3.7D} + \frac{13}{Re} \right) \right) \right) \quad (1.23)$$

valid for Reynolds number range of  $4000 \leq Re \leq 4 \times 10^8$  and relative roughness range of  $10^{-5} \leq \left(\frac{\varepsilon}{D}\right) \leq 5 \times 10^{-2}$

Haaland [33]:

$$\frac{1}{\sqrt{f}} = -1.8 \log \left( \left( \frac{\varepsilon}{3.7D} \right)^{1.11} + (6.9/Re) \right) \quad (1.24)$$

valid for Reynolds number range of  $4000 \leq Re \leq 10^8$  and relative roughness range of  $10^{-6} \leq \left(\frac{\varepsilon}{D}\right) \leq 5 \times 10^{-2}$

Serghides [34]:

$$\frac{1}{\sqrt{f}} = A - \frac{(B-A)^2}{C-2B+A} \quad (1.25)$$

where

$$A = -2 \log \left( \frac{\varepsilon}{3.7D} + \frac{12}{Re} \right) \quad (1.26)$$

$$B = -2 \log \left( \frac{\varepsilon}{3.7D} + \frac{2.51A}{Re} \right) \quad (1.27)$$

$$C = -2 \log \left( \frac{\varepsilon}{3.7D} + \frac{2.51B}{Re} \right) \quad (1.28)$$

valid for Reynolds number range of  $2300 \leq Re \leq 10^8$  and relative roughness range of  $10^{-6} \leq \left(\frac{\varepsilon}{D}\right) \leq 5 \times 10^{-2}$

Tsal [35]:

$$A = 0.11 \left( \frac{68}{Re} + \frac{\varepsilon}{D} \right)^{0.25} \quad (1.29)$$

If  $A \geq 0.018 \rightarrow f = A$ ,

If  $A < 0.018 \rightarrow f = 0.0028 + 0.85A$

valid for Reynolds number range of  $4000 \leq Re \leq 10^8$  and relative roughness range of  $0 \leq \frac{\varepsilon}{D} \leq 5 \times 10^{-2}$

Manadilli [36]:

$$\frac{1}{\sqrt{f}} = -2 \log \left( \frac{\frac{\varepsilon}{D}}{3.7} + \frac{95}{Re^{0.983}} - \frac{96.82}{Re} \right) \quad (1.30)$$

valid for Reynolds number range of  $4000 \leq Re \leq 10^8$  and relative roughness range of  $0 \leq \frac{\varepsilon}{D} \leq 5 \times 10^{-2}$

Pimentel et al. [37] studied on the incompressible fully developed turbulent flow of ducts which had rough walls. They investigated the both symmetric and asymmetric ducts. A semi-analytical method was presented by using a modified turbulence model to show the surface roughness influence. For circular ducts and parallel plates, the velocity distribution and friction factor were presented.

Romeo et al. [38]:

$$\frac{1}{\sqrt{f}} = -2 \log \left( \frac{\frac{\varepsilon}{D}}{3.7} + \frac{95}{Re^{0.983}} - \frac{96.82}{Re} \right) \quad (1.31)$$

valid for Reynolds number range of  $3000 \leq Re \leq 1.5 \times 10^8$  and relative roughness range of  $0 \leq \frac{\varepsilon}{D} \leq 5 \times 10^{-2}$

Sonnad and Goudar [39];

$$\frac{1}{\sqrt{f}} = 0.8686 \ln \left[ \frac{0.4587Re}{(S-0.31)^{(S+1)}} \right] \quad (1.32)$$

where

$$S = 0.124Re \frac{\varepsilon}{D} + \ln(0.4587Re) \quad (1.33)$$

valid for Reynolds number range of  $4000 \leq Re \leq 10^8$  and relative roughness range of  $10^{-6} \leq \frac{\varepsilon}{D} \leq 5 \times 10^{-2}$

Shockling et al. [40] presented in their paper the mean flow measurements for fully developed turbulent pipe flow. The range of the Reynolds number of the study was between  $57 \times 10^3$  to  $21 \times 10^6$ . In this range, the flow presented hydraulically smooth, transitionally rough, and fully rough behaviors. They achieved the ratio for characteristic roughness height over pipe diameter as 1:17000 by using a honing tool to prepare the surface. It was obtained from their study that equivalent sand-grain roughness was three times root-mean-square roughness height.

Buzelli [41]:

$$\frac{1}{\sqrt{f}} = \alpha - \frac{\alpha + 2 \log\left(\frac{B}{Re}\right)}{1 + \frac{2.18}{B}} \quad (1.34)$$

where

$$\alpha = \frac{0.744 \ln(Re) - 1.41}{1 + 1.32 \sqrt{\varepsilon/D}} \quad (1.35)$$

$$B = \frac{\varepsilon/D}{3.7} Re + 2.51\alpha \quad (1.36)$$

valid for Reynolds number range of  $2300 \leq Re \leq 10^8$  and relative roughness range of  $10^{-6} \leq \frac{\varepsilon}{D} \leq 5 \times 10^{-2}$

Cheng [42]:

$$\frac{1}{f} = \left(\frac{Re}{64}\right)^\alpha \left(1.8 \log \frac{Re}{6.8}\right)^{2(1-\alpha)b} \left(2 \log \frac{3.7D}{\varepsilon}\right)^{2(1-a)(1-b)} \quad (1.37)$$

where

$$\alpha = \frac{1}{1 + \left(\frac{Re}{2720}\right)^9} \quad (1.38)$$

$$b = \frac{1}{1 + \left(\frac{Re}{160} \frac{D}{\varepsilon}\right)^2} \quad (1.39)$$

Avci and Karagoz [43]:

$$f = \frac{6.4}{\left[\ln(Re) - \ln\left(1 + 0.01 Re \frac{\varepsilon}{D} \left(1 + 10 \sqrt{\frac{\varepsilon}{D}}\right)\right)\right]^{2.4}} \quad (1.40)$$

valid for Reynolds number range of  $2300 \leq Re \leq 10^8$  and relative roughness range of  $0 \leq \frac{\varepsilon}{D} \leq 5 \times 10^{-2}$

Papaevangelou [44]:

$$f = \frac{0.2479 - 0.0000947(7 - \log Re)^4}{\left(\log\left(\frac{\varepsilon}{3.615D} + \frac{7.366}{Re^{0.9142}}\right)\right)^2} \quad (1.41)$$

valid for Reynolds number range of  $4000 \leq Re \leq 10^8$  and relative roughness range of  $10^{-6} \leq \frac{\varepsilon}{D} \leq 5 \times 10^{-2}$ .

Brkic [45]:

$$f = \left[-2 \log\left(10^{-0.4343\beta} + \frac{\varepsilon}{3.71D}\right)\right]^{-2} \quad (1.42)$$

where

$$\beta = \ln \frac{Re}{1.816 \ln\left(\frac{1.1Re}{\ln\left(1 + \frac{1.1}{Re}\right)}\right)} \quad (1.43)$$



valid for Reynolds number range of  $4000 \leq Re \leq 10^8$  and relative roughness range of  $0 \leq \frac{\varepsilon}{D} \leq 5 \times 10^{-2}$

Fang et al. [46]:

$$f = 1.613 \left[ \ln \left( 0.234 (\varepsilon/D)^{1.1007} - \frac{60.525}{Re^{1.1105}} + \frac{56.291}{Re^{1.0712}} \right) \right]^{-2} \quad (1.44)$$

valid for Reynolds number range of  $3000 \leq Re \leq 10^8$  and relative roughness range of  $0 \leq \frac{\varepsilon}{D} \leq 5 \times 10^{-2}$

Ghanbari et al. [47]:

$$f = \left[ -1.52 \log \left( \left( \frac{\varepsilon/D}{7.21} \right)^{1.042} + \left( \frac{2.731}{Re} \right)^{0.9152} \right) \right]^{-2.169} \quad (1.45)$$

valid for Reynolds number range of  $2300 \leq Re \leq 10^8$  and relative roughness range of  $0 \leq \frac{\varepsilon}{D} \leq 5 \times 10^{-2}$

Bellos et al. [48]:

$$f = \left( \frac{64}{Re} \right)^a \left[ 0.75 \ln \frac{Re}{5.37} \right]^{2(a-1)b} \left[ 0.88 \ln 3.41 \frac{D}{\varepsilon} \right]^{2(a-1)(1-b)} \quad (1.46)$$

where

$$a = \frac{1}{1 + \left( \frac{Re}{2712} \right)^{8.4}} \quad (1.47)$$

$$b = \frac{1}{1 + \left( \frac{Re/D}{150} \right)^{1.8}} \quad (1.48)$$

Genic et al. [49] studied on the pipe flows in smooth, rough and transition regimes, and proposed friction factor correlations. The proposed equations are valid for the Reynolds number range of  $2 \times 10^3 < Re < 4 \times 10^3$  and  $4 \times 10^3 < Re < 35.5 \times 10^6$ , respectively.

$$f = 0.032 + 0.00052(Re - 2000)\left(\frac{\varepsilon}{D}\right)^{0.8} + 0.089 \quad (1.49)$$

$$f = \left\{ -1.8 \log \left[ \frac{7.35 - 1200\left(\frac{\varepsilon}{D}\right)^{1.25}}{Re} \right] + \left(\frac{\varepsilon}{3.15D}\right)^{1.15} \right\}^{-2} \quad (1.50)$$

### 1.1.3 Non-Newtonian fluid flow in smooth pipes

Non-Newtonian fluids can be expressed by different rheological models such as the Bingham plastic, the Power Law, and the Herschel-Bulkley model. The Herschel-Bulkley model is a generalized model to describe the relationship between the strain and shear by combining Bingham Plastic and Power-Law models, and quite suitable to describe the behavior of non-Newtonian fluids. Detailed information about these rheological models for non-Newtonian fluids is presented in section 2.2.

Metzner and Reed [50] proposed a friction factor of pseudoplastic non-Newtonian fluid flows in smooth pipes for the laminar regime. They used the generalized Reynolds number  $N_{Reg}$  concept.

$$f_F = 16/N_{reg} \quad (1.51)$$

$$N_{Reg} = \frac{D^n V^{2-n} \rho}{g_c K (8)^{n-1}} \quad (1.52)$$

Where  $f_F$  is the Fanning friction factor which is  $1/4$  times of the Darcy friction factor  $f_D$ .  $D$  is the diameter of the pipe ( $L$ ),  $V$  is the average fluid velocity ( $LT^{-1}$ ),  $n$  is the flow behavior index of power-law model (*dimensionless*),  $\rho$  is the fluid density ( $ML^{-3}$ ),  $g_c$  is conversion factor ( $32.17 \text{ lb}_m \cdot \text{ft} / \text{lb}_f \cdot \text{sec}^2$ ),  $K$  is the consistency index ( $ML^{-1}T^{n-2}$ ) of power-law model.

Dodge and Metzner [51] performed an extensive theoretical and experimental study and suggested the following correlation for the friction factor of the non-Newtonian fluids flow through smooth pipes. The presented equation is widely accepted in the industry. Even though it is widely accepted, it has some restrictions. For example, there is no data for the fluids which have a flow behavior index smaller than 0.4 ( $n < 0.4$ ) and not sufficient data available for the higher generalized Reynolds numbers.

$$\frac{1}{\sqrt{f}} = \frac{4}{(n)^{0.75}} \log \left[ N_{Reg} f \left( 1 - \frac{n}{2} \right) \right] - \frac{0.40}{(n)^{1.2}} \quad (1.53)$$

where  $N_{Reg}$  is the generalized Reynolds Number for Power-Law fluid and can be calculated as in Eq. 1.52.

Reed and Pilehvari presented a correlation [52] by modifying the Dodge and Metzner [51] 's correlation to compute Herschel-Bulkley fluid's Fanning friction factor for smooth pipes as;

$$\frac{1}{\sqrt{f_F}} = \frac{4}{N^{0.75}} \log \left[ N_{Reg} f_F \left( 1 - \frac{N}{2} \right) \right] - \frac{0.40}{N^{1.2}} \quad (1.54)$$

where N is the generalized flow behavior index presented as;

$$\frac{1}{N} = \frac{(1-2m)\tau_w + 3m\tau_y}{m(\tau_w - \tau_y)} + \frac{2m(1+m)[(1+2m)\tau_w^2 + m\tau_y\tau_w]}{m(1+m)(1+2m)\tau_w^2 + 2m(1+m)\tau_w\tau_y + 2m^3\tau_y^2} \quad (1.55)$$

In Eq. 1.55,  $m$  represents flow behavior index of Herschel-Bulkley Fluid (dimensionless),  $\tau_y$  is the Yield Stress or Point ( $ML^{-1}T^{-2}$ ),  $\tau_w$  is the Wall Shear Stress ( $ML^{-1}T^{-2}$ ).

$N_{Reg}$  is the generalized Reynolds Number for Herschel-Bulkley Fluid and presented as

$$N_{Reg} = \frac{D^N V^{2-N} \rho}{K(8)^{N-1}} \quad (1.56)$$

Where D is the diameter of the pipe (L), V is the average fluid velocity ( $LT^{-1}$ ), N is the generalized flow behavior index of Herschel-Bulkley model (*dimensionless*),  $\rho$  is the fluid density ( $ML^{-3}$ ), K is the consistency index ( $ML^{-1}T^{n-2}$ ) of Herschel-Bulkley model.

Melton and Malone [53] suggested their method to predict friction pressures for the non-Newtonian fracturing fluids.

$$\tau = AD^e (\gamma)^s \quad (1.57)$$

Where  $A$ ,  $e$  and  $s$  are experimentally obtained constants. Lord et al. [54] confirmed the following equation to overcome data collection from multiple pipes.

$$e = (s - 0.2) \quad (1.58)$$

The relation between  $\tau$  and  $\gamma$  is expected to present a straight line in a logarithmic plot from the equation proposed by Melton and Malone. While this expectation appears to be true for thin fluids, fracturing gels presents curvature.

Shah [55] in order to present a prediction of friction pressures for fracturing gels, employed the approach presented by Dodge and Metzner [51].

$$f = f_{\infty} + A(N_{Reg})^{-B} \quad (1.59)$$

where constants ( $f_{\infty}$ ,  $A$ ,  $B$ ) are functions of flow behavior index of power-law model ( $n$ ).

#### 1.1.4 Non-Newtonian fluid flow in rough pipes

Szilas et al. [56] presented a detailed theoretical analysis for the non-Newtonian fluids in rough pipes. They came up with a new friction factor equation for turbulent flows of power-law type fluids that worked between smooth and wholly rough wall turbulence in the transition region. They evaluated the accuracy of their equation by performing in situ measurements on a crude oil pipeline.

$$\frac{1}{\sqrt{4f}} = -2.0 \log \left[ \frac{\varepsilon/D}{3.71} + \frac{10^{-\beta/2}}{N_{Reg}(4f)^{(2-n)/2n}} \right] \quad (1.60)$$

$$\beta = 1.51^{1/n} \left( \frac{0.707}{n} + 2.12 \right) - \frac{4.015}{n} - 1.057 \quad (1.61)$$

In Eq. 1.61,  $n$  is flow behavior index of power-law fluid and  $\beta$  represents a coefficient to be used in the Eq. 1.60.

Heywood and Cheng [57] presented a study in which the investigations for the head loss prediction methods in turbulent pipe flow of non-Newtonian fluids were performed. They aimed to state that for non-Newtonian fluid flows in turbulent regimes, considering the difference in predictions of head losses carries great importance.

Garcia and Steffe [58] in their study compared the friction factor equations for non-Newtonian pipe flows. Friction factor relationships for non-Newtonian fluids were summarized and it was stated that these relationships alter remarkably according to the  $n$  (flow behavior index),  $Re$  (Reynolds), and  $He$  (Hedstrom) numbers.

Khan [59] in his paper discussed the estimation of head loss for non-Newtonian fluids (in particular a power-law fluid and its flow) through straight and curved pipes. He examined the relationship between the frictional factor and Reynolds number for the flow of polymeric solutions through straight and curved pipes.

Hemeida [60] presented a paper where the effect of wall roughness in turbulent pipe flow of pseudoplastic crude oil was investigated and field data from pipelines were evaluated. An equation was presented for the pipe flows of turbulent pseudoplastic fluids to estimate the laminar sublayer thickness.

Reed and Pilehvari [52] proposed a Fanning friction factor correlation for the turbulent flow of Herschel-Bulkley fluid in rough pipes. The correlation was based on a modification of the Colebrook equation [18] and has not been verified with experimental data yet. The proposed correlation is presented below.

$$\frac{1}{\sqrt{f_F}} = -4.0 \log \left[ \frac{\varepsilon/D}{3.7} + \frac{1.26 N^{-1.2}}{N_{Reg} f^{(1-\frac{N}{2}) N^{-0.75}}} \right] \quad (1.62)$$

Where  $f_F$  is the Fanning friction factor,  $\varepsilon/D$  is the relative roughness,  $N$  is the generalized flow behaviour index of Herschel-Bulkley model, and  $N_{Reg}$  is the generalized Reynolds Number.

Kawase et al. [61] proposed a friction factor correlation for the power-law fluids in rough pipes as follows:

$$\frac{1}{\sqrt{f_F}} = 3.57 \log \left[ \frac{N_{Reg} \left( \frac{1}{n^{0.615}} \right)}{N_{Reg} \left( \frac{1}{n^{0.615}} \right) \left( 10^{\frac{8.5n-3.75}{5.756}} \left( \frac{\varepsilon}{2D} \right)^{(-1.14/n) + 6.5(1/n(1+0.75n))} \right)} \right] \quad (1.63)$$

In Eq. 1.63, different from Eq. 1.62,  $n$  is the flow behavior index of power-law fluid (dimensionless).

Langelandsvik et al. [62] pointed out the significant difference of transitionally rough behavior from Colebrook roughness function. They found the equivalent sand-grain roughness 1.6 times of commercial steel pipe's roughness height.

Avci and Karagoz [63] proposed an explicit friction factor equation as a function of Reynolds number and relative roughness for both smooth and rough walls of turbulent pipe and channel flows. By using the available experimental data from the literature, they determined the model constants. The proposed equation was obtained from a new logarithmic velocity profile.

Dosunmu and Shah [64], for non-Newtonian fluids flow through pipes and annular sections, came up with a paper in which they evaluated friction factor correlations and presented equivalent diameter definitions. Presenting a friction factor correlation for rough pipe and annular flows of non-Newtonian fluids to predict frictional pressure losses was the objective other their study.

Dosunmu and Shah [65] for various flowrates, performed measurements for the pressure drop across a straight pipe. They investigated the behaviours of surfactant solutions of their turbulent flows. An analytical Fanning friction factor equation for purely viscous Power-Law fluids were derived.

Diogo and Vilela [66] experimentally investigated the turbulent water flows through plastic pipes. Based on the experimental study they performed, they determined the friction factors. Important variations of absolute roughness values for the different pipes were obtained.

## **1.2 Aim of the Study**

- The first aim of the presented study is to identify if the roughness height of the commercially available galvanized pipes varies with the diameters of the pipes.
- Investigating the fluid temperature effects on frictional pressure losses and proposing friction factor correlations for both Newtonian and non-Newtonian fluid flows through rough pipes are other aims of this study. It is seen that in the literature, there is not any correlation for friction factor that includes fluid temperature and roughness parameters together.

Other objectives of this study are;

- Developing a mathematical model for Newtonian fluid flow (water) through rough pipes under fluid temperature conditions and,
- Validating the developed mathematical model with experimental results.

## 2.THEORY

### 2.1 Geometry of the Model and Main Equations of Turbulent Pipe Flow

The geometry of the model and main equations of turbulent pipe flow is presented. The schematic drawing of the experimentally investigated pipe flow is shown in Figure 2.1.

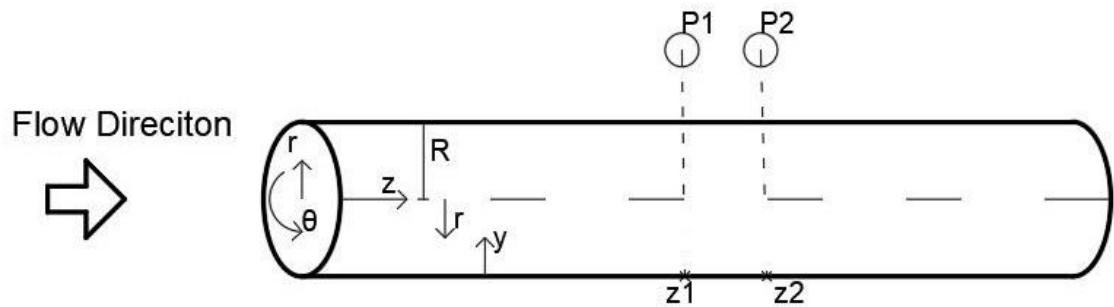


**Figure 2.1** Schematic drawing of the experimentally investigated pipe flow

To investigate the presented flow, the Navier-Stokes equations in cylindrical coordinates are analyzed.

Flow of incompressible fluids are expressed with the Navier-Stokes equations. These equations give the fundamentals of the fluid flow. In order to account for turbulence, Reynolds averaging is applied.

Pipes of the test section are axisymmetric, the Navier-Stokes equation in all directions of cylindrical coordinates  $(r, \theta, z)$  are presented in this section.

$$u_z = u, u_r = v, u_\theta = w \quad (2.1)$$



In this case, the velocity field is:

$$\vec{V} = (u, v, w) \quad (2.2)$$

The Reynolds Averaged Navier-Stokes (RANS) equations are written as the continuity and the momentum equations.

Continuity eq.:

$$\frac{1}{r} \frac{\partial(rv)}{\partial r} + \frac{1}{r} \frac{\partial w}{\partial \theta} + \frac{\partial u}{\partial z} = 0 \quad (2.3)$$

Momentum eq. in  $r$  dir.:

$$\begin{aligned} \frac{\partial v}{\partial t} + \frac{1}{r} \frac{\partial[r(vv)]}{\partial r} + \frac{1}{r} \frac{\partial(vw)}{\partial \theta} + \frac{\partial(vu)}{\partial z} - \frac{vw}{r} = -\frac{1}{\rho} \frac{\partial p}{\partial r} + \frac{1}{r} \frac{\partial(r\tau_{rr})}{\partial r} + \frac{1}{r} \frac{\partial(\tau_{\theta r})}{\partial \theta} + \frac{\partial(\tau_{rz})}{\partial z} - \frac{\tau_{\theta\theta}}{r} + \rho g_r + \\ \frac{1}{r} \frac{\partial[r(-\overline{v'v'})]}{\partial r} + \frac{1}{r} \frac{\partial(-\overline{v'w'})}{\partial \theta} + \frac{\partial(-\overline{v'u'})}{\partial z} - \frac{-\overline{w'w'}}{r} \end{aligned} \quad (2.4)$$

Momentum eq. in  $\theta$  dir.:

$$\begin{aligned} \frac{\partial w}{\partial t} + \frac{1}{r} \frac{\partial[r(wv)]}{\partial r} + \frac{1}{r} \frac{\partial(ww)}{\partial \theta} + \frac{\partial(wu)}{\partial z} + \frac{vw}{r} = -\frac{1}{\rho r} \frac{\partial p}{\partial \theta} + \frac{1}{r} \frac{\partial(r\tau_{r\theta})}{\partial r} + \frac{1}{r} \frac{\partial(\tau_{\theta\theta})}{\partial \theta} + \frac{\partial(\tau_{z\theta})}{\partial z} + \frac{\tau_{r\theta}}{r} + \\ \rho g_\theta + \frac{1}{r} \frac{\partial[r(-\overline{w'v'})]}{\partial r} + \frac{1}{r} \frac{\partial(-\overline{w'w'})}{\partial \theta} + \frac{\partial(-\overline{w'u'})}{\partial z} + \frac{-\overline{w'v'}}{r} \end{aligned} \quad (2.5)$$

Momentum eq. in  $z$  dir.:

$$\begin{aligned} \frac{\partial u}{\partial t} + \frac{1}{r} \frac{\partial[r(uv)]}{\partial r} + \frac{1}{r} \frac{\partial(uw)}{\partial \theta} + \frac{\partial(uu)}{\partial z} = -\frac{1}{\rho} \frac{\partial p}{\partial z} + \frac{1}{r} \frac{\partial(r\tau_{rz})}{\partial r} + \frac{1}{r} \frac{\partial(\tau_{\theta z})}{\partial \theta} + \frac{\partial\tau_{zz}}{\partial z} + \rho g_z + \frac{1}{r} \frac{\partial[r(-\overline{u'v'})]}{\partial r} + \\ \frac{1}{r} \frac{\partial(-\overline{u'w'})}{\partial \theta} + \frac{\partial(-\overline{u'u'})}{\partial z} \end{aligned} \quad (2.6)$$

Necessary assumptions are assigned to simplify RANS equations as follows.

- Fully developed turbulent flow. (In the axial direction, there is no velocity variation ( $\partial/\partial z \rightarrow 0$ )).
- Fluid flow is only in the Z direction. ( $v=w=0$ ).
- Steady-state condition. (All partial derivatives with respect to time are zero  $\partial/\partial t \rightarrow 0$ ).
- Incompressible fluid.
- Isothermal system (Physical properties do not change).

Viscous stresses  $\tau_{ij}$  are expressed as;

$$\tau_{rr} = \nu \left[ \frac{4}{3} \frac{\partial v}{\partial r} - \frac{2}{3} \left( \frac{1}{r} \frac{\partial w}{\partial \theta} + \frac{\partial u}{\partial z} + \frac{v}{r} \right) \right] \quad (2.7)$$

$$\tau_{\theta\theta} = \nu \left[ \frac{4}{3} \left( \frac{1}{r} \frac{\partial w}{\partial \theta} \frac{v}{r} \right) - \frac{2}{3} \left( \frac{\partial v}{\partial r} + \frac{\partial u}{\partial z} \right) \right] \quad (2.8)$$

$$\tau_{zz} = \nu \left[ \frac{4}{3} \frac{\partial u}{\partial z} - \frac{2}{3} \left( \frac{1}{r} \frac{\partial(rv)}{\partial r} + \frac{1}{r} \frac{\partial w}{\partial \theta} \right) \right] \quad (2.9)$$

$$\tau_{r\theta} = \nu \left[ \frac{\partial(w/r)}{\partial r} + \frac{1}{r} \frac{\partial v}{\partial \theta} \right] \quad (2.10)$$

$$\tau_{\theta z} = \nu \left[ \frac{\partial w}{\partial z} + \frac{1}{r} \frac{\partial u}{\partial \theta} \right] \quad (2.11)$$

$$\tau_{rz} = \nu \left[ \frac{\partial u}{\partial r} + \frac{\partial v}{\partial z} \right] \quad (2.12)$$

According to the assumptions, RANS equation in z direction is re-arranged as;

$$\frac{1}{\rho} \frac{\partial P}{\partial z} = \frac{1}{r} \frac{\partial(r\tau_{rz})}{\partial r} + \frac{1}{r} \frac{\partial[r(-\overline{u'v'})]}{\partial r} \quad (2.13)$$

$$\frac{1}{\rho} \frac{\partial P}{\partial z} = \frac{1}{r} \frac{\partial}{\partial r} [r(\tau_{rz} - \overline{u'v'})] \quad (2.14)$$

However, since the Navier-Stokes equations have nonlinearity, still there are velocity fluctuations in the RANS equations. The nonlinear term due to the convective acceleration,  $-\overline{u'v'}$ , which is the Reynolds stress, appears. Therefore, the RANS equation needs to be closed to have an equation with only pressure and mean velocity. For this purpose, in order to solve the ‘‘closure problem’’, the Reynolds stress is modeled as a function of the mean flow by eliminating any fluctuation velocity.

### 2.1.1 Mixing length model

The mixing length model describes momentum transfer that occurs in turbulent flows. The mixing length is a distance of a fluid particle that moves through while conserving its specific properties before it loses them by mixing the surrounding fluid which happens due to the momentum exchange.

Turbulent viscosity,  $\nu_t$  (eddy viscosity) which is introduced by Boussinesq [67], and mixing length,  $l_m$ , which is introduced by Prandtl [68] are the phenomenons where the mixing length model is based on.

$$l_m^2 \left| \frac{\partial u}{\partial r} \right| = \nu_t \quad (2.15)$$

$$-\overline{u'v'} = \nu_t \frac{\partial u}{\partial r} \quad (2.16)$$

$$-\overline{u'v'} = l_m^2 \left| \frac{\partial u}{\partial r} \right| \frac{\partial u}{\partial r} \quad (2.17)$$

When the mixing length model is applied to the re-arranged RANS equation;

$$\frac{1}{\rho} \frac{\partial P}{\partial z} = \frac{1}{r} \frac{\partial}{\partial r} \left[ r \left( \nu \frac{\partial u}{\partial r} + l_m^2 \left| \frac{\partial u}{\partial r} \right| \frac{\partial u}{\partial r} \right) \right] = \frac{1}{r} \frac{\partial}{\partial r} \left[ r \left( (\nu + \nu_t) \frac{\partial u}{\partial r} \right) \right] \quad (2.18)$$

Then, the effective viscosity concept is presented and after some more re-arrangements, the governing equation that finite difference method to be applied;

$$\nu + \nu_t = \nu_e \quad (2.19)$$

$$(\nu + \nu_t) \frac{\partial u}{\partial r} = \nu_e \frac{\partial u}{\partial r} = T \quad (2.20)$$

$$\frac{1}{\rho} \frac{\partial P}{\partial z} = \frac{1}{r} \frac{\partial}{\partial r} (rT) \quad (2.21)$$

$$\frac{\partial P}{\partial z} = C_p \quad (2.22)$$

$$\frac{C_p}{\rho} r = \frac{\partial}{\partial r} (rT) \quad (2.23)$$

The mixing length is expressed as;

$$l_m = Ky \quad (2.24)$$

where K is the von Karman constant and y is the distance from the wall.

At the wall, the mixing length approaches zero due to the dominance of the viscous effect.

Van Driest [69] presented a damping function to represent this behavior for the smooth wall as;

$$f_{\mu} = 1 - \exp\left(-\frac{y^+}{A^+}\right) \quad (2.25)$$

where  $A^+$  is the viscous damping constant and commonly picked as 26. The flow presents fully turbulent behavior around three times of viscous damping constant which is about  $A^+ = 75$ .

Turbulent mixing becomes more significant at a rough wall against a smooth wall. The viscous layer near the wall diminishes. van Driest [69] proposed an additional term for damping function for rough walls as;

$$f_{\mu} = 1 - \exp\left(-\frac{y^+}{A^+}\right) + \exp\left(-\frac{y^+ R^+}{A^+ k^+}\right) \quad (2.26)$$

$R^+$  was given 60 and around 60 damping about to disappear. While  $k^+ = R^+$  fully rough surface is obtained as there is no damping present.  $k^+$  is the roughness height.

Krogstad [70] extended Van Driest's [69] damping function for turbulent boundary layers on rough surfaces. Krogstad's damping function is used to predict roughness as;

$$f_{\mu} = 1 - \exp\left(-\frac{y^+}{A^+}\right) + \exp\left(-\frac{y^+}{A^+} \left(\frac{R^+}{k^+}\right)^{\frac{3}{2}}\right) \sqrt{1 + \exp\left(-\frac{R^+}{k^+}\right)} \quad (2.27)$$

$y^+$  represents the dimensionless wall distance and it is expressed as;

$$y^+ = \frac{y u_*}{\nu} \quad (2.28)$$

$u_*$  represents the shear velocity and it is expressed as;

$$u_* = \sqrt{\frac{\tau_w}{\rho}} \quad (2.29)$$

$\tau_w$  represents the wall shear stress and for the stated pipe flow it is expressed as;

$$\tau_w = -\frac{C_p R}{2} \quad (2.30)$$

## 2.2 Fluid Behavior Classification

Fluid behaviors are classified according to the relationship between the shear stress and the shear rate of fluids. The direct proportion can be seen between shear stress and shear rate for the Newtonian fluids but non-Newtonian fluids have different nature from Newtonian fluids. Therefore, for non-Newtonian fluids, the relation between shear stress and shear rate does not consist of direct proportion.

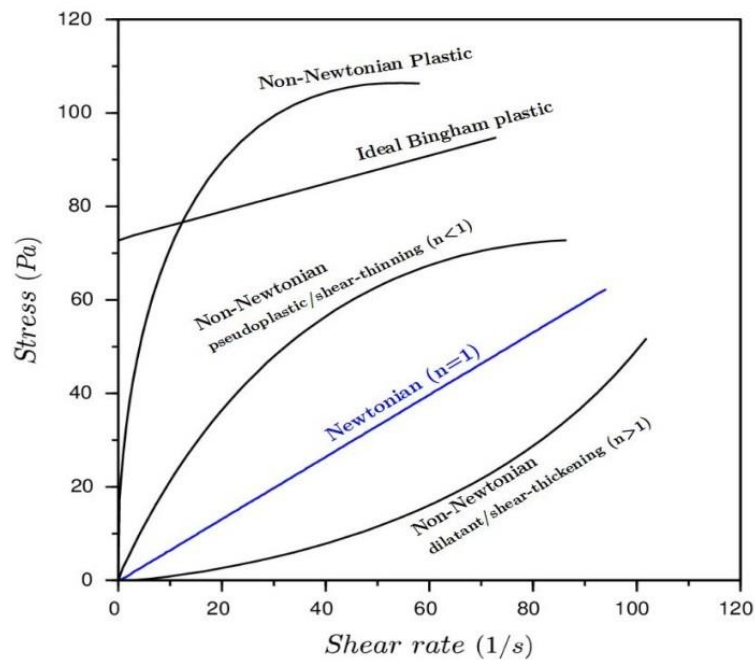


**Figure 2.2** Non-Newtonian fluid classification based on the shear stress and shear rate relation

In order to express the behavior of a fluid, rheological models are used. Rheological models identify the behaviors of the fluids and predict frictional pressure losses in pipe flows by mathematically expressing the relations between shear stresses and shear rates.

To calculate the pressure loss of the non-Newtonian fluid flow correctly, it is critical to choose the appropriate rheological model that represents the fluid behavior. Power-Law, Bingham Plastic, and Herschel-Bulkley models are generally used to describe the rheological behavior of the non-Newtonian fluids.

### 2.2.1 Newtonian model

This model expresses the Newtonian fluid behavior. In this model, a direct proportion between shear stress and shear rate is seen.

The direct proportion corresponds to dynamic viscosity which can be obtained also from the slope of shear stress – shear rate plot.

$$\tau = \mu\gamma \quad (2.31)$$

where  $\tau$  is the Shear Stress ( $ML^{-1}T^{-2}$ ),  $\mu$  is the Dynamic Viscosity ( $ML^{-1}T^{-1}$ ), and  $\gamma$  is the Shear Rate ( $T^{-1}$ ).

### 2.2.2 Power-Law model

This model explains non-Newtonian fluid behavior by introducing flow behaviour index ( $n$ ) and consistency index ( $K$ ).

$n$  constant is the behavior characterizing parameter. For  $n < 1$ , the Power Law model is used for pseudoplastic fluids, for  $n = 1$  it is used for Newtonian fluids and for  $n > 1$  it is used for dilatant fluids.

In case of the Power-Law model:

$$\tau = K\gamma^n \quad (2.32)$$

where  $\tau$  is the Shear Stress ( $ML^{-1}T^{-2}$ ),  $n$  is the flow behavior index and it is dimensionless,  $K$  is the Consistency Index ( $ML^{-1}T^{n-2}$ ) depends on  $n$ , and  $\gamma$  is the Shear Rate ( $T^{-1}$ ).

Dial readings from the viscometer are used for Power-Law model to determine flow behavior index and consistency index.

$$\text{Flow Behaviour Index } (n) = 3.32 \log \left( \frac{\theta_{600}}{\theta_{300}} \right) \quad (2.33)$$

$$\text{Consistency Index } (K) = \frac{\theta_{300}}{511^n} \quad (2.34)$$

### 2.2.3 Bingham Plastic model

Bingham Plastic is a fluid behavior where there is initial shear stress in it to start the flow. That initial shear stress is named as yield stress. Fluids cannot flow until that yield stress is exceeded. After it reaches, a linear plot occurs that represents the shear stress and shear rate relation. The slope of this plot gives the plastic viscosity ( $\mu_p$ ).

$$\tau = \tau_y + \mu_p \gamma \quad (2.35)$$

where  $\tau$  is the Shear Stress ( $ML^{-1}T^{-2}$ ),  $\tau_y$  is the Yield Stress or Point ( $ML^{-1}T^{-2}$ ),  $\mu_p$  is the Plastic Viscosity ( $ML^{-1}T^{-1}$ ), and  $\gamma$  is the Shear Rate ( $T^{-1}$ ).

600 rpm and 300 rpm dial readings from the viscometer are used to calculate the plastic viscosity and yield point.

$$\text{Plastic Viscosity } (\mu_p) = \theta_{600} - \theta_{300} \quad (2.36)$$

$$\text{Yield Point } (\tau_y) = \theta_{300} - \mu_p \quad (2.37)$$

### 2.2.4 Herschel-Bulkley model

This model is also named as Modified or Yield Power Law model. Non-Newtonian fluid behavior is explained with 3 parameters which is the combination of Bingham Plastic and Power Law models and that causes more accuracy.

For the Herschel-Bulkley model, the relation is:

$$\tau = \tau_y + K\gamma^n \quad (2.38)$$

where  $\tau$  is the Shear Stress ( $ML^{-1}T^{-2}$ ),  $\tau_y$  is the Yield Stress or Point ( $ML^{-1}T^{-2}$ ),  $n$  is the flow behavior index and it is dimensionless,  $K$  is the Consistency Index ( $ML^{-1}T^{n-2}$ ) depends on  $n$ , and  $\gamma$  is the Shear Rate ( $T^{-1}$ ).

This model has also the yield stress parameter which represents the flow initiation as Bingham Plastic does. On the other hand, it has flow behavior and consistency index parameters similar to Power-Law model. This model can be used to describe three previous rheological models (Newtonian, Bingham Plastic and Power Law) by

changing its parameters. The model represents Newtonian while  $n=1$ ,  $K=\mu$ ,  $\tau_y=0$  ; represents Power Law while  $n=1$ ,  $\tau_y=0$  ; and represents Bingham Plastic while  $n=1$ ,  $K=\mu_p$ ,  $\tau_y$ =Yield Point.

In this model, the yield stress is calculated with 3 rpm and 6 rpm dial readings which are known as low shear rate shear stress, and by adding yield point parameters into the Power Law model equation, flow behavior and consistency indexes are determined.

$$\text{Yield Point } (\tau_y) = 2\theta_3 - \theta_6 \quad (2.39)$$

$$\text{Flow Behaviour Index } (n) = 3.32 \log \left( \frac{\theta_{600} - \tau_y}{\theta_{300} - \tau_y} \right) \quad (2.40)$$

$$\text{Consistency Index } (K) = \frac{\theta_{300} - \tau_y}{511^n} \quad (2.41)$$



### **3. EXPERIMENTAL STUDY**

In this study, extensive experimental work is conducted by using the flow loop which is located in the fluid mechanics and hydraulics laboratory of the Civil Engineering Department at Izmir Katip Celebi University.

Flows of water and two different CMC (Carboxymethyl Cellulose) polymeric solutions are experimentally investigated in the flow loop.

The test section of the flow loop consists of 10 m long galvanized pipes. The diameters of the pipes are 40 mm, 50 mm, 80 mm, and 90 mm.

Water is the first fluid (F-1) that is experimentally studied. Also, two different polymeric solutions are used in the experiments. Polymeric solutions are named as F-2 (non-Newtonian Fluid - 2) and F-3 (non-Newtonian Fluid - 3). F-2 consists of 5.6 kg high viscous CMC polymer per 1 m<sup>3</sup> of water, and F-3 consists of 9.6 kg low viscous CMC polymer per 1 m<sup>3</sup> of water.

All Specifications of the experiments are presented in Table 3.1.

**Table 3.1** Specifications of the experiments

<b>Specifications of the Experimental Study</b>	<b>Values</b>
Test Section Length (m)	10
Pipe Diameters (mm)	40, 50, 80, 90
Flow Rate Range (m <sup>3</sup> /hr)	6-90
Fluid Temperature (°C)	20, 40, 50, 60
Fluid Types	F-1 (Water) F-2 (5.6 kg High Viscous CMC / 1.0 m <sup>3</sup> ) F-3 (9.6 kg Low Viscous CMC / 1.0 m <sup>3</sup> )

### **3.1 Experimental Setup**

The flow loop consists of a storage tank, mixer, centrifugal pump, control valve, electromagnetic flowmeter, heating resistors, thermocouple, temperature control panel, test section which is formed by galvanized pipes with varying diameters, pressure transducers and, return line. The schematic drawing of the flow loop is represented in Figure 3.1 and actual views of the flow loop that consists galvanized pipes with different diameters is shown in Figure 3.2.

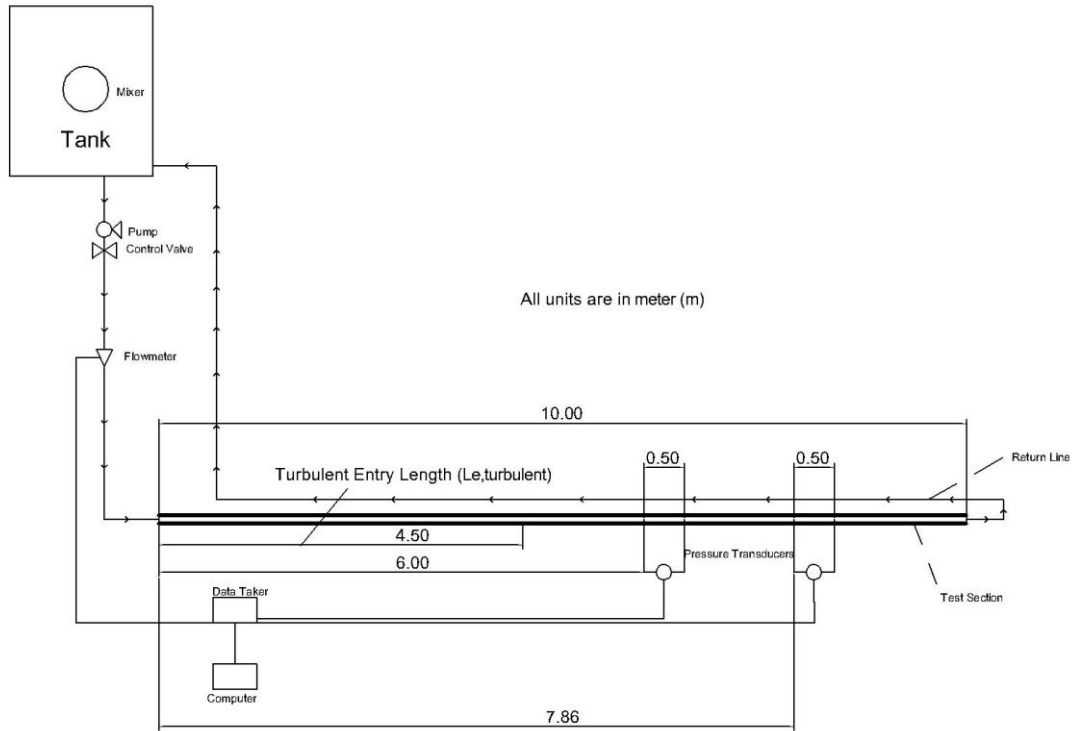


**Figure 3.1** Schematic drawing of the flow loop (plan view)

In this study, investigations of turbulent flow are performed at where it is fully developed. In order to have a fully developed flow, hydrodynamic entry length has to be determined properly. The non-dimensional hydrodynamic entry length of the pipe for turbulent flow is approximately calculated as [71];

$$\frac{L_{e,turbulent}}{D} = 4.4Re^{\frac{1}{6}} \quad (3.1)$$

Minimum Reynolds number of the experimental study is  $3.2 \times 10^3$  and the maximum is  $8.6 \times 10^4$ . Minimum pipe diameter of the experimental study is 40 mm and the maximum is 90 mm. The maximum turbulent entrance length in this case will be for the situation where the Reynolds number is  $8.6 \times 10^4$  and pipe diameter is 90 mm.

$$L_{e,turbulent} \cong 4.5 \text{ m} \quad (3.2)$$

In this study, in order to stay in the region where the flow is fully developed, measuring locations of two pressure transducers are placed at 6–6.5 m and 7.9–8.4 m from the entrance, respectively. These lengths are more than the required ones.



**Figure 3.2** Izmir Katip Celebi University Civil Engineering (IKCU-CE) Flow Loop and galvanized pipes with different diameters (a. 40 mm, b. 50 mm, c. 80 mm, d. 90 mm)

Fluids of the experimental study are stored in the storage tank and there is a mixer mounted on top of the tank to provide temperature at every location of fluid uniformly. The motor of the mixer is shown in the red circle in Figure 3.3 and the mixing attachments are shown in Figure 3.4, respectively.



**Figure 3.3** Storage tank and mixer

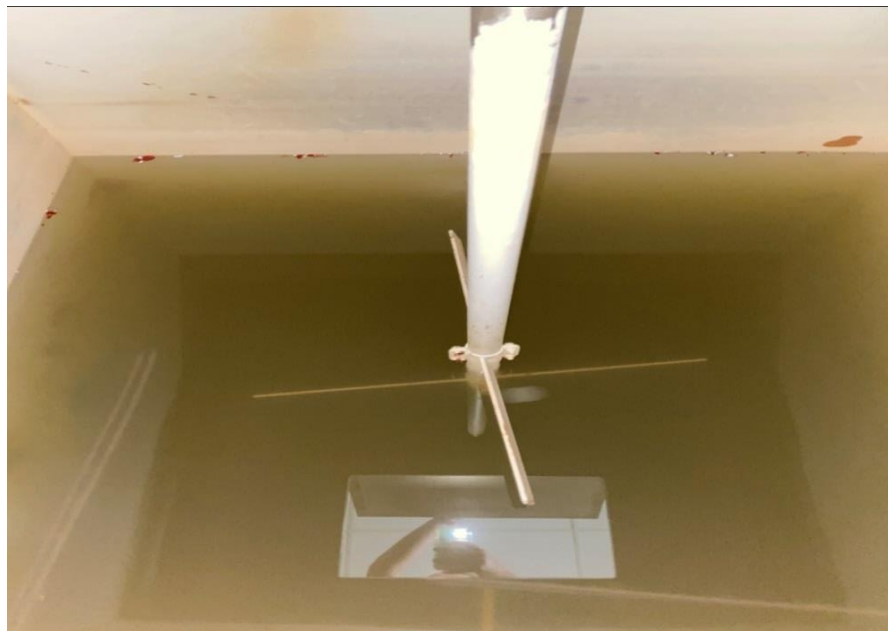


**Figure 3.4** Mixing attachments of the mixer

Experimental study consists of temperature variations. Therefore, a control panel is used to set different temperatures of the fluid as shown in Figure 3.5. Temperature variations are provided by heating resistors and one of the heating resistors is shown in Figure 3.6.



**Figure 3.5** Temperature control panel



**Figure 3.6** Heating resistor

A centrifugal pump is placed between the inlet pipe and the storage tank. To achieve different flow rates, a valve is mounted on the beginning of the inlet pipe and used to set the rate of flow that comes from the tank into the system. The centrifugal pump is presented in Figure 3.7.





**Figure 3.7** Centrifugal pump

The electromagnetic flowmeter is located on the inlet pipe to see the flowrate that goes through the flow loop. The electromagnetic flowmeter is shown in Figure 3.8.



**Figure 3.8** Electromagnetic flowmeter

Pressure transducers are used to measure pressure losses. They are placed at the fully developed section of the flow loop. The pressure transducers are shown in Figure 3.9.



**Figure 3.9** Pressure transmitters

A data acquisition device that collects real-time measured data from the flowmeter and the pressure transducers is connected to the computer. According to the collected data, necessary readings and calculations are performed. The data acquisition device is presented in Figure 3.10.



**Figure 3.10** Data acquisition device

In order to obtain pressure values from pressure transducers, they are switched on by using a power supply. The power supply is shown in Figure 3.11, and real-time data readings on the computer are presented in Figure 3.12.



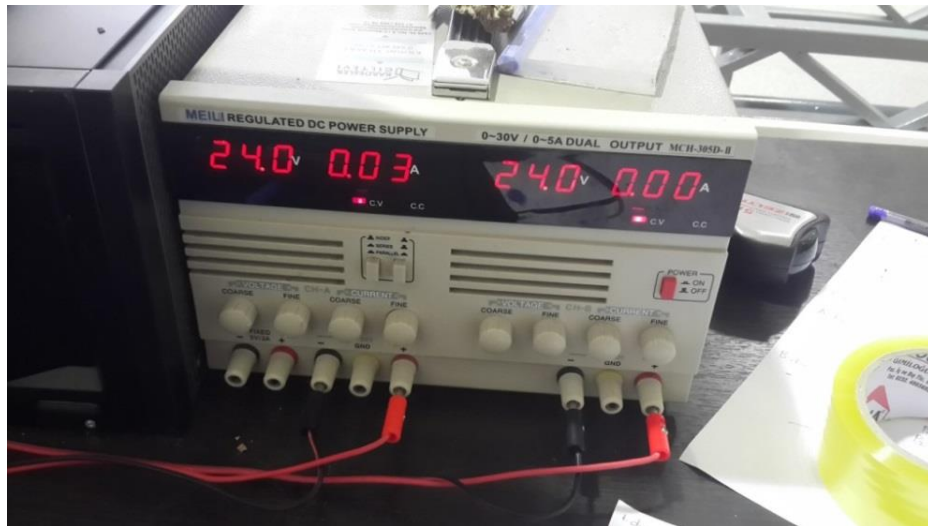


**Figure 3.11** Power supply

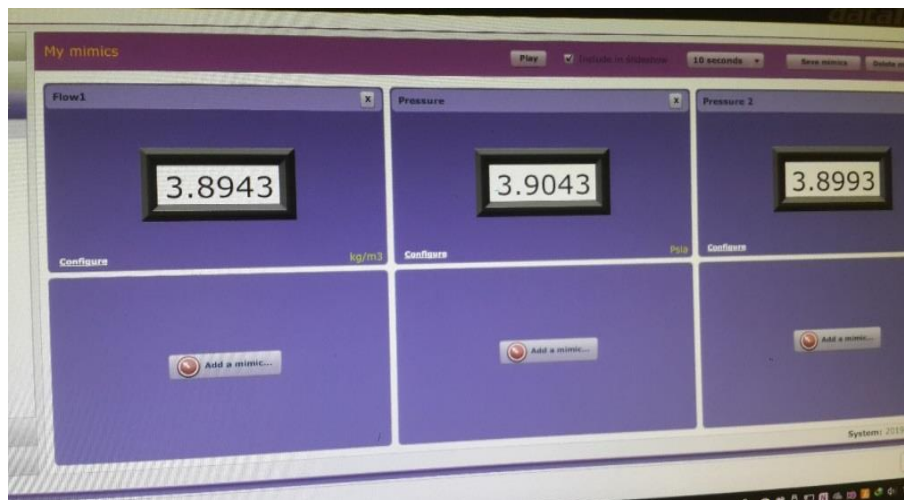


**Figure 3.12** Real-time data readings

### **3.2 Experiment Procedures**

The experimental procedure can be divided into two categories. The first one is for the water, and the second one is for the polymeric solutions to investigate both Newtonian and non-Newtonian fluid flows experimentally.

All experimental procedure, both for Newtonian and non-Newtonian fluid flows, starts with assembling the test section of the flow loop. After that initial tests are conducted by using water to check the accuracy of measurements obtained from the pressure transducers.

Water flow experiments starts by filling the storage tank with pure water at room temperature. The temperature of the water inside the tank is always checked by the temperature control panel or the fluid is heated if it is necessary for the experiments. The heating resistors inside the tank increase the temperature of the fluid and also maintain them. The mixer which is mounted on top of the tank provides homogenous temperature distribution.

As the electricity is given to the system by the power supply, initial electrical current values of the electromagnetic flowmeter and pressure transducers are double-checked to see if the electrical current gives accurate numbers on the computer. Then, experimental work continues by changing the flow rates to desired values using the control valve.

Stabilization of the fluid flow against fluctuations has great importance for the sake of accurate calculations. Therefore, data collection from the electromagnetic flowmeter and pressure transducers for each flowrate have 10 minutes time intervals.

Non-Newtonian fluid flow experiments have the same routine except for the preparation of the fluid in the beginning. The non-Newtonian polymers are added into the water at room temperature very slowly using sieves to prevent any aggregation. Then the mixture is heated if the experiments are going to be performed in different temperatures. The mixer which is used to provide homogenous temperature distribution also helps to overcome the aggregation.

## **4.MATHEMATICAL MODEL TO PREDICT PRESSURE LOSS OF TURBULENT NEWTONIAN FLUID FLOW IN ROUGH PIPES CONSIDERING FLUID TEMPERATURE EFFECTS**

In order to accurately predict the pressure loss of a turbulent Newtonian fluid flow in the rough pipe under temperature effects, a mathematical model is proposed. To obtain a solution for the turbulent transport term in governing equations, the mixing length model is used. After applying the mixing length model, an explicit solution of the governing equation is obtained by using the finite difference method. Estimations of pressure losses from the proposed model are compared to experimental pressure loss values. The accuracy of the proposed model is analyzed. Model development and comparison processes are presented in this chapter.

### **4.1 Explicit Solution of the Governing Equation**

#### **4.1.1 Finite difference method**

The finite difference method to achieve an explicit solution is applied to the governing equation presented in Eq. 2.23. The finite difference scheme is shown in Figure 4.1

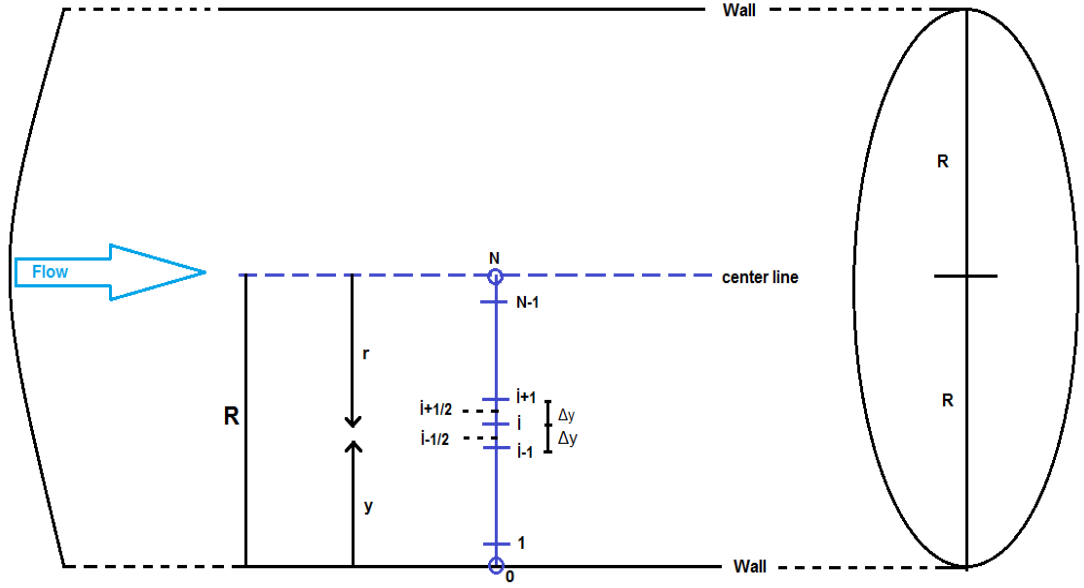


**Figure 4.1** Finite difference scheme of the experimentally investigated pipe flow

The application of the finite difference method is shown below.

$$\frac{c_p}{\rho} r_i = \frac{(rT)_{i+\frac{1}{2}} - (rT)_{i-\frac{1}{2}}}{\Delta y} \quad (4.1)$$

$$\frac{c_p}{\rho} r_i \Delta y = r_{i+\frac{1}{2}} v_{e_{i+\frac{1}{2}}} \frac{u_{i+1} - u_i}{\Delta y} - r_{i-\frac{1}{2}} v_{e_{i-\frac{1}{2}}} \frac{u_i - u_{i-1}}{\Delta y} \quad (4.2)$$

$$A_i = \frac{r_{i+\frac{1}{2}} v_{e_{i+\frac{1}{2}}}}{\Delta y} \quad (4.3)$$

$$C_i = \frac{r_{i-\frac{1}{2}} v_{e_{i-\frac{1}{2}}}}{\Delta y} \quad (4.4)$$

$$A_i + C_i = B_i \quad (4.5)$$

$$-A_i u_{i+1} + B_i u_i - C_i u_{i-1} = -\frac{c_p}{\rho} r_i \Delta y \quad (4.6)$$

$$-\frac{c_p}{\rho} r_i \Delta y = D_i \quad (4.7)$$

$$-A_i u_{i+1} + B_i u_i - C_i u_{i-1} = D_i \quad (4.8)$$

If the RANS equation (Eq. 2.18) is recalled, it is seen that the effective kinematic viscosity has to be determined in order to achieve the mean velocity of the flow. Therefore, the determination of effective kinematic viscosity ( $\nu_e$ ) with finite difference method is

$$\nu + \nu_t = \nu_e \quad (4.9)$$

$$\nu_{ti} = \frac{\nu_{ti} + l_m^2 \frac{u_{i+1} - u_i}{\Delta y} |_{new}}{2} \quad (4.10)$$

As the effective kinematic viscosity is determined, solution vectors for boundary conditions are achieved by applying the Thomas algorithm. Thomas algorithm is used to solve tridiagonal systems of equations by adopting the Gauss elimination method.

After applying the Thomas algorithm, the following expression for the velocity at a node is obtained.

$$u_N = \frac{F_{N-1} + \Delta y B_{CN}}{1 - E_{N-1}} \quad (4.11)$$

where  $u_N$  is the velocity at Nth node,  $\Delta y$  is the distance between nodes, BCN is the boundary condition at Nth node, E and F represent the algorithm parameters at different boundary conditions.

## 4.2 Flow Chart of the Computer Program

In order to predict frictional pressure loss in a rough pipe under temperature effects, a computer code is written for the developed mathematical model by using the Matlab program.

The developed code allows the user to set the accuracy for calculations by changing the number of nodes and tolerance limits for the error between experimental and model velocities.

The developed Matlab code is quite user-friendly since it directly requires the main parameters of the pipe flow.

Input parameters of the Matlab code are as follows;

- Pipe radius,
- Dynamic viscosity and density of the water (either from a table or by using correlations),

Dynamic viscosity correlation for water according to its temperature is given by (T is in Kelvin)

$$\mu(T) = 2.414 \times 10^{-5} x 10^{\frac{247.8}{T-140}} \quad (4.12)$$

Density correlation for water according to its temperature is given by Kell [72] (T is in Celcius)

$$\rho(T) = \frac{a_0 + a_1 T + a_2 T^2 + a_3 T^3 + a_4 T^4 + a_5 T^5}{1 + b T} \quad (4.13)$$

$$a_1 = 17.801161 \times 10^{-3} \quad (4.14)$$

$$a_2 = -7.942501 \times 10^{-6} \quad (4.15)$$

$$a_3 = -52.56328 \times 10^{-9} \quad (4.16)$$

$$a_4 = 137.6891 \times 10^{-12} \quad (4.17)$$

$$a_5 = -364.4647 \times 10^{-15} \quad (4.18)$$

$$b = 17.735441 \times 10^{-3} \quad (4.19)$$

- Roughness height,
- Number of nodes,
- Number of iterations,
- Error tolerance,
- Pressure difference

And the program gives the mean flow velocity as the output.

The flow chart of this computer program is presented in Figure 4.2.

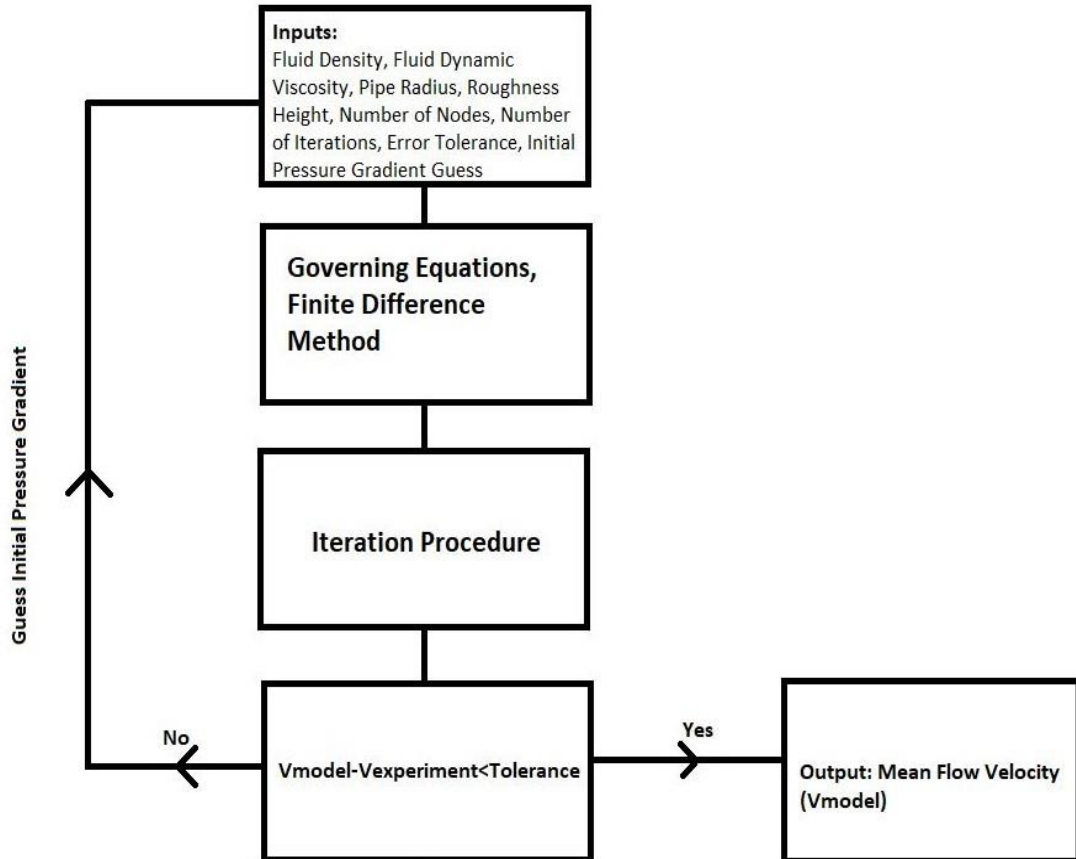


**Figure 4.2** Flow chart of the computer program

## **5.RESULTS AND DISCUSSION**

In this chapter, pipe roughness determination for the galvanized pipes, and friction factor correlations for Newtonian and non-Newtonian fluid flows in rough pipes with fluid temperature effects are presented. Moreover, the efficiency of the developed mathematical model to predict frictional pressure losses of Newtonian fluid flows in rough pipes considering the fluid temperature effects is presented. Detailed comparisons with the presented experimental study and literature are performed in order to validate the accuracy of proposed friction factor correlations and developed mathematical model.

### **5.1 Determination of Pipe Roughness Values for Galvanized Pipes**

Galvanized pipes with four different diameters of 40, 50, 80, and 90 mm are used during the experiments of this study. Experimental and Colebrook [18] friction factors are compared to obtain roughness values of the galvanized pipes. Comparisons are shown in Figures 5.1 – 5.4, and real roughnesses for each pipe are presented in Table 5.1.



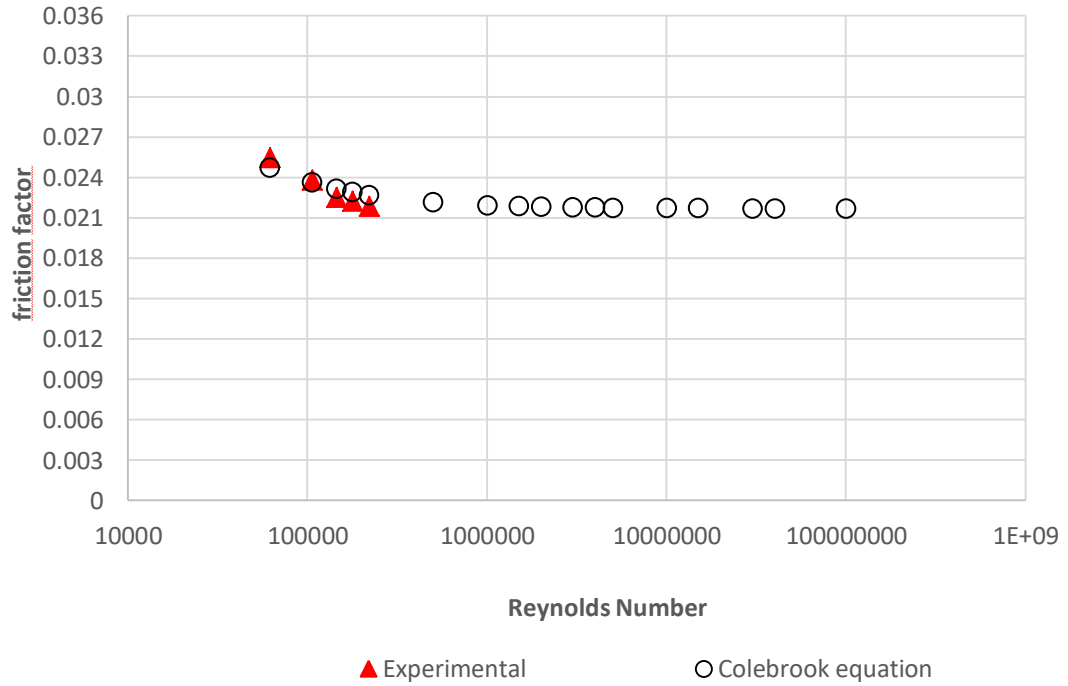


**Figure 5.1** Experimental and Colebrook friction factor comparisons for 40 mm pipe diameter and room temperature

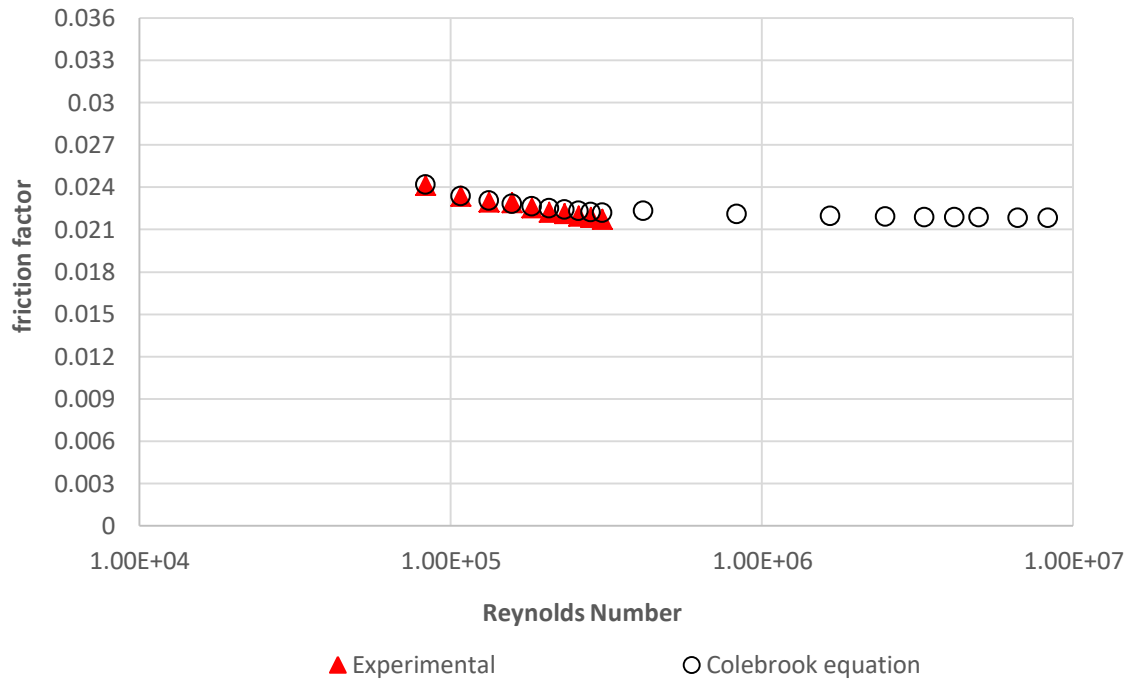


**Figure 5.2** Experimental and Colebrook friction factor comparisons for 50 mm pipe diameter and room temperature

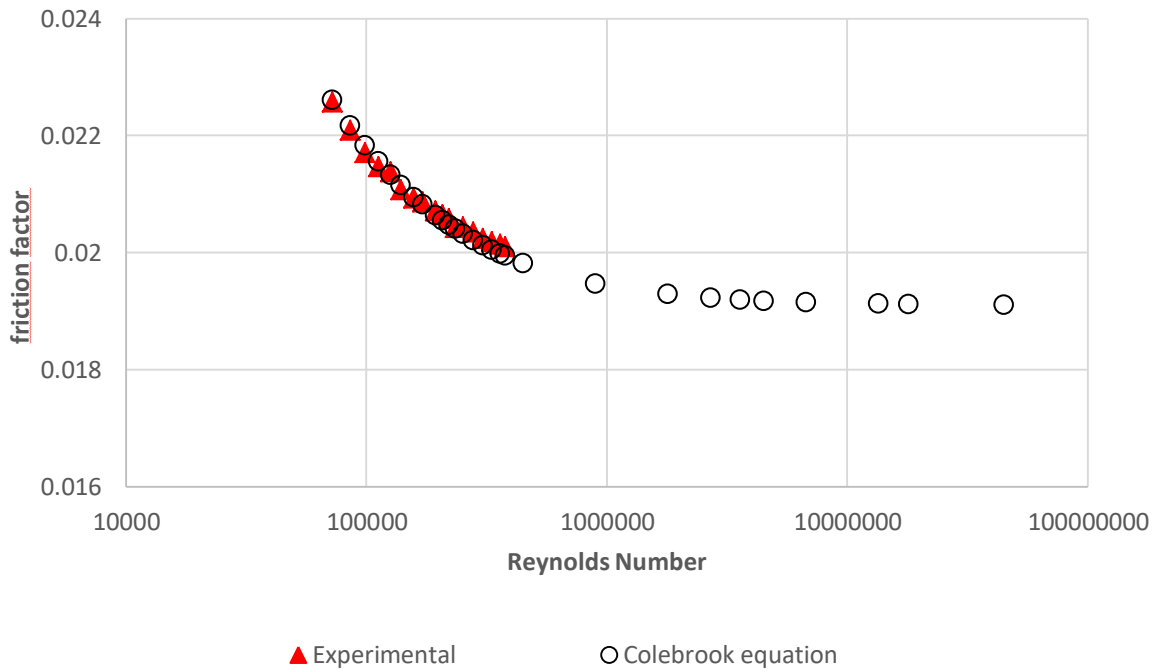


**Figure 5.3** Experimental and Colebrook friction factor comparisons for 80 mm pipe diameter and room temperature

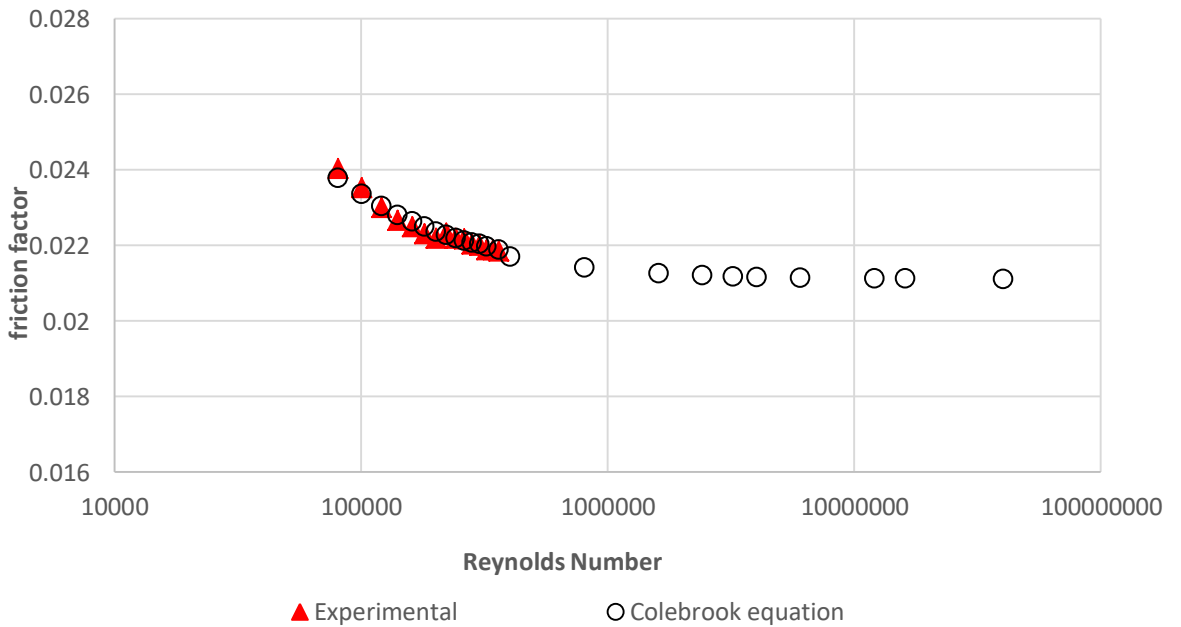


**Figure 5.4** Experimental and Colebrook friction factor comparisons for 90 mm pipe diameter and room temperature

It is seen from the plotted figures that for all pipe diameters experimentally obtained points and Colebrook equation points appear to agree in general.

**Table 5.1** Proposed pipe roughness values for galvanized pipes (Sorgun and Muftuoglu [73])

<b>Pipe Roughness</b>	<b>40 mm</b>	<b>50 mm</b>	<b>80 mm</b>	<b>90 mm</b>
Commercial Value (mm)	0.15	0.15	0.15	0.15
Proposed Value (mm)	0.052	0.06	0.07	0.12

Table 5.1 shows that while the roughnesses of pipes are stated as constant for all pipe diameters commercially, actually they vary significantly with pipe diameters. The predicted pumping requirements which are based on the frictional pressure losses can be affected from this variation.

## **5.2 A New Friction Factor Formula for Water Flow through Rough Pipes with Fluid Temperature Effects**

Variables that affect the friction factor are investigated by performing dimensional analysis. The effective major variables of friction factor are presented as;

$$f = func(V, \rho, \mu, D, \varepsilon, C_p, k) \quad (5.1)$$

where  $V$  is the fluid velocity ( $L/T$ ),  $\rho$  is the fluid density ( $M / L^3$ ),  $\mu$  is the dynamic viscosity ( $M / LT$ ),  $D$  is the pipe diameter ( $L$ ),  $\varepsilon$  is the pipe roughness ( $L$ ),  $c_p$  is the specific heat ( $L^2/(T^2 \Theta)$ ),  $k$  is the thermal conductivity ( $ML/(T^3 \Theta)$ ),  $\Theta$  is the fluid temperature.

Another dimension in addition to Mass, Length, and Time is introduced to represent the Temperature.

In the dimensional analysis, since the Temperature is introduced as a new dimension, four variables, which are velocity, viscosity, diameter, and thermal conductivity, are selected as repeating variables. The following dimensionless groups are obtained as the Buckingham- $\pi$  theorem is applied for dimensional analysis. For this reason the following three dimensionless groups are presented as:

$$\pi_1 = \frac{\rho V D}{\mu} \quad (5.2)$$

$$\pi_2 = \frac{\varepsilon}{D} \quad (5.3)$$

$$\pi_3 = \frac{c_p \mu}{k} \quad (5.4)$$

Pipe roughness values are determined by performing the experimental study as stated above. Then, based on the experimental data, a friction factor correlation in terms of dimensionless groups which consist of Reynolds Number, relative roughness, and Prandtl Number is proposed based on the experimental data. The proposed equation is presented as;

$$f = \left( \frac{\pi_1}{1000} \right)^{-1.218} + 7.384\pi_2 + 0.00185\pi_3 \quad (5.5)$$

where  $\pi_1$  is the Reynolds Number (Re) ,  $\pi_2$  is the relative roughness and  $\pi_3$  is the Prandtl Number (Pr).

The proposed equation is valid for the range of Reynolds number as  $Re > 5 \times 10^4$  and for the range of temperature as  $25^\circ \text{C} \leq \text{Temperature} \leq 60^\circ \text{C}$ .

Using the proposed friction factor correlation, the frictional pressure can be obtained from the equation which is presented below.

$$\frac{\Delta P}{\Delta L} = \frac{f \rho V^2}{2D} \quad (5.6)$$

Comparisons of all experimental and calculated friction factors are represented in Figure 5.5. In Figure 5.5, the solid line shows the perfect match and the dashed lines represent the difference in the range of  $\pm 20\%$ . A good agreement between experimental and calculated friction factors for most of the cases are seen in Figure 5.5.

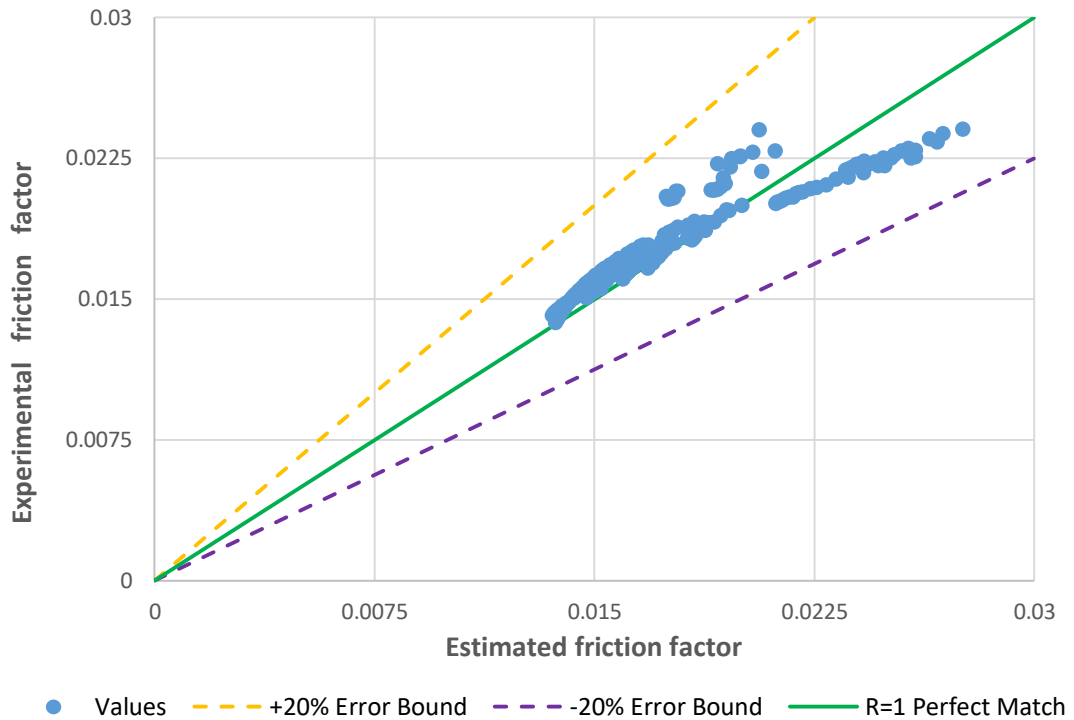


**Figure 5.5** Experimental and calculated friction factor comparisons using Eq. 5.5

Different error metrics to evaluate the performance of the proposed friction factor equation are shown in Table 5.2.

In this table, RMSE expresses the Root Mean Square Error, AAE expresses the Average Absolute Error and AAPE expresses the Average Absolute Percentage Error. The proposed equation is developed with 95% level of confidence and 0.86  $R^2$  value.

**Table 5.2** Performance of the developed friction factor equation in terms of error metrics

$R^2$	RMSE	AAE	AAPE (%)
0.87	0.011	0.0007	3.94

The proposed equation is the first equation in the literature that includes temperature effects and roughness for the pressure difference determination of fully turbulent flow of Newtonian fluids considering the fluid temperature effects. The proposed equation is compared with explicit equations available in the literature for both smooth and rough pipes. For smooth pipes, the proposed equation is compared with explicit equations of Blasius [5] and Taler [10]. Figure 5.6 shows the reasonable accuracy which is obtained between the explicit formulas of proposed equation, Blasius [5] and Taler [10].

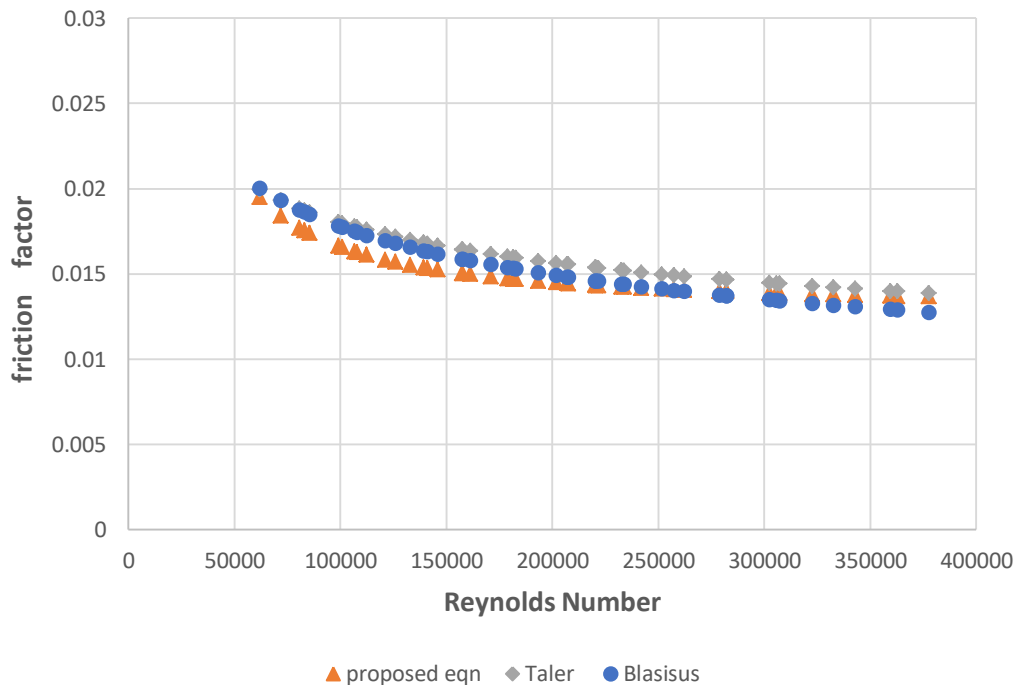


**Figure 5.6** Proposed friction factor comparisons with Blasius [5] and Taler [10] formulas for smooth pipes

For rough pipe comparisons, the relation between the proposed equation and the Colebrook equation [18] is investigated. In Figure 5.7, plotted points show the comparison between the experimental data, the proposed equation and the Colebrook equation. Satisfactory agreement is obtained for the proposed equation when compared with experimental data, and Colebrook equation. Slightly better performance of Colebrook equation than the proposed equation is realized.

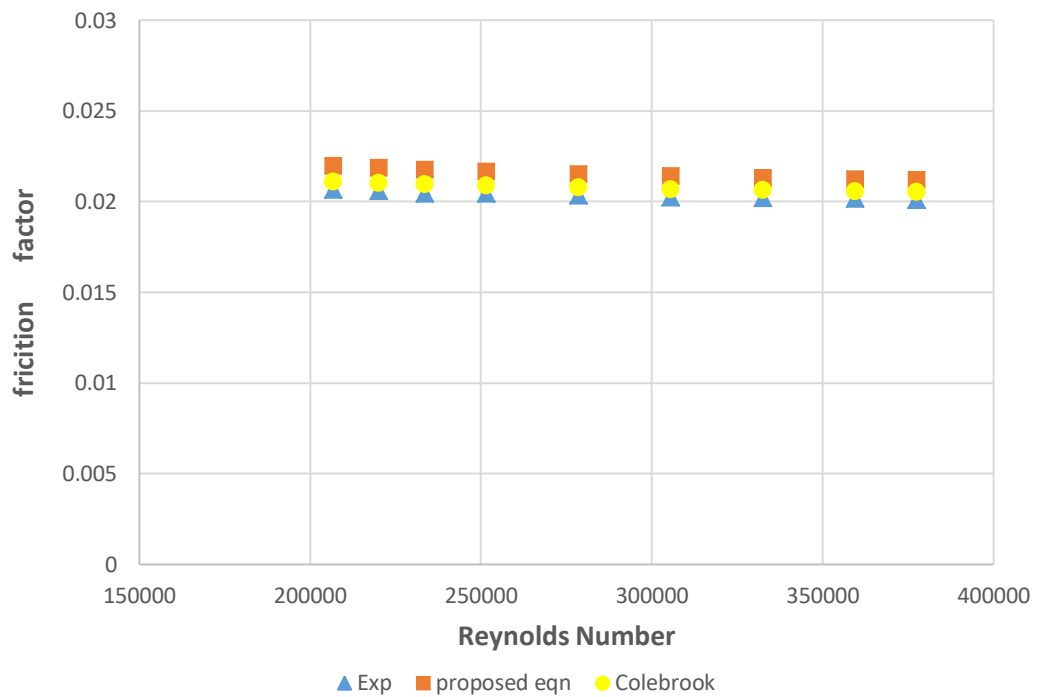


**Figure 5.7** Proposed friction factor comparisons with experimental data and Colebrook [18] formula for rough pipes

Colebrook equation does not take temperature effects into account. Therefore, it is seen from Figure 5.8 where the Colebrook equation overpredicts the friction factor at 40°C fluid temperature. On the other hand, the proposed equation presents better performance which shows its superiority over the Colebrook equation at high fluid temperatures.

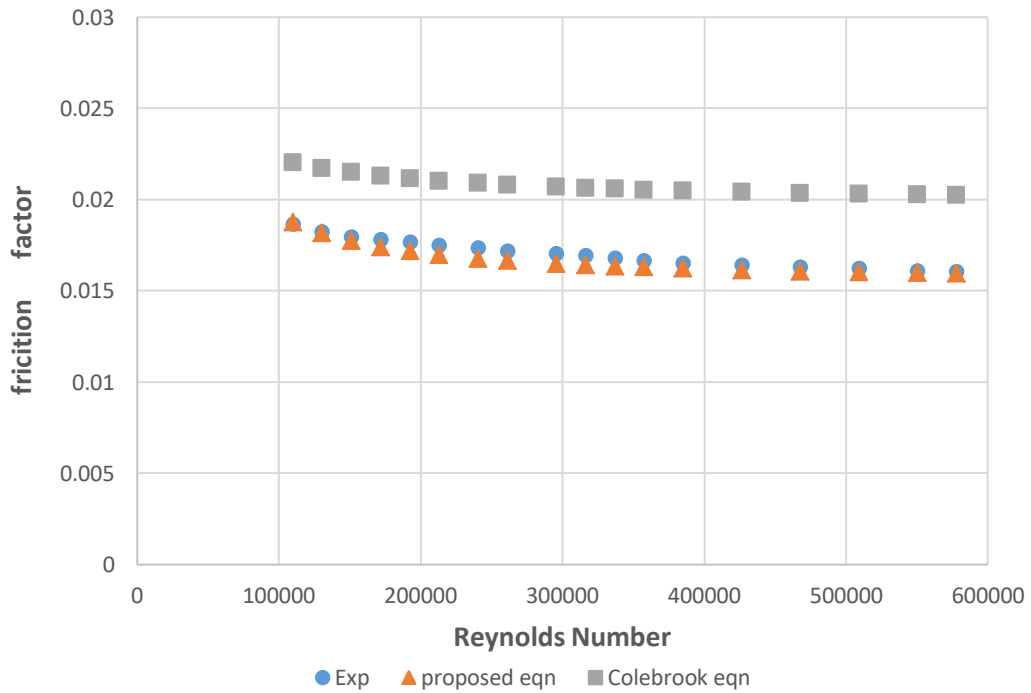


**Figure 5.8** Proposed friction factor comparisons with experimental data at 40°C and Colebrook [18] formula for rough pipes

In Figure 5.9-5.11, dimensionless parameter effects on friction factor in the rough pipe are presented. A similar trend of the Moody Chart can be seen for the Reynolds Number in Figure 5.9 where the inverse ratio between Reynolds Number and friction factor is shown. In Figure 5.10, the relation between relative roughness and friction factor is shown with the direct proportion. Figure 5.11 shows another direct proportion for Prandtl Number and friction factor. As the relation between Prandtl Number and temperature presents an inverse ratio, friction factor decreases while fluid temperature increases.



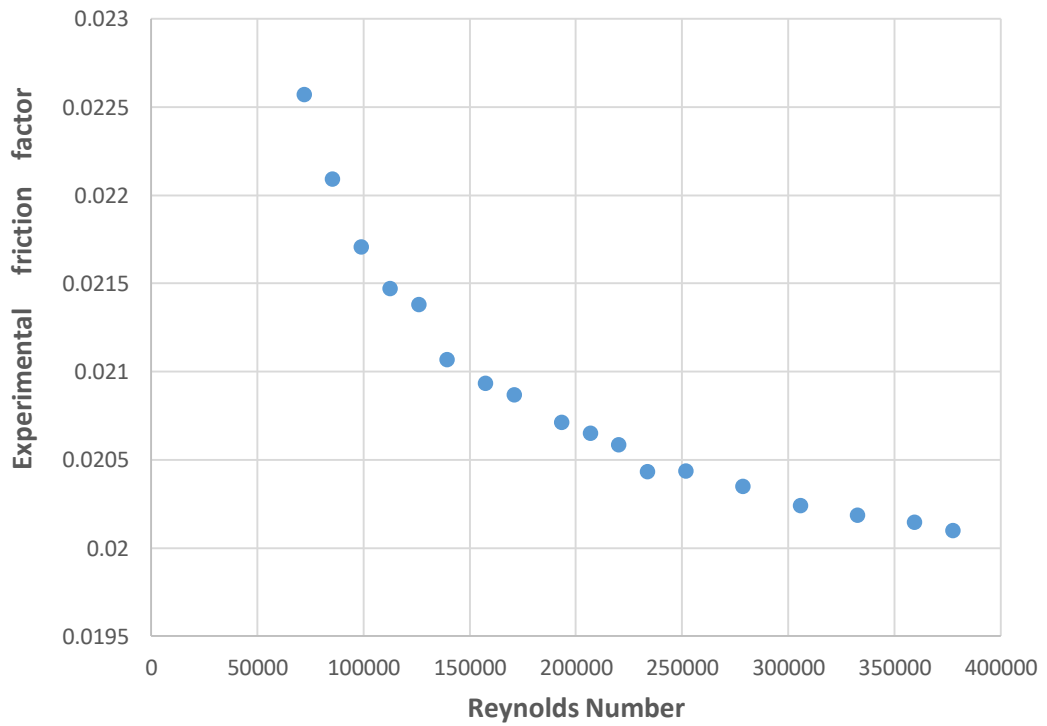


**Figure 5.9** The relation between the friction factor and  $\pi_1$  (Reynolds Number) for 80 mm Pipe diameter and room temperature

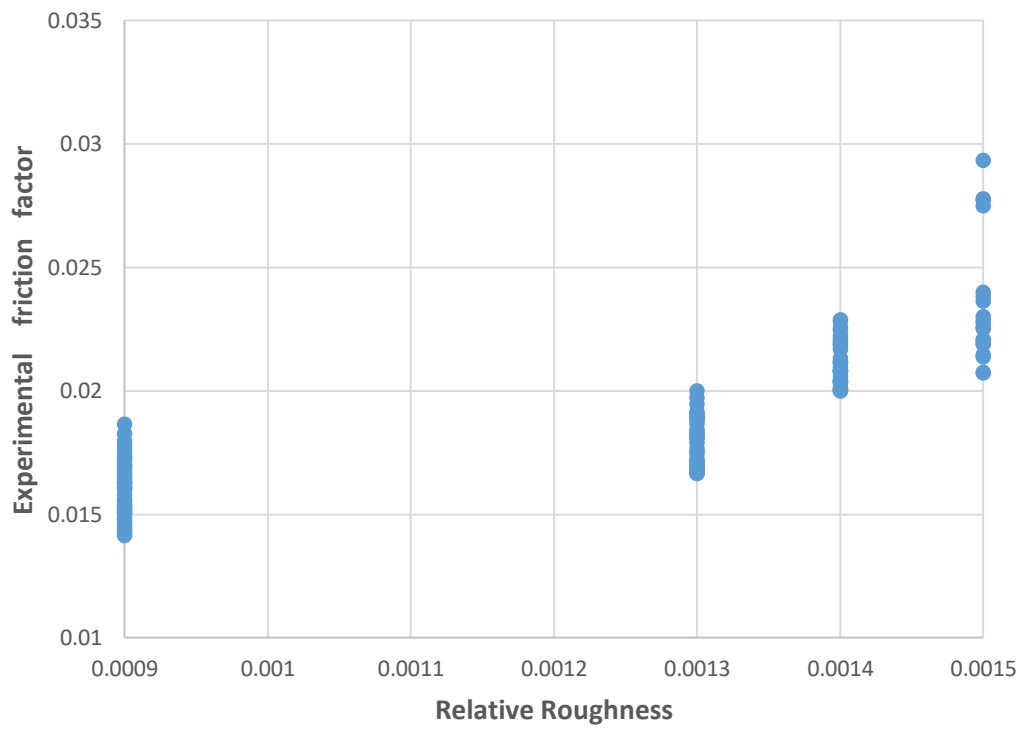


**Figure 5.10** The relation between the friction factor and  $\pi_2$  (Relative Roughness)

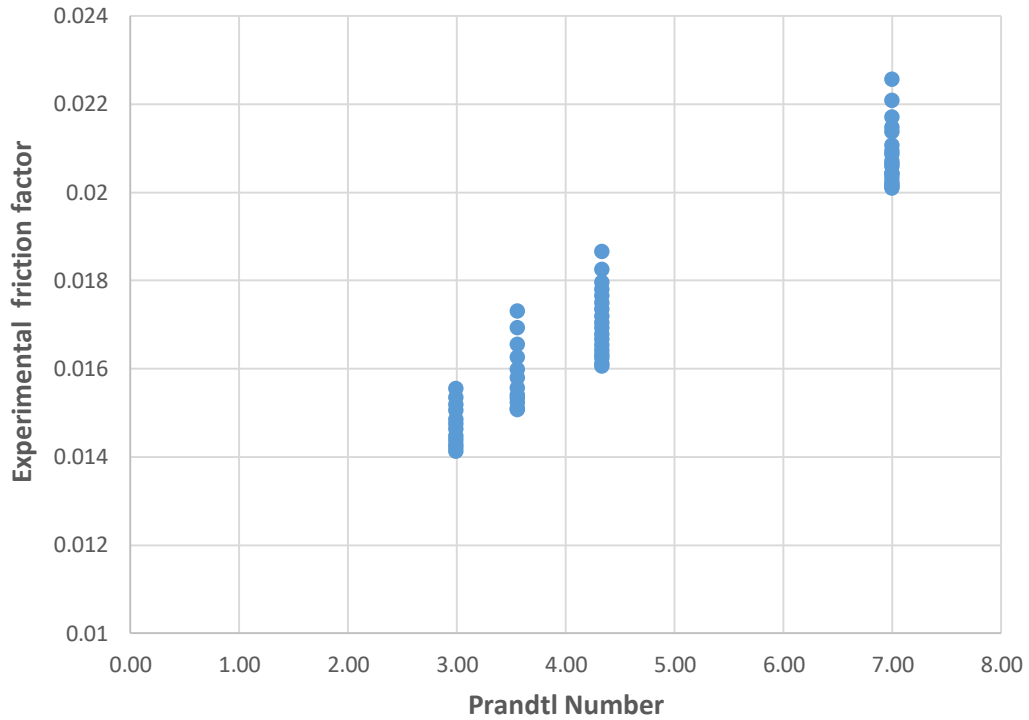


**Figure 5.11** The relation between the friction factor and friction and  $\pi_3$  (Prandtl Number)

In order to evaluate the effectiveness of the developed friction factor equation an F test is performed. A linear regression analysis is conducted using Reynolds Number, Relative Roughness and Prandtl number as predictor variables and friction factor as the response variable. From the F test analysis, the obtained F value is used to determine if the regression model presents statistically significance.

**Table 5.3** F test results

$k'$	$n'$	SSE	SSR	$v'_1$	$v'_2$	$f'$	$f'_{cr}$
3	117	9.39049E-05	0.001203	3	113	482.6216	2.6856

where;

$k'$  is the number of independent variables in model,  $n'$  is the number of total data,  $SSE$  is the sum of squares error,  $SSR$  is the sum of squares due to regression,  $v'_1$  is the numerator degrees of freedom,  $v'_2$  is the denominator degrees of freedom,  $f'$  is the F test value and  $f'_{cr}$  is the critical F test value.

SSE (sum of squares error) is represented with the following equation.

$$SSE = \sum_{i=1}^n (Y_{i,exp} - Y_{i,pre})^2 \quad (5.7)$$

where;

$Y_{i,exp}$  represents experimental data, and  $Y_{i,pre}$  represents predicted data with regression.

SSR (sum of squares due to regression) is represented with the following equation.

$$SSR = \sum_{i=1}^n (Y_{i,pre} - Y_{mean})^2 \quad (5.8)$$

where;

$Y_{i,pre}$  represents predicted data with regression, and  $Y_{mean}$  represents mean experimental data.

$v'_1$ , the numerator degrees of freedom and,  $v'_2$ , the denominator degrees of freedom are calculated as;

$$v'_1 = k' \quad (5.9)$$

$$v'_2 = n' - k' - 1 \quad (5.10)$$

F test value,  $f'$ , is calculated as;

$$f' = \left( \frac{SSR}{v'_1} \right) / \left( \frac{SSE}{v'_2} \right) \quad (5.11)$$

Critical F test value,  $f'_{cr}$ , is obtained from F distribution tables of desired significance level. Numerator and denominator degrees of freedom values are picked from the those tables. In this study, alpha=0.05 significance level is chosen. Critical F test value is obtained according to the table as 2.685.

Since the F test value is bigger than the F critical value, it is concluded that the joint effect of all variables in the developed equation is significant at the level of probability (alpha=0.05).

The proposed equation, Eq. 5.5, can be inserted into Eq. 5.6 to compute frictional pressure losses. In Figures 5.12 and 5.13, for low and high pressure gradient values, comparisons between experimental data and calculated results are presented. These figures show the accuracy of the proposed friction factor equation for predicting frictional pressure losses.

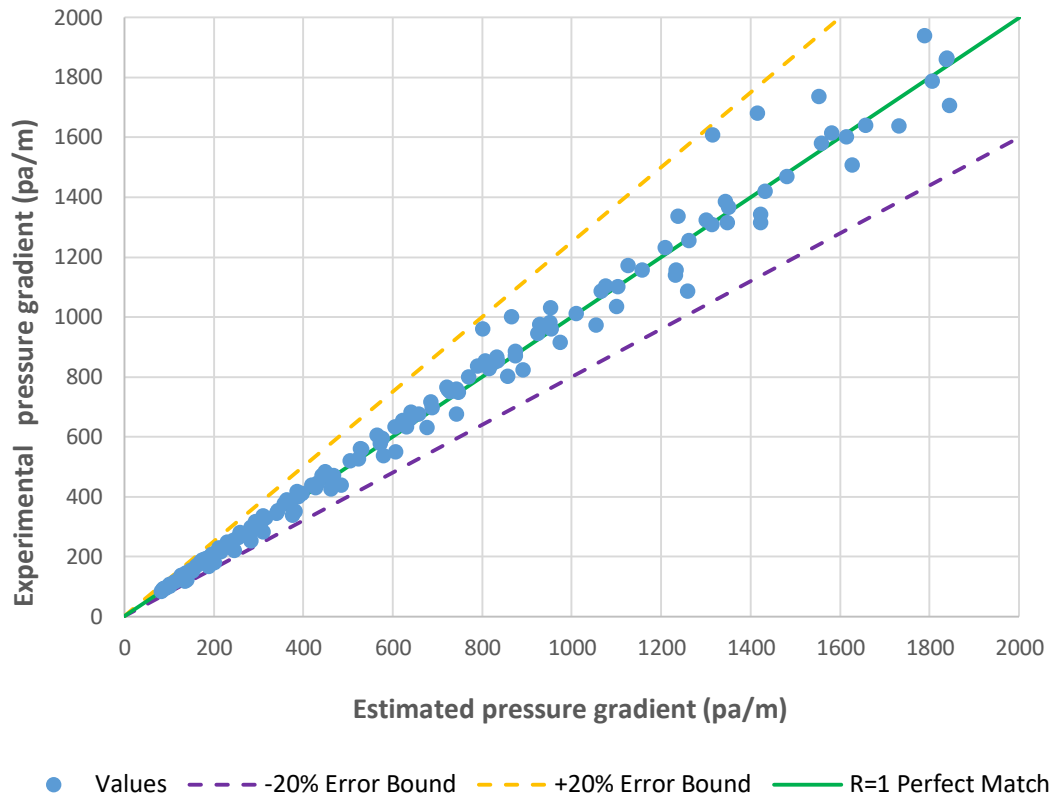


**Figure 5.12** Calculated and experimental data comparisons for low pressure gradient values

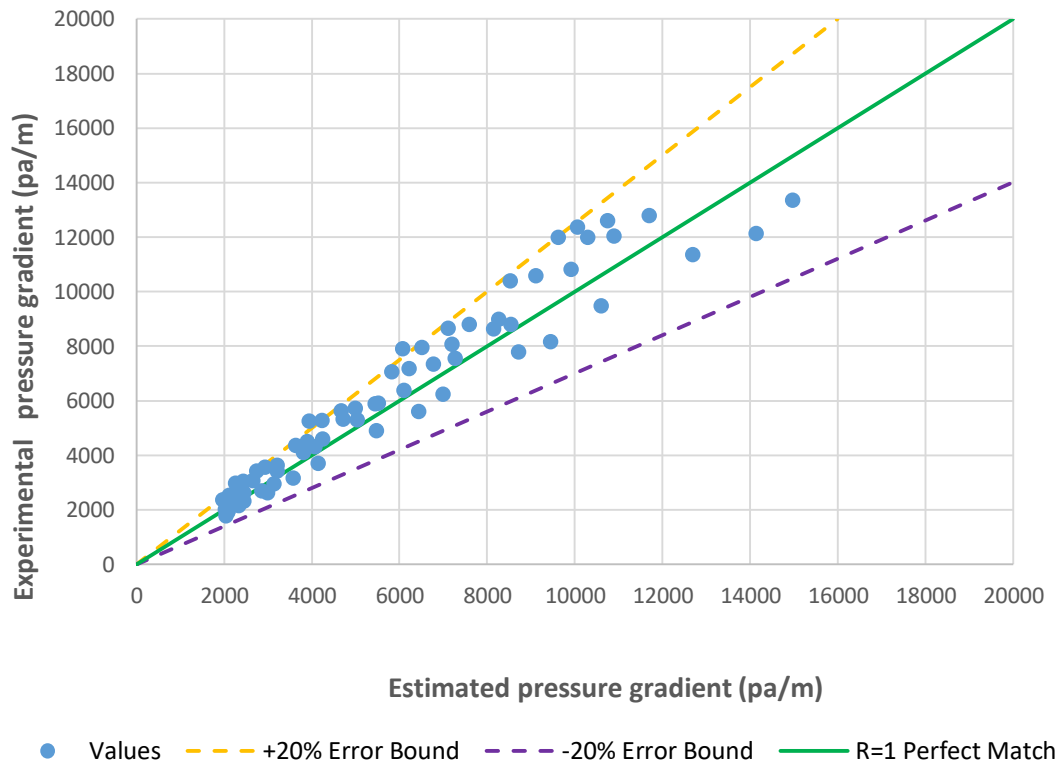


**Figure 5.13** Calculated and experimental data comparisons for high pressure gradient values

### 5.3 A New Friction Factor Formula for non-Newtonian Fluid Flow through Rough Pipes

Rheological models of the non-Newtonian fluids are investigated in order to obtain the best model that represents the polymeric solutions of the experimental study. Detailed comparisons of the Power-Law, Bingham Plastic, and Herschel-Bulkley models are performed for F-2 and F-3 fluids. Results show that the behavior of the polymeric solutions which are used in the experimental study is represented by Herschel-Bulkley model better than other models.

In Figures 5.14-5.16, the shear stress and shear rate relation of F-2 fluid (5.6 kg High Viscous CMC per 1.0 m<sup>3</sup> of water) for Power-Law, Bingham Plastic, and Herschel-Bulkley models are presented, respectively.

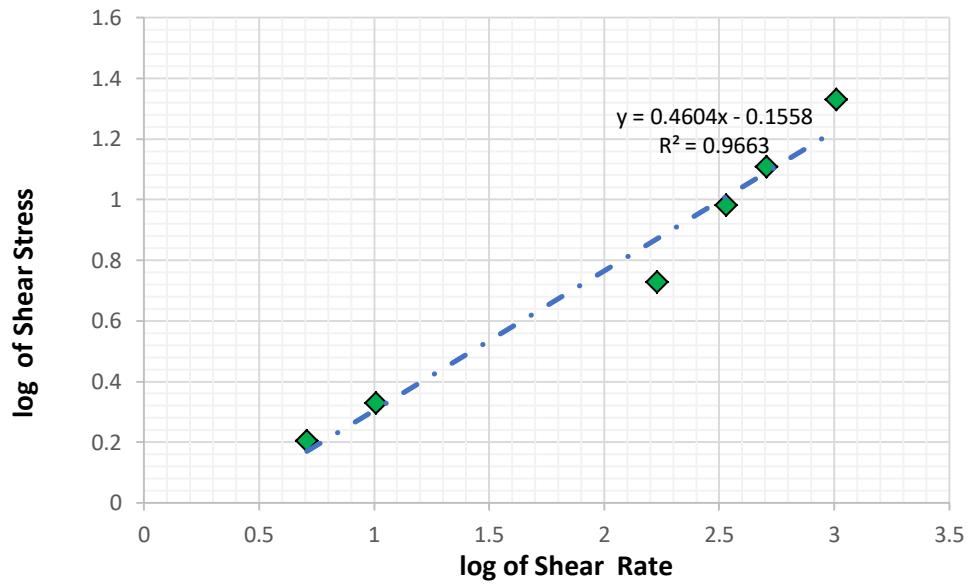


**Figure 5.14** Shear stress and shear rate relation of F-2 fluid for Power-Law model

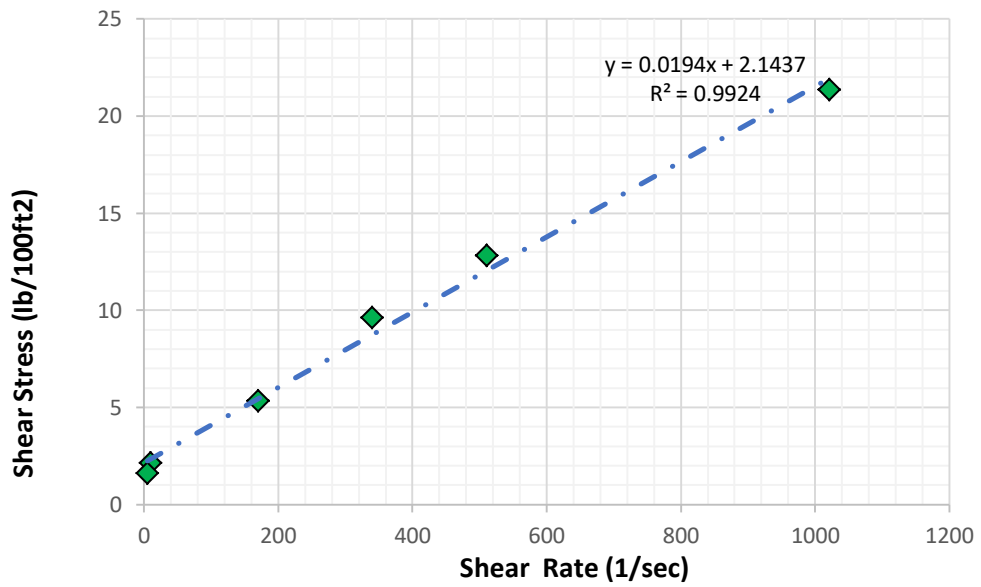


**Figure 5.15** Shear stress and shear rate relation of F-2 fluid for Bingham Plastic model

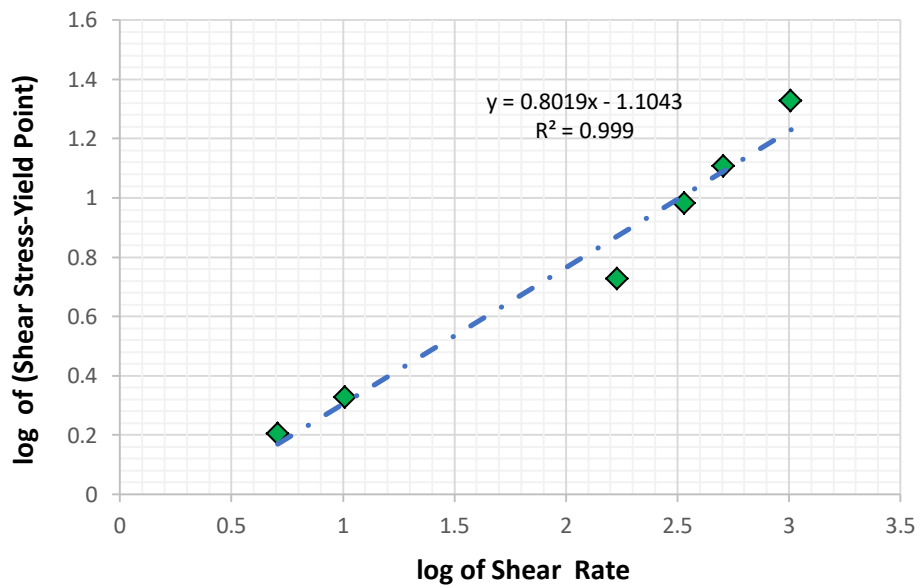


**Figure 5.16** Shear stress and shear rate relation of F-2 fluid for Herschel-Bulkley model

In Figures 5.17-5.19, the shear stress and shear rate relation of F-3 fluid (9.6 kg Low Viscous CMC per 1.0 m<sup>3</sup> of water) for Power-Law, Bingham Plastic, and Herschel-Bulkley models are presented, respectively.

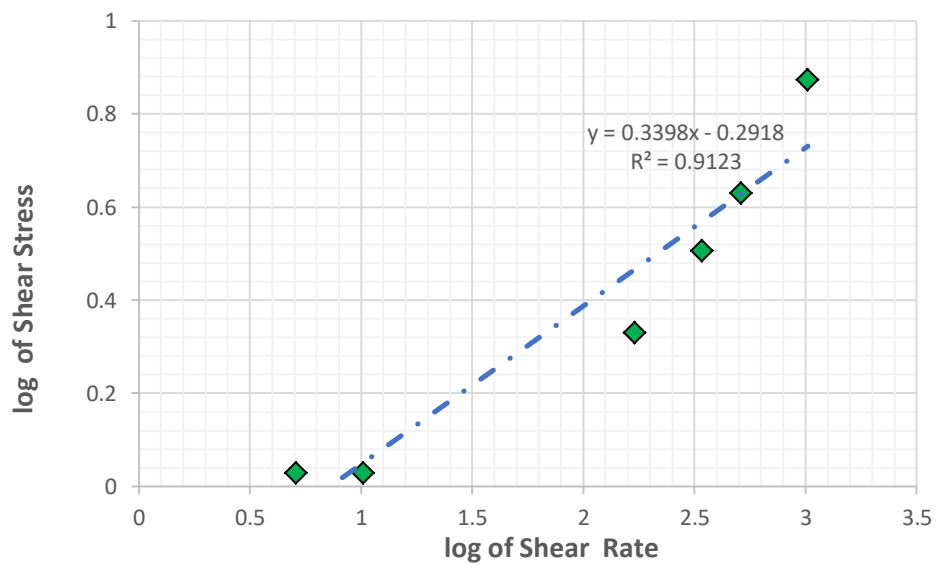


**Figure 5.17** Shear stress and shear rate relation of F-3 fluid for Power-Law model

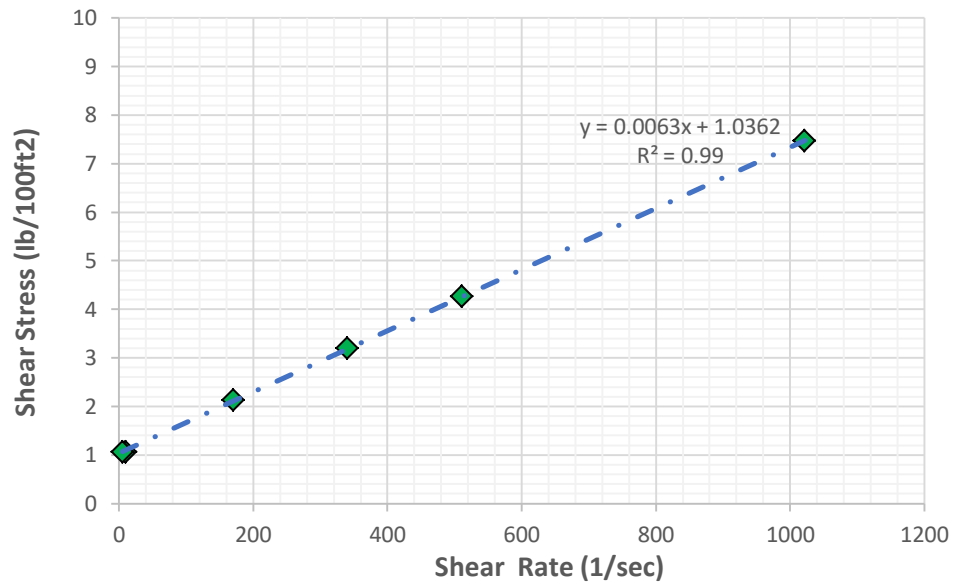


**Figure 5.18** Shear stress and shear rate relation of F-3 fluid for Bingham Plastic model

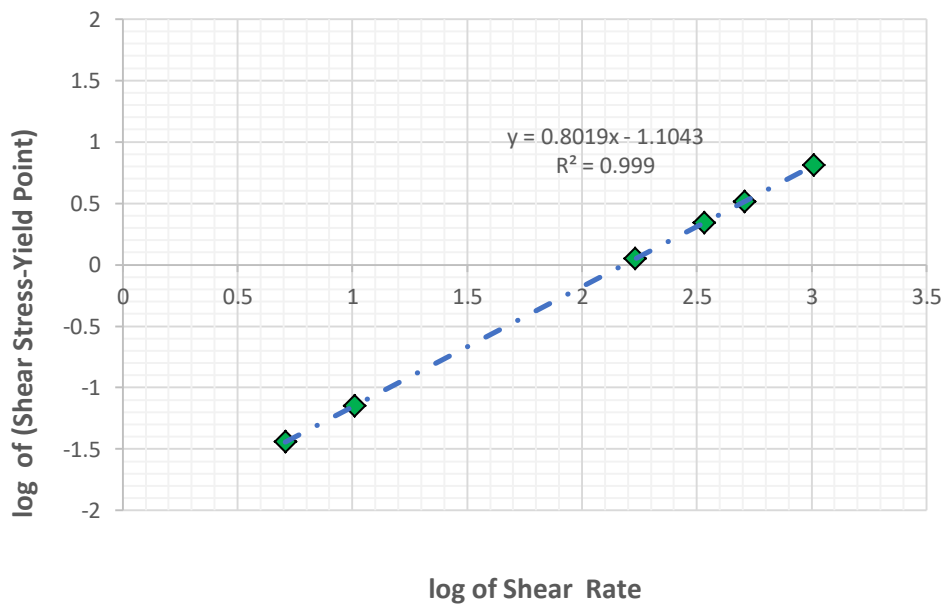


**Figure 5.19** Shear stress and shear rate relation of F-3 fluid for Herschel-Bulkley model

In Table 5.4, comparison of rheological models and the parameters for F-2 (5.6 kg High Viscous CMC polymer per 1.0 m<sup>3</sup> of water) are presented.



**Table 5.4** Comparison of rheological models and the parameters for F-2 fluid

	<b>Power-Law Model</b>	<b>Bingham Plastic Model</b>	<b>Herschel-Bulkley Model</b>
<b>Average Error(%)</b>	13.72	11.61	5.41
<b>R<sup>2</sup></b>	0.9663	0.992	0.999
<b>Plastic Viscosity (cp)</b>		0.02	
<b>Yield Point [lb/100 ft<sup>2</sup>]</b>		2.15	1.46
<b>Flow Behavior Index</b>	0.46		0.85
<b>Consistency Index [lb-s/100 ft<sup>2</sup>]</b>	0.70		0.0574

In Table 5.5, comparison of rheological models and the parameters for F-3 (9.6 kg Low Viscous CMC polymer per 1.0 m<sup>3</sup> of water) are presented.

**Table 5.5** Comparison of rheological models and the parameters for F-3 fluid

	<b>Power-Law Model</b>	<b>Bingham Plastic Model</b>	<b>Herschel-Bulkley Model</b>
<b>Average Error(%)</b>	17.24	0.90	0.74
<b>R<sup>2</sup></b>	0.912	0.999	0.999
<b>Plastic Viscosity (cp)</b>		0.0063	
<b>Yield Point [lb/100 ft<sup>2</sup>]</b>		1.0362	1.018
<b>Flow Behavior Index</b>	0.34		0.9847
<b>Consistency Index [lb-s/100 ft<sup>2</sup>]</b>	0.51		0.007

Therefore, according to the best model that represents the behavior of CMC solutions of the experimental study, the proposed friction factor equation is developed for Herschel-Bulkley fluid as;

$$f_F = \frac{0.06 N^{3.34}}{\left[ \log_{10} \left( \frac{\varepsilon/D}{3.7} + 9.86 (N_{Reg})^{-N} \right) \right]^2} \quad (5.7)$$

Eq. 5.7 can also be used for Power-Law model, if the Generalized Fluid Behavior Index,  $N$ , is changed with the Power-Law model's Fluid Behavior Index,  $n$ .

According to the presented fanning friction factor equation in Eq. 5.7, pressure gradient to determine pressure drop in a pipe can be calculated as;

$$\frac{\Delta p}{L} = \frac{2f_F \rho V^2}{D} \quad (5.8)$$

Experimental data from the Flow Loop is used to evaluate the accuracy of the proposed friction factor correlation. Moreover, the comparisons for the proposed correlation are performed with the correlations from the available literature for Herschel-Bulkley fluids.

Experimental pressure gradient data of the two types of fluids, F-2 and F-3 with yield-pseudoplastic Herschel-Bulkley behavior, which flow through in 50 mm, 80 mm, and 90 mm pipe diameters are tested with the proposed friction factor equation and comparison with Reed and Pilehvari [52] correlation is performed. As a result, a good agreement between experimental data and proposed friction factor correlation is obtained from Figures 5.20-5.25. It is seen from the figures that the proposed correlation shows better performance than Reed and Pilehvari [52] equation in almost all situations.

From Figures 5.26-5.28, it is seen that when the friction factor variation is investigated for F-2 and F-3 fluids, three different roughness height values (0.06 mm, 0.07 mm, and 0.12 mm) and for the large range of generalized Reynolds numbers ( $3.2 \times 10^3 - 8.6 \times 10^4$ ), the success of proposed equation for predicting friction factors can be clearly noticed. For low and high generalized Reynolds number values, Reed and Pilehvari [52] correlation converges with the proposed correlation.

If the predicted friction factor values from the proposed correlation are compared with the measured friction factor values and values obtained from the Reed and Pilehvari [52] correlation for F-2 and F-3 fluids, the gap between the proposed and Reed and Pilehvari correlation becomes more noticeable as the friction factor increases as shown in Figure 5.29.

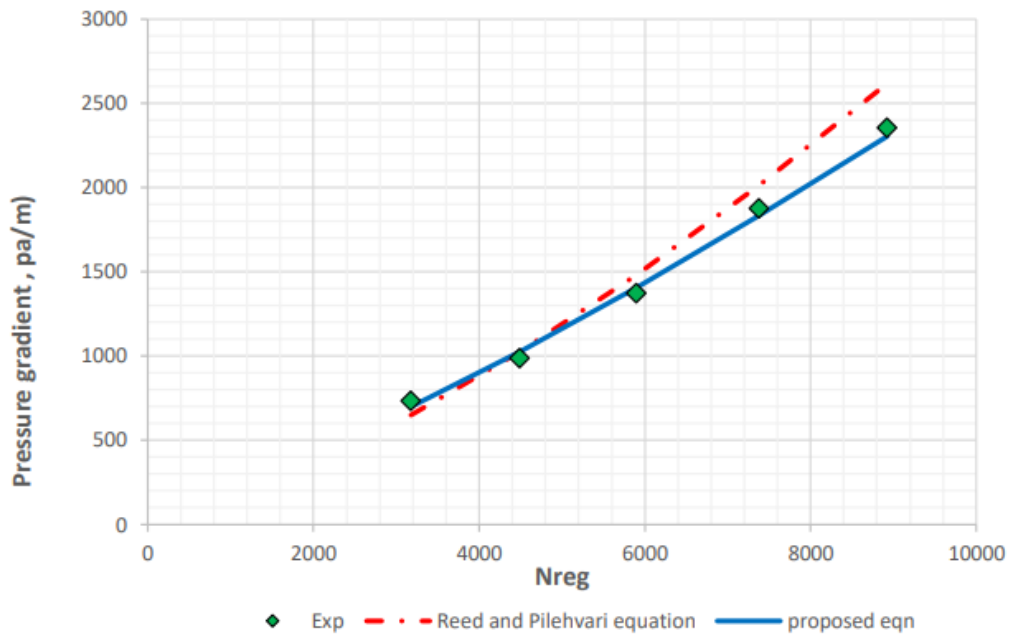


**Figure 5.20** Measured and estimated pressure gradient comparisons for F-2 and 50 mm pipe diameter

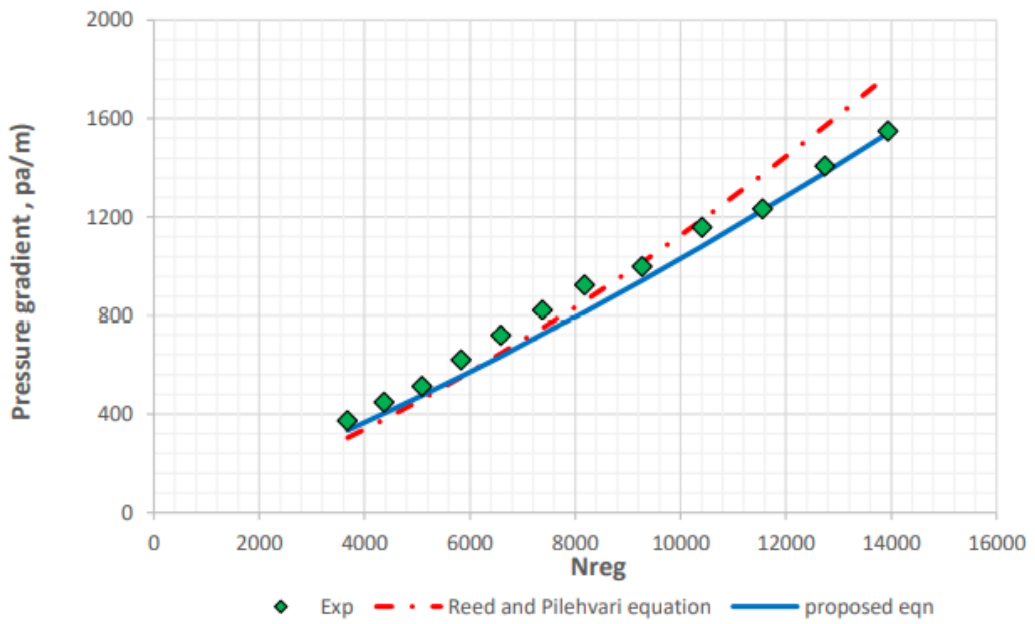


**Figure 5.21** Measured and estimated pressure gradient comparisons for F-2 and 80 mm pipe diameter

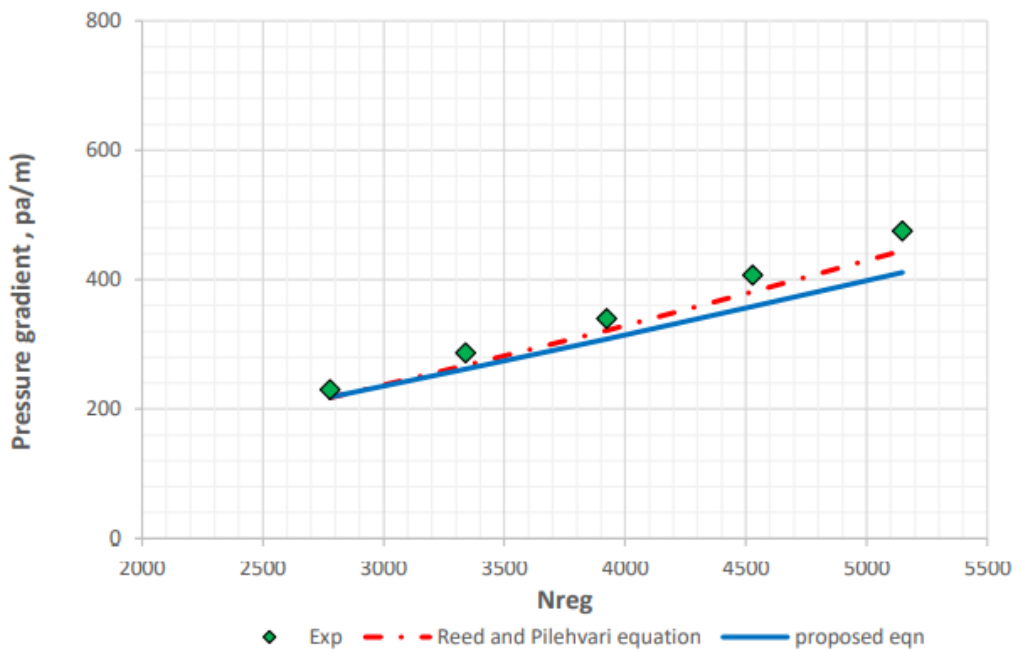


**Figure 5.22** Measured and estimated pressure gradient comparisons for F-2 and 90 mm pipe diameter

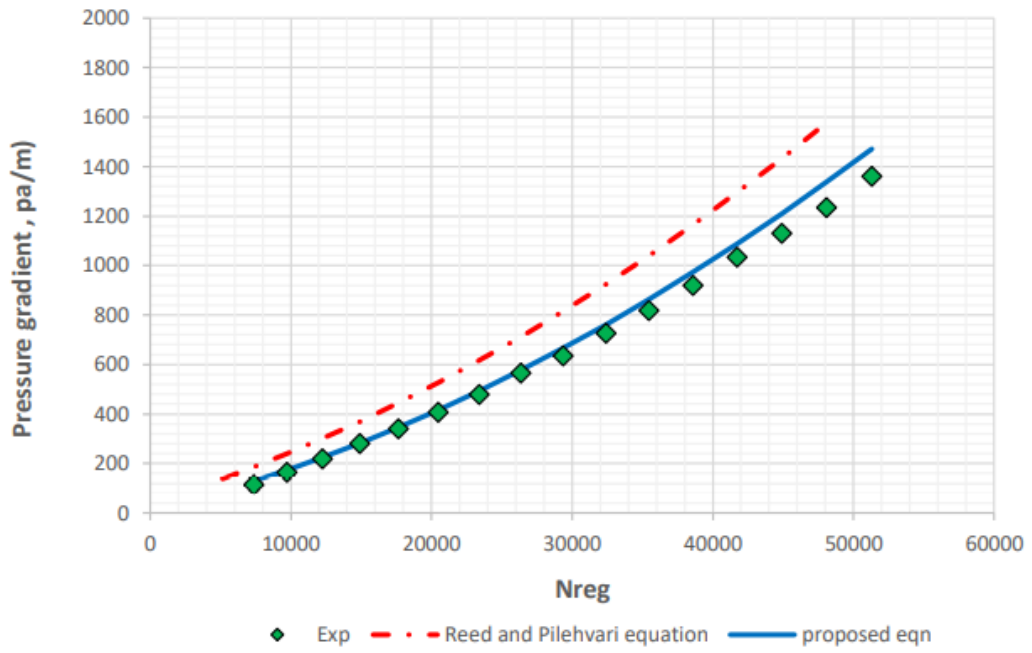


**Figure 5.23** Measured and estimated pressure gradient comparisons for F-3 and 90 mm pipe diameter

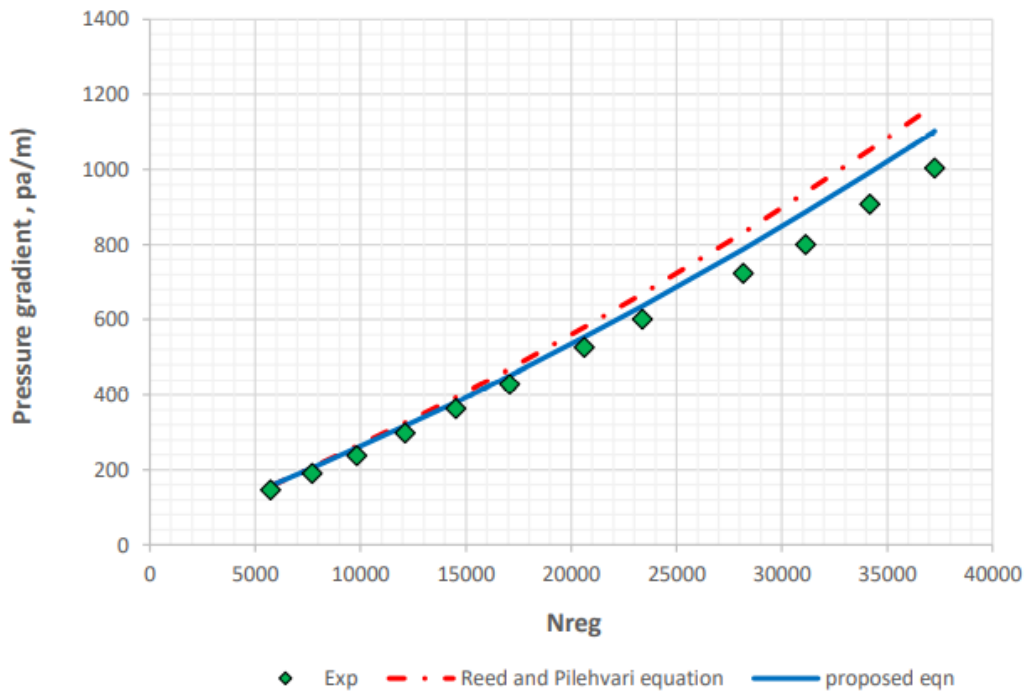


**Figure 5.24** Measured and estimated pressure gradient comparisons for F-3 and 80 mm pipe diameter

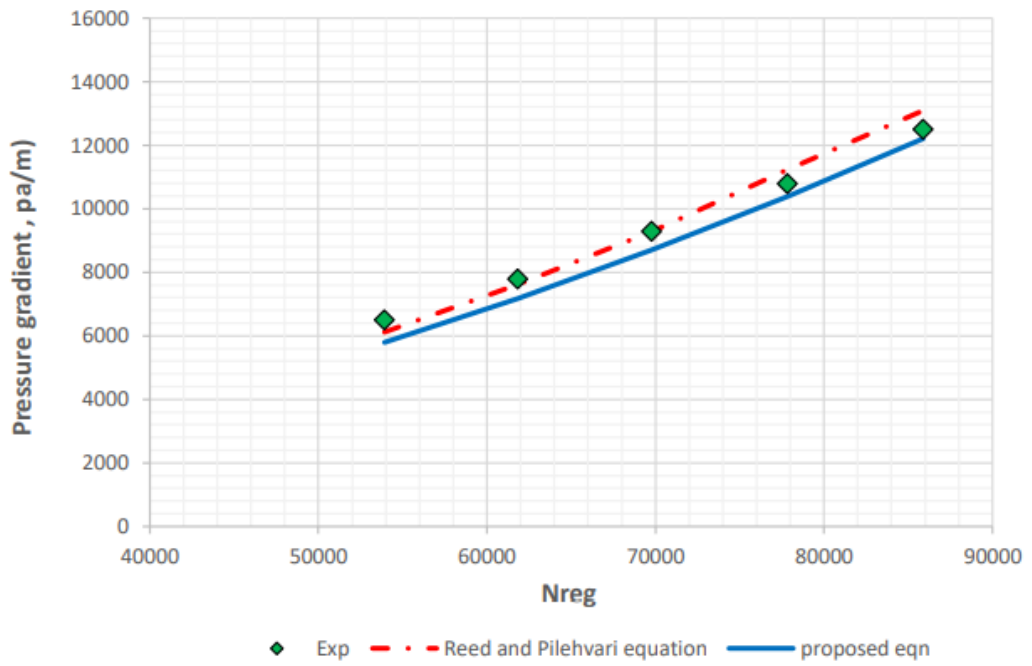


**Figure 5.25** Measured and estimated pressure gradient comparisons for F-3 and 50 mm pipe diameter

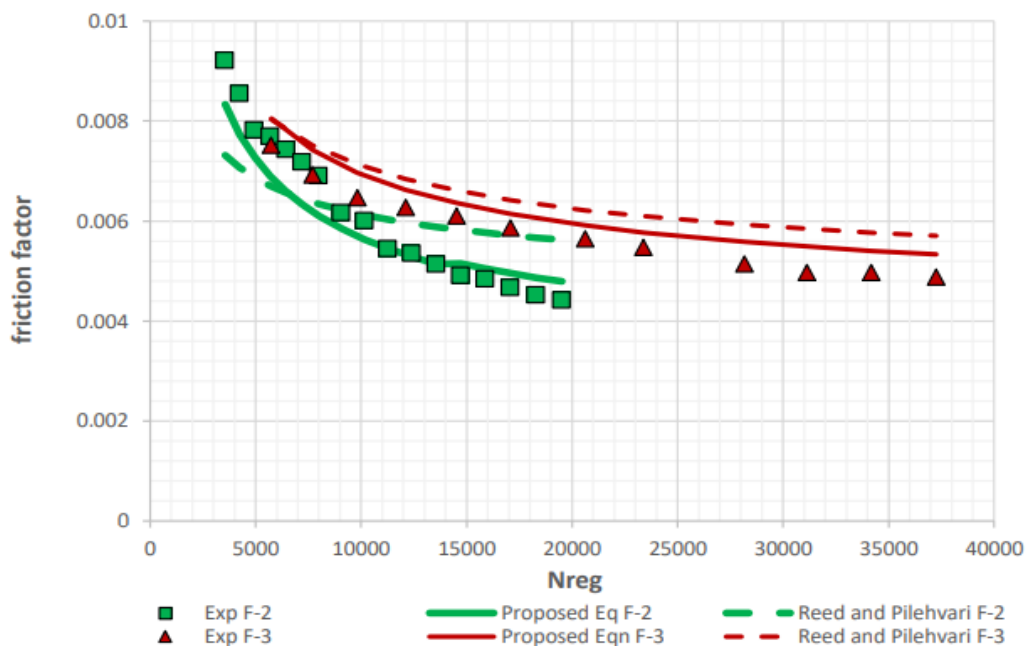


**Figure 5.26** Obtained friction factor values for  $\epsilon/D = 0.000875$

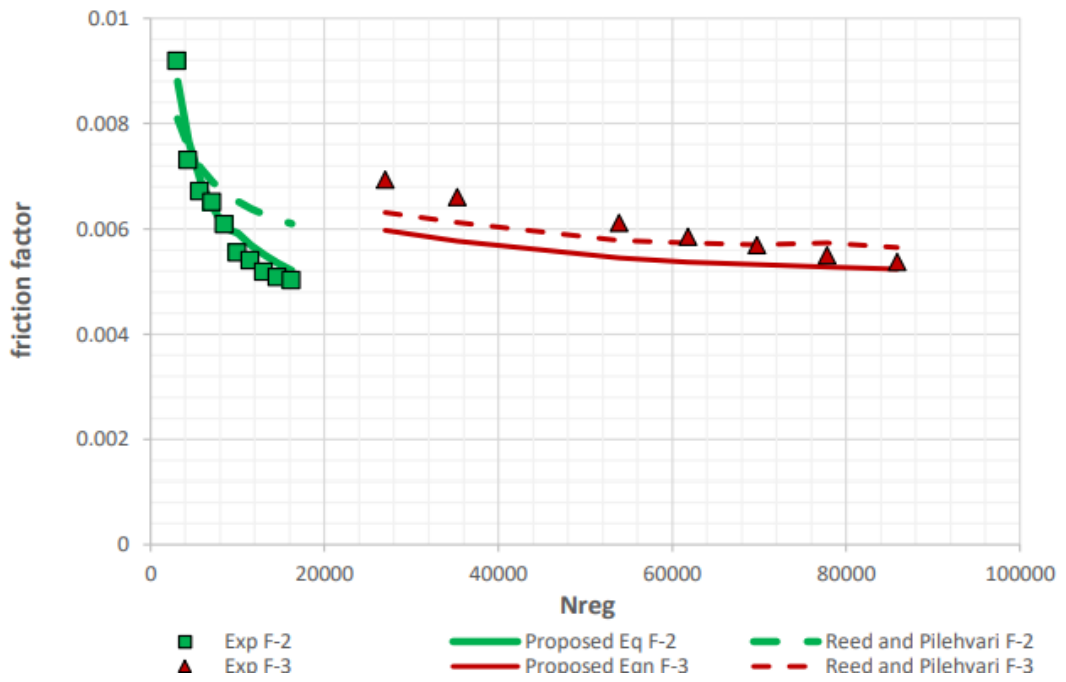


**Figure 5.27** Obtained friction factor values for  $\epsilon/D = 0.0012$

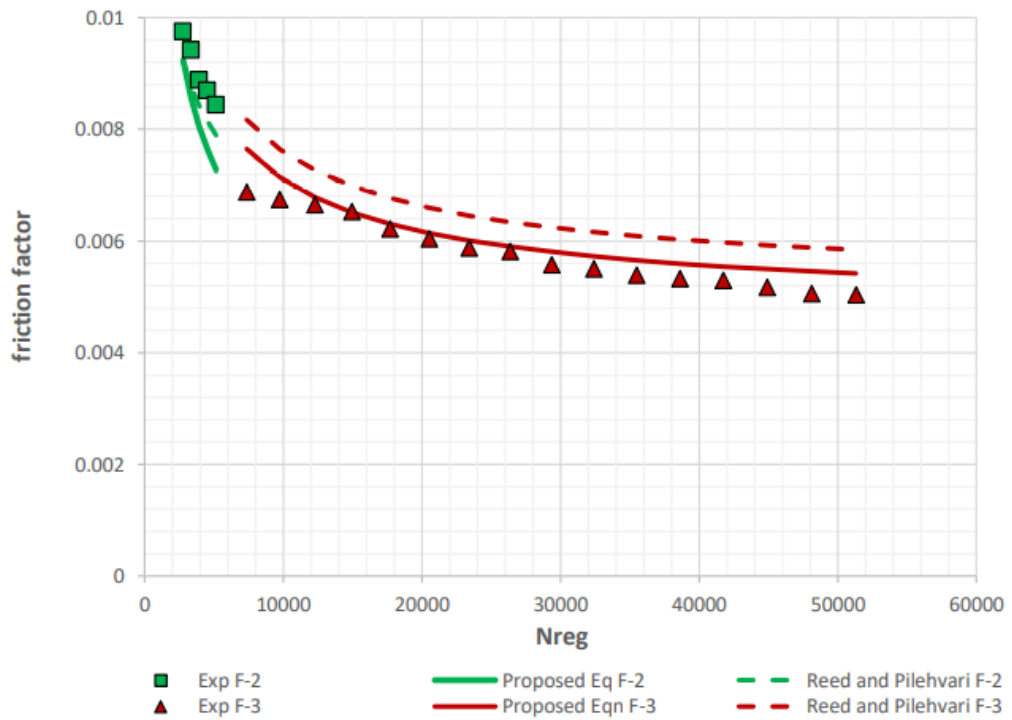


**Figure 5.28** Obtained friction factor values for  $\epsilon/D = 0.001337$

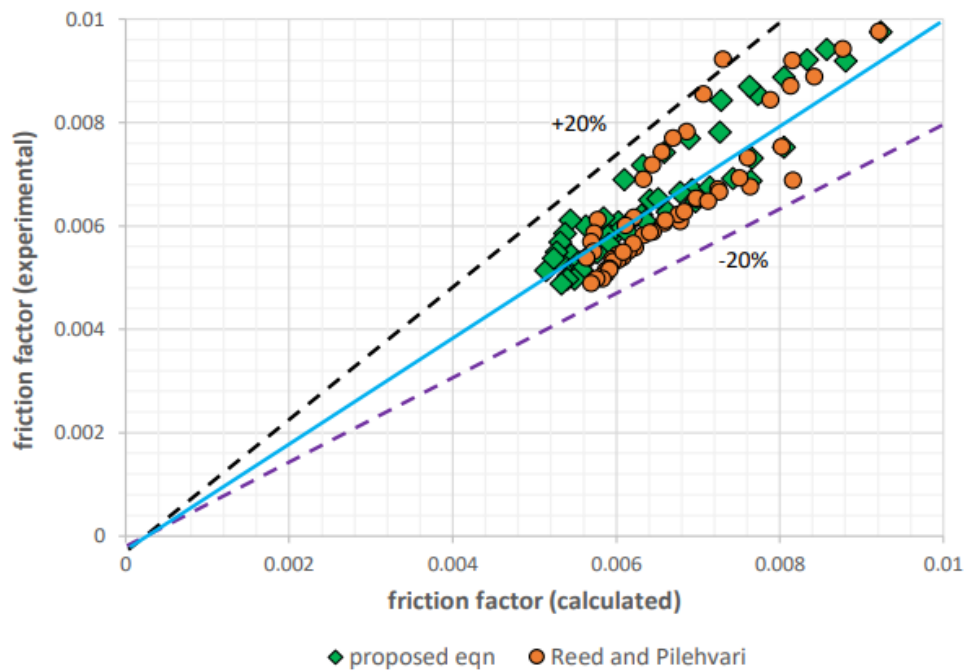


**Figure 5.29** Comparison of measured friction factors with estimated friction factors for F-2 and F-3 fluids using the proposed correlation, and Reed and Pilehvari [52] correlation

In terms of error metrics, the performance of the proposed friction factor correlation is shown in Table 5.6. The level of confidence and  $R^2$  values are 95% and 0.85, respectively.

**Table 5.6** Performance of developed friction factor equation

$R^2$	RMSE	AAE	AAPE (%)
0.85	0.0037	0.0004	6.07

RMSE: Root Mean Square Error, AAE: Average Absolute Error, AAPE: Average Absolute Percentage Error



## 5.4 Comparison of the Pressure Gradients between The Developed Mathematical Model and Experimental Study

The performance of the developed mathematical model for Newtonian fluid flow in rough pipes considering the fluid temperature effects is presented in this section by analyzing the accuracy of it for various flowrates, pipe diameters, and fluid temperatures which are obtained from the performed experimental study. Comparisons with the conducted experiments are shown in detail.

### 5.4.1 Comparisons for 40 mm pipe diameter

In Figures 5.30 - 5.33, in order to express the performance of the developed mathematical model, experimental and model pressure gradient comparisons for 40 mm pipe diameter and for all fluid temperatures are presented. It is seen that there is a good agreement between experimental and model pressure gradient data for all fluid temperatures.

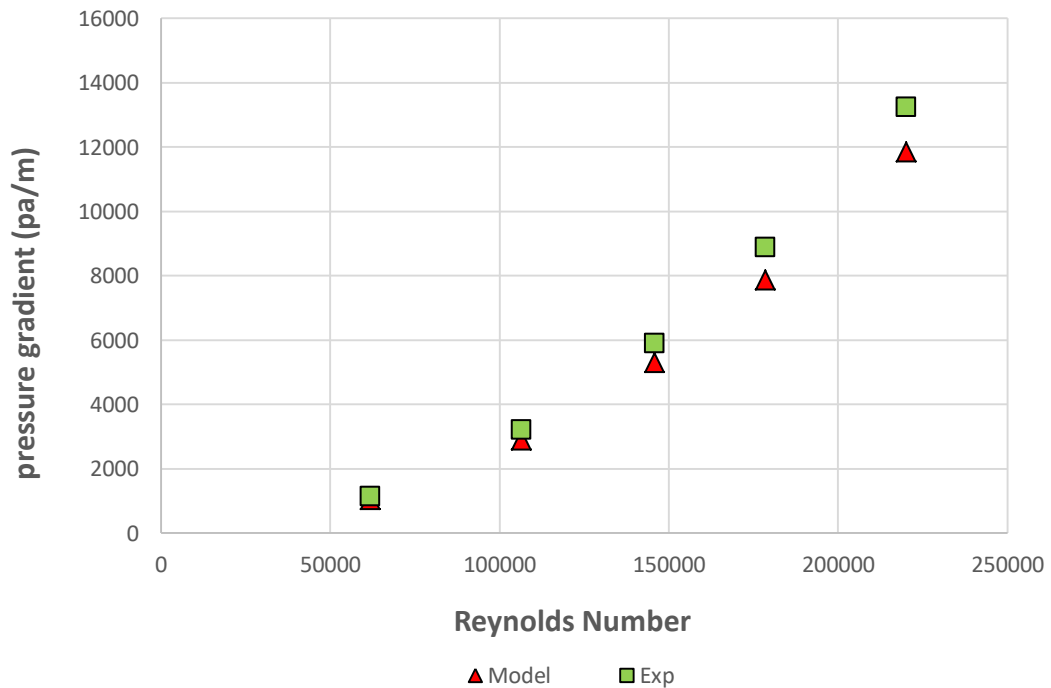


**Figure 5.30** Measured and predicted pressure gradient comparisons for 40 mm pipe diameter and 20 °C fluid temperature

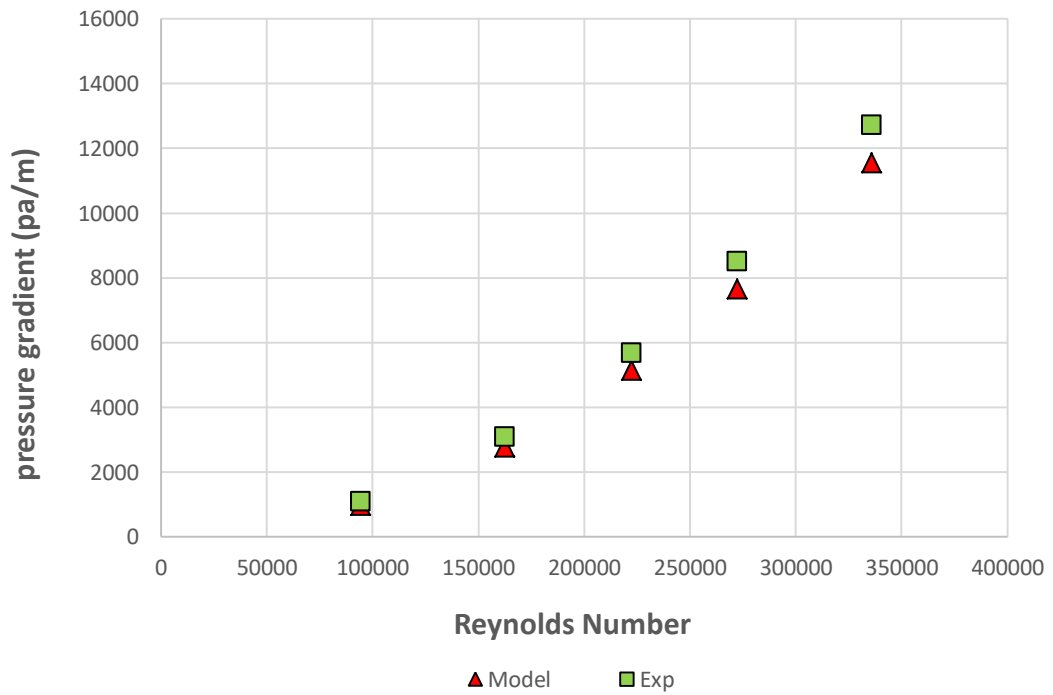


**Figure 5.31** Measured and predicted pressure gradient comparisons for 40 mm pipe diameter and 40 °C fluid temperature

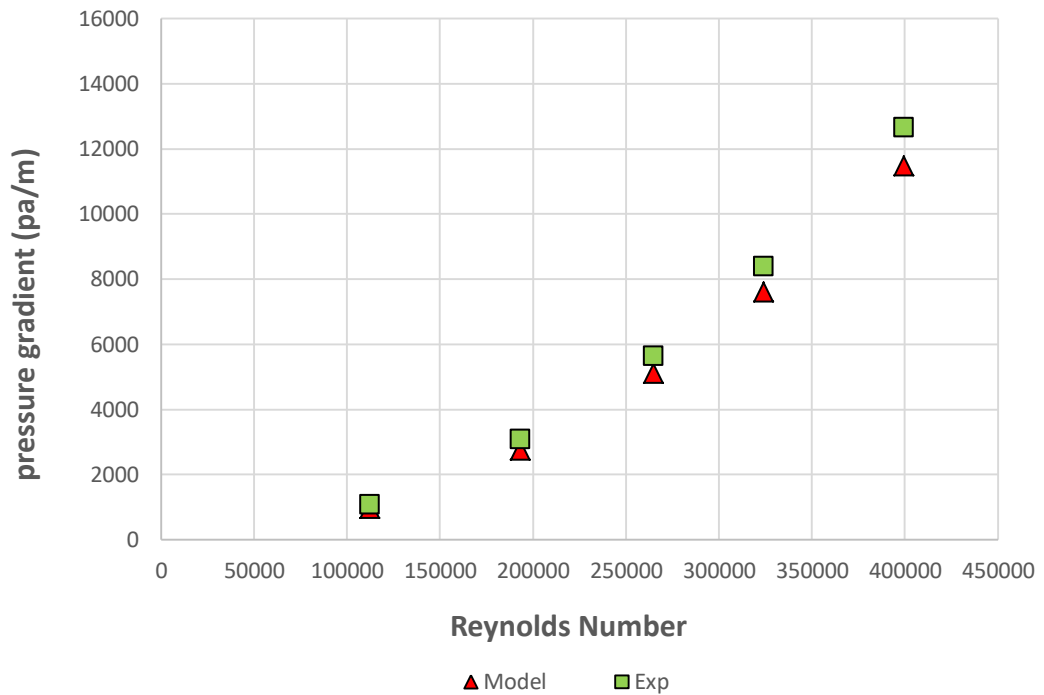


**Figure 5.32** Measured and predicted pressure gradient comparisons for 40 mm pipe diameter and 50 °C fluid temperature

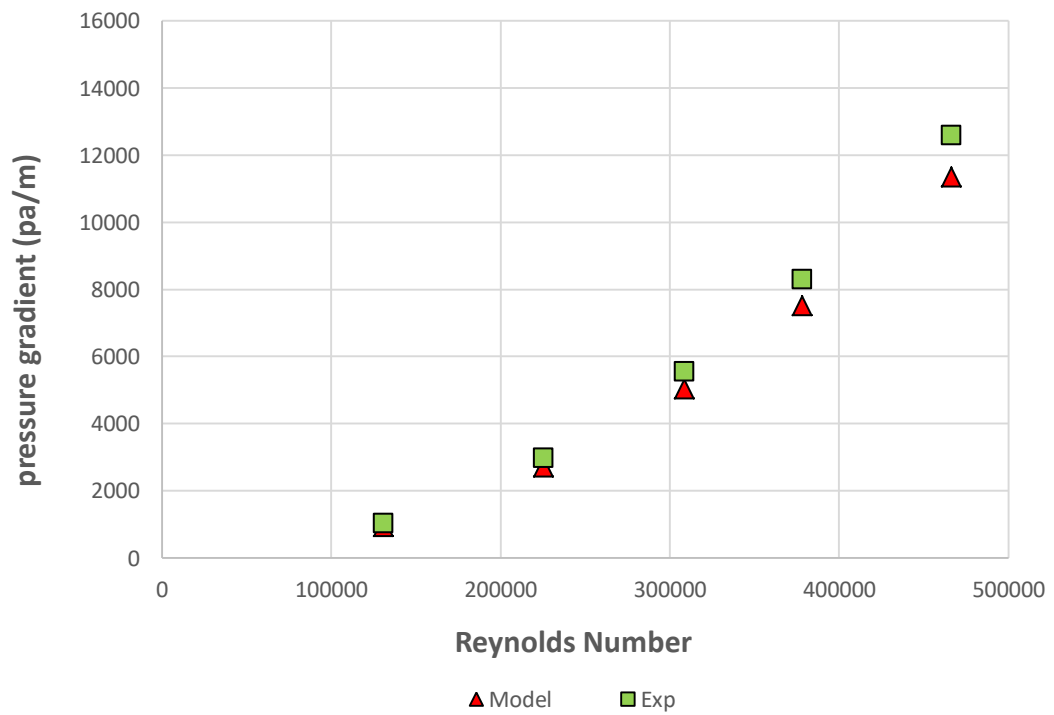


**Figure 5.33** Measured and predicted pressure gradient comparisons for 40 mm pipe diameter and 60 °C fluid temperature

#### 5.4.2 Comparisons for 50 mm pipe diameter

In Figures 5.34 - 5.37, in order to express the performance of the developed mathematical model, experimental and model pressure gradient comparisons for 50 mm pipe diameter and for all fluid temperatures are presented. Satisfactory agreement between the experimental and model pressure gradient data is observed.

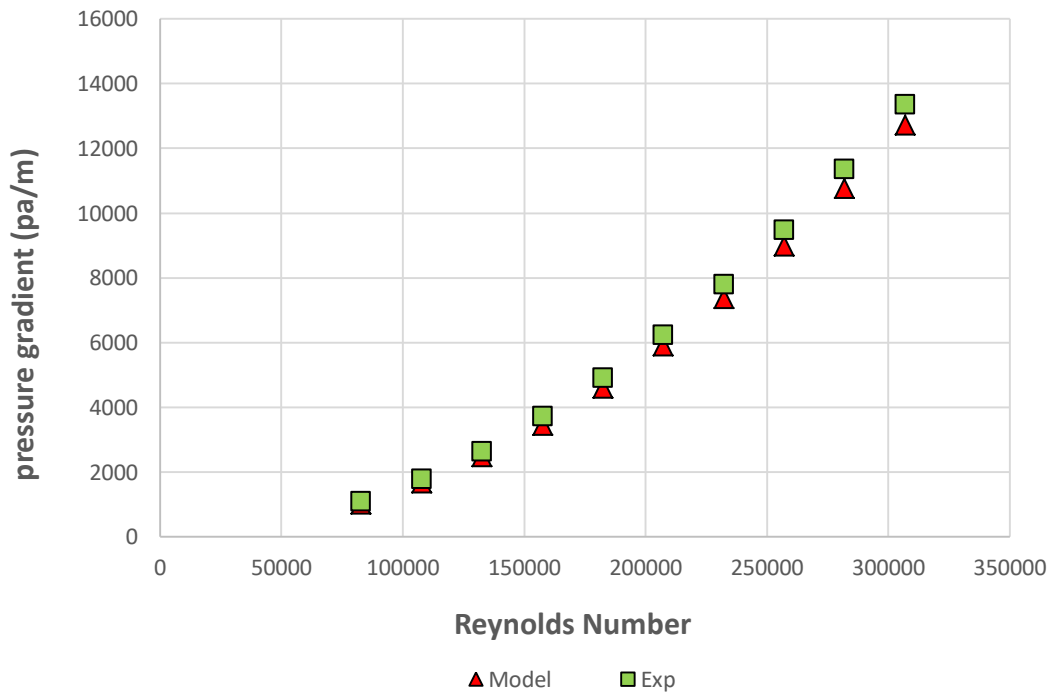


**Figure 5.34** Measured and predicted pressure gradient comparisons for 50 mm pipe diameter and 20 °C fluid temperature

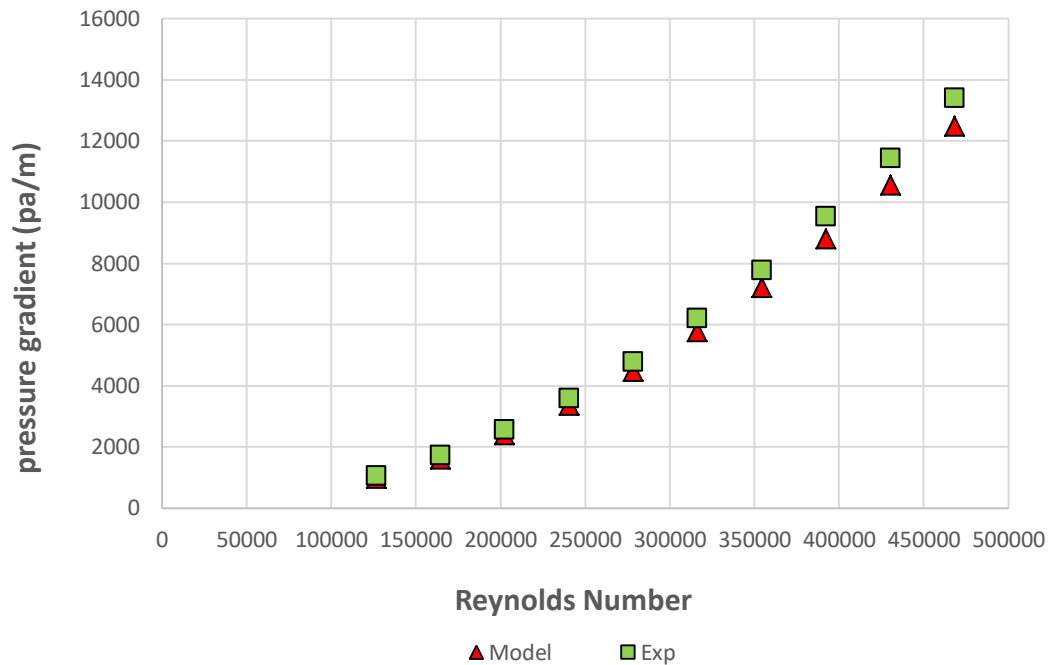


**Figure 5.35** Measured and predicted pressure gradient comparisons for 50 mm pipe diameter and 40 °C fluid temperature

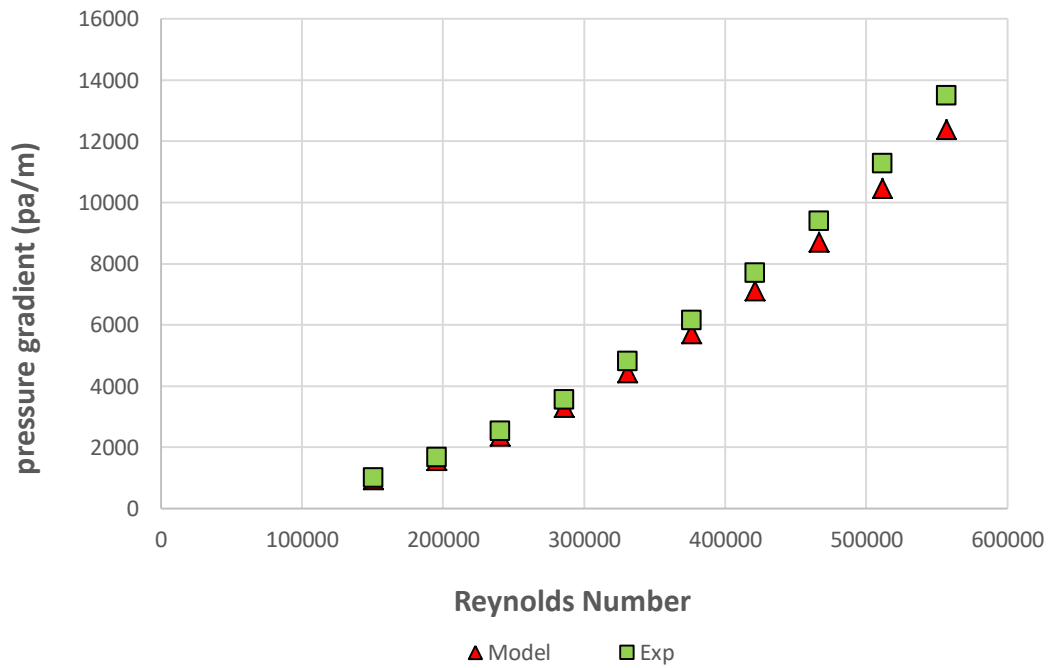


**Figure 5.36** Measured and predicted pressure gradient comparisons for 50 mm pipe diameter and 50 °C fluid temperature

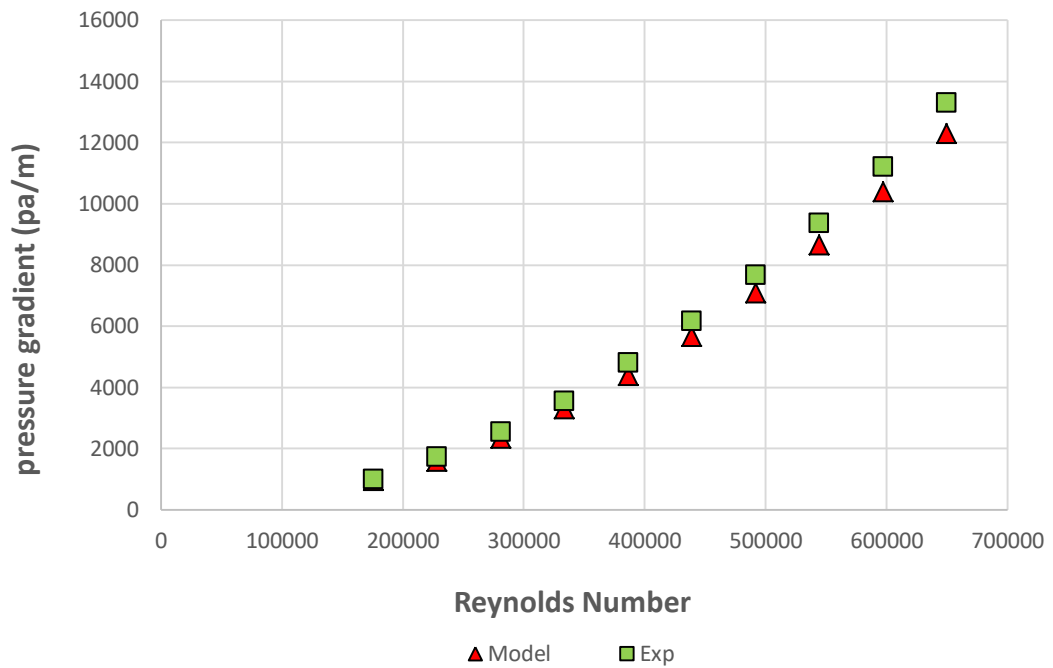


**Figure 5.37** Measured and predicted pressure gradient comparisons for 50 mm pipe diameter and 60 °C fluid temperature

### 5.4.3 Comparisons for 80 mm pipe diameter

In Figures 5.38 - 5.41, in order to express the performance of the developed mathematical model, experimental and model pressure gradient comparisons for 80 mm pipe diameter and for all fluid temperatures are presented. The simulation shows good agreement between experimental and model pressure gradient data in general. It is observed that at high Reynolds numbers, the model slightly overestimates pressure gradients for all fluid temperatures.

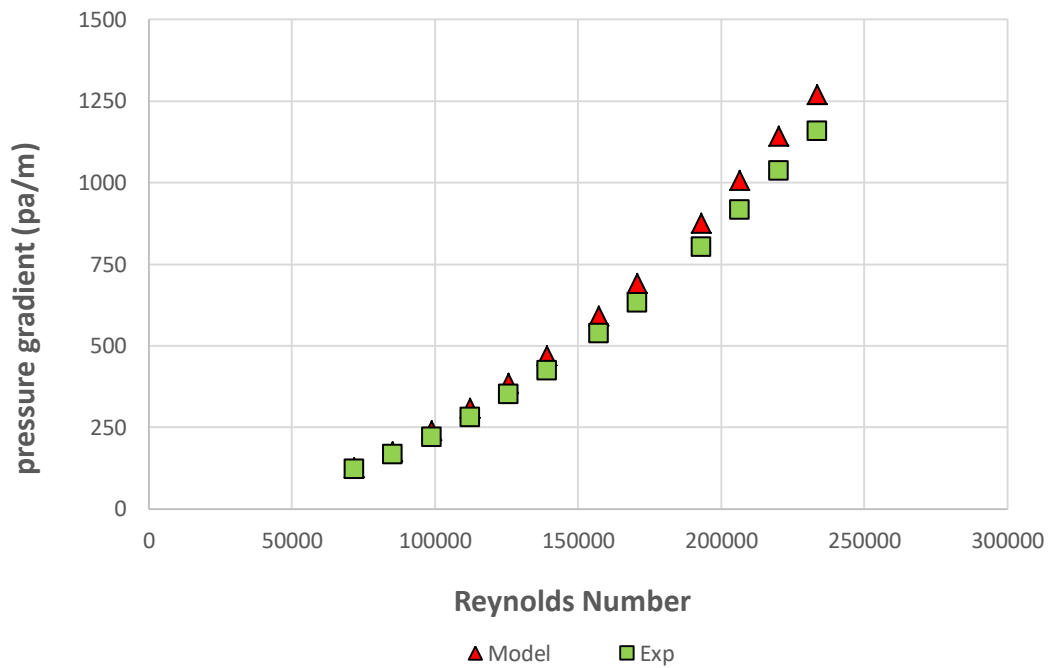


**Figure 5.38** Measured and predicted pressure gradient comparisons for 80 mm pipe diameter and 20 °C fluid temperature

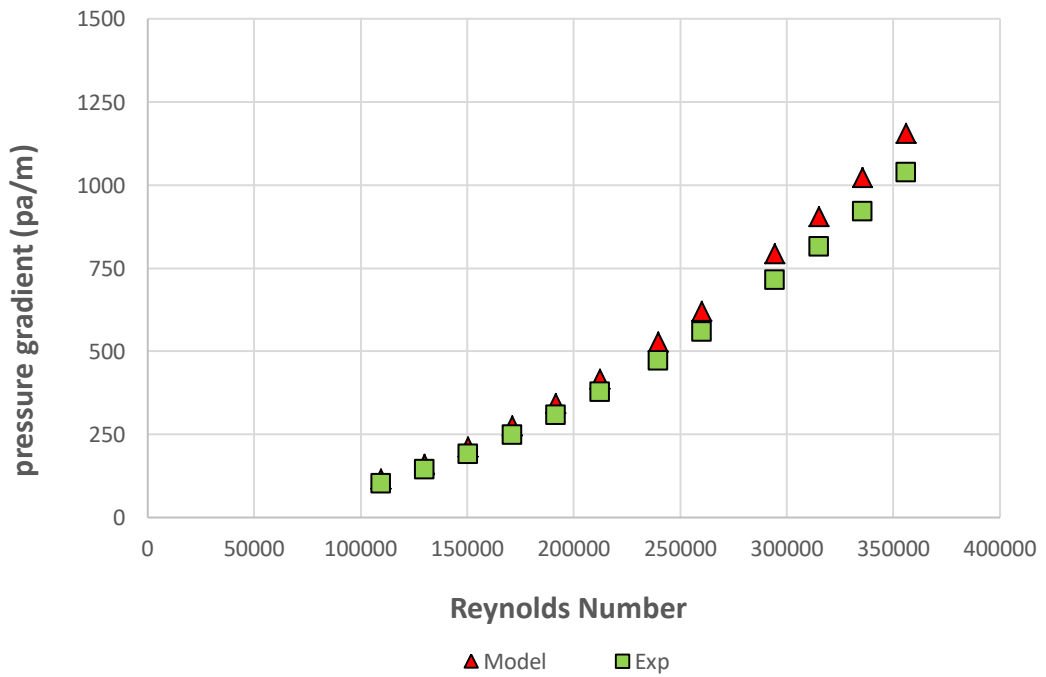


**Figure 5.39** Measured and predicted pressure gradient comparisons for 80 mm pipe diameter and 40 °C fluid temperature

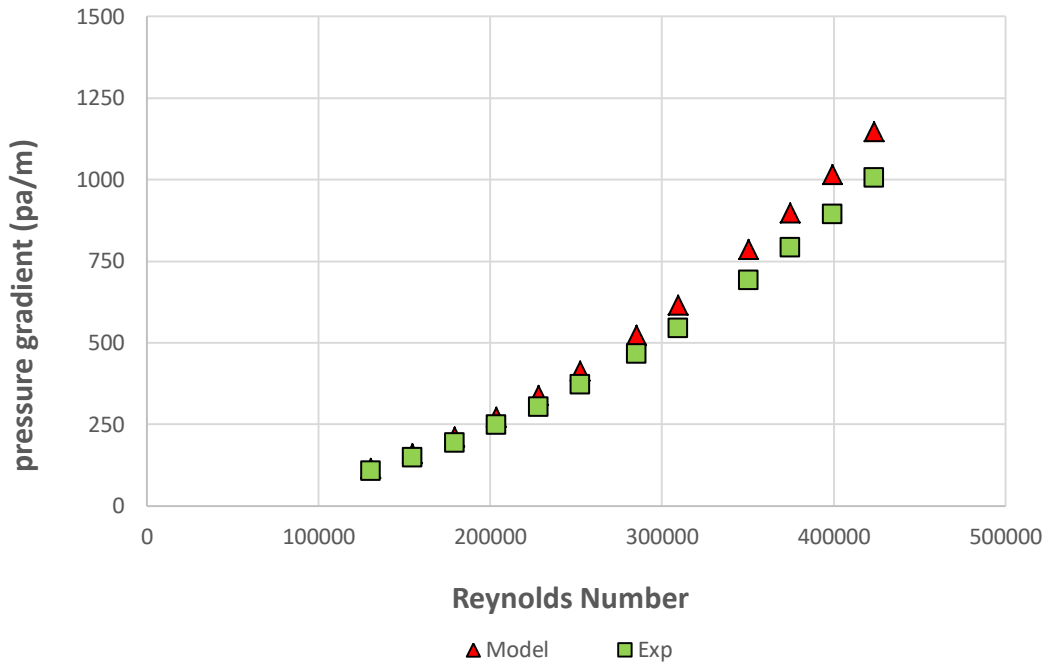


**Figure 5.40** Measured and predicted pressure gradient comparisons for 80 mm pipe diameter and 50 °C fluid temperature

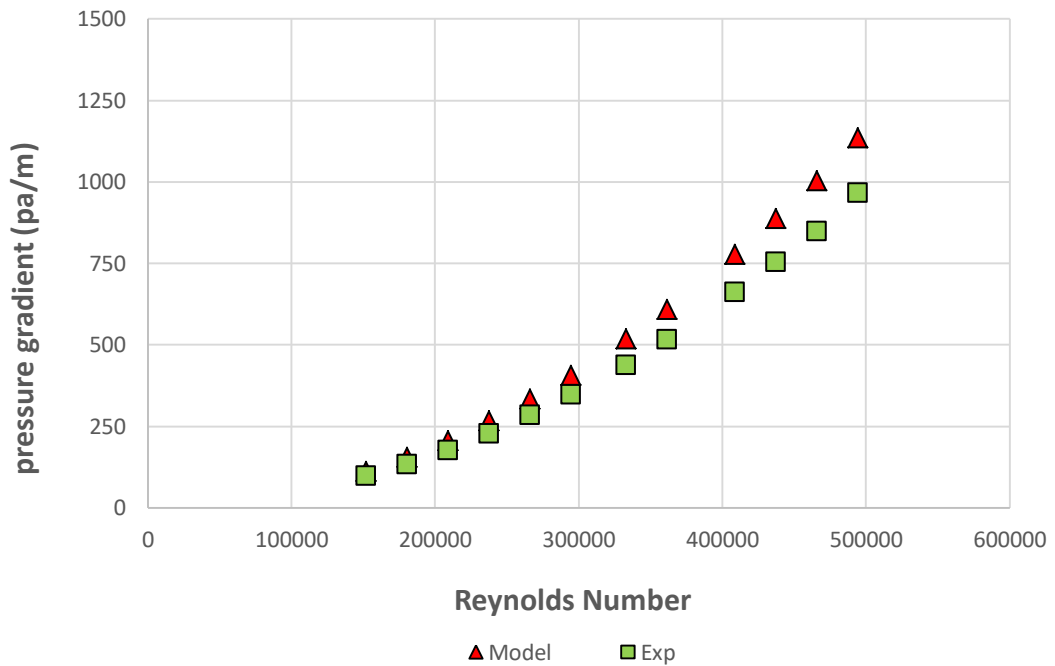


**Figure 5.41** Measured and predicted pressure gradient comparisons for 80 mm pipe diameter and 60 °C fluid temperature

#### 5.4.4 Comparisons for 90 mm pipe diameter

In Figures 5.42 - 5.45, in order to express the performance of the developed mathematical model, experimental and model pressure gradient comparisons for 90 mm pipe diameter and for all fluid temperatures are presented. If the results of the developed model are analyzed, the model presents reasonable accuracy with experimental data within an average error of 12.4%.



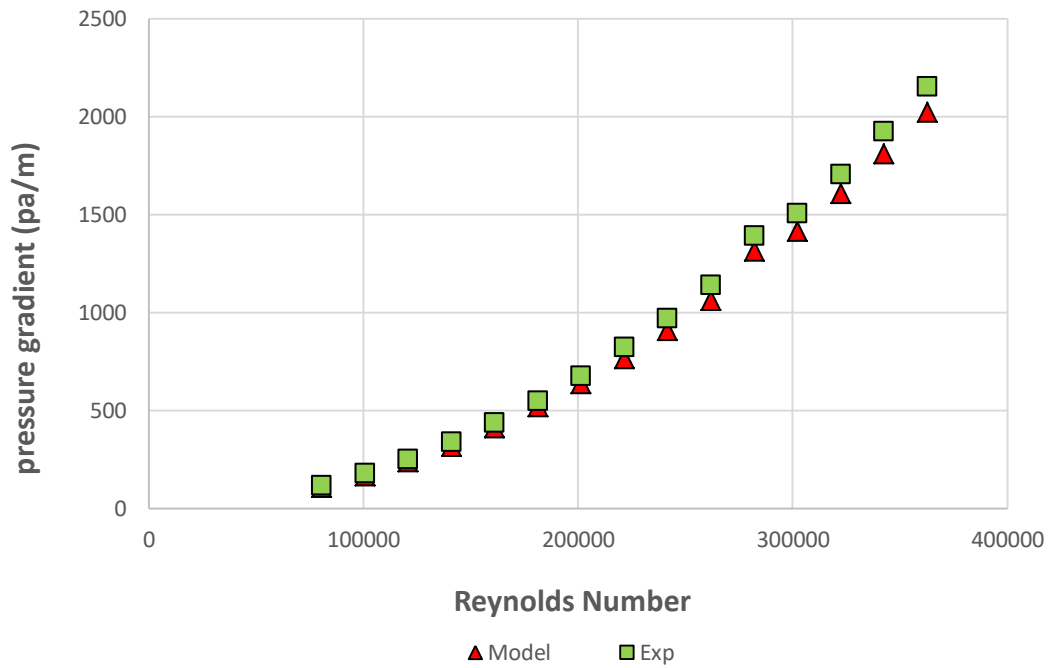


**Figure 5.42** Measured and predicted pressure gradient comparisons for 90 mm pipe diameter and 20 °C fluid temperature

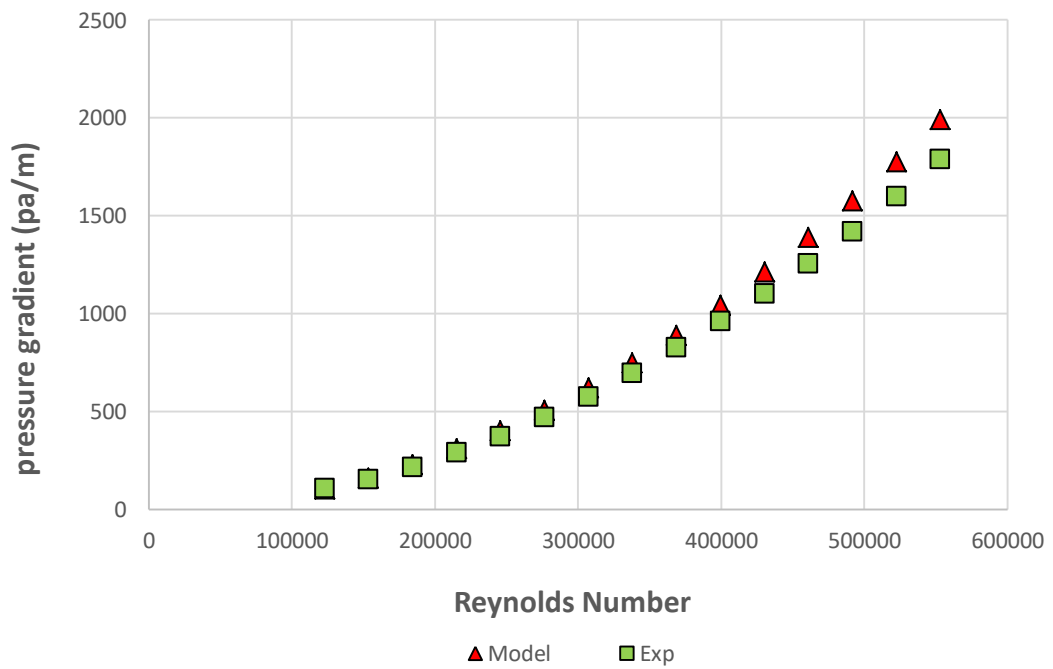


**Figure 5.43** Measured and predicted pressure gradient comparisons for 90 mm pipe diameter and 40 °C fluid temperature

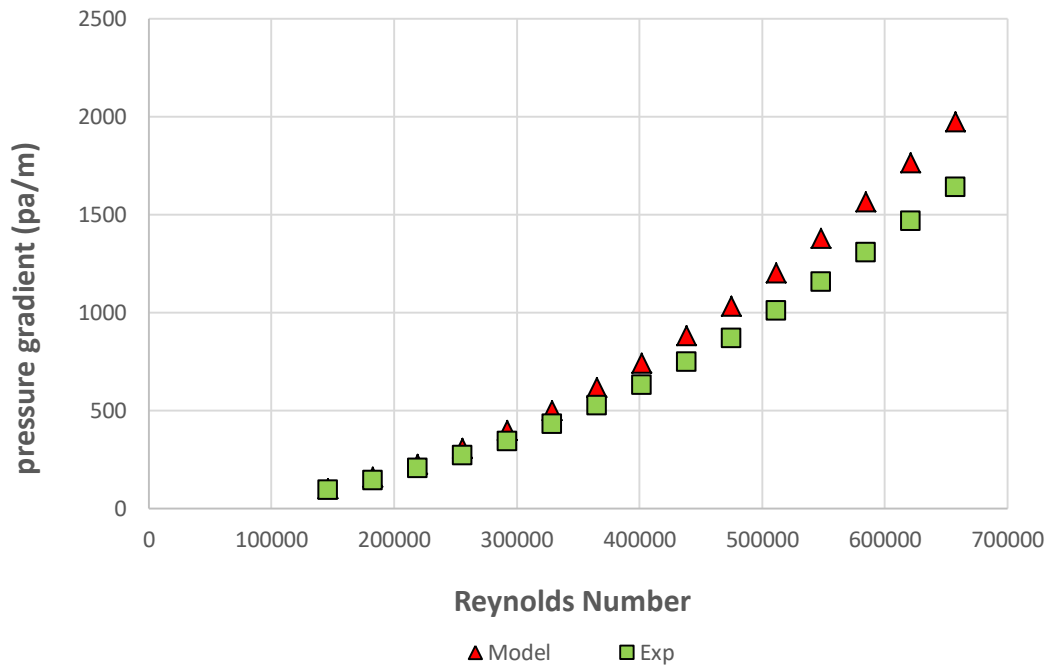


**Figure 5.44** Measured and predicted pressure gradient comparisons for 90 mm pipe diameter and 50 °C fluid temperature

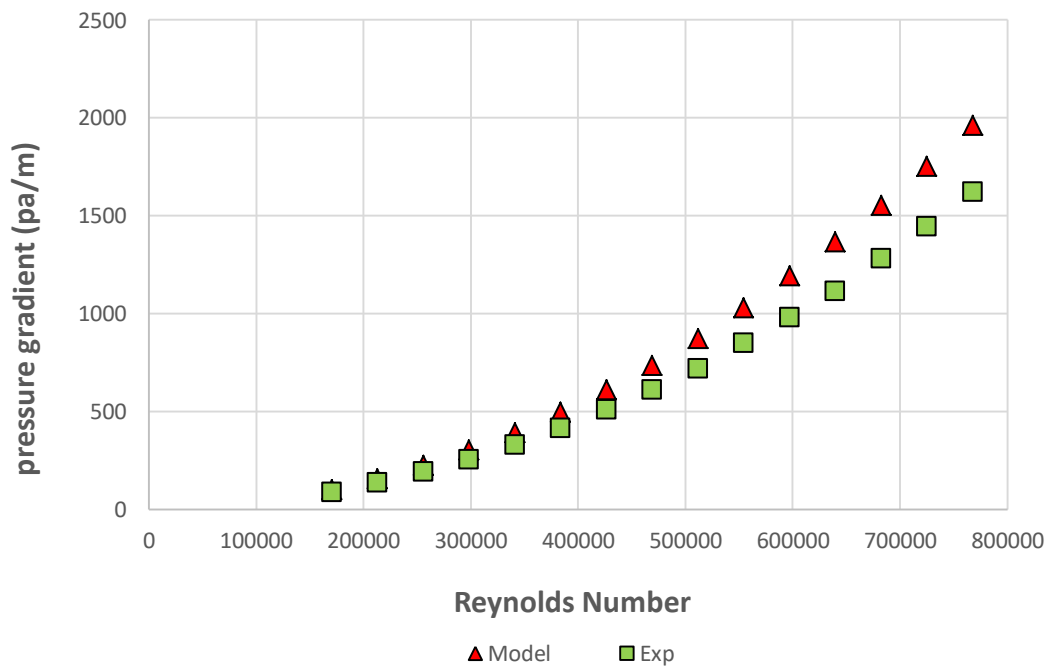


**Figure 5.45** Measured and predicted pressure gradient comparisons for 90 mm pipe diameter and 60 °C fluid temperature

Comparisons of experimental (measured) and model (predicted) pressure gradients of low pressure gradient values and high pressure gradient values for all fluid temperatures are shown in Figures 5.46 and 5.47, respectively. In these figures, predicted pressure gradient values are represented on the x-axis and measured pressure gradient values are represented on the y-axis. Solid lines on the figures show the perfect match and dashed lines on the figures show  $\pm 20\%$  error margin. All of the points fall into the error margin as observed from the figures. For all pipe diameters and fluid temperatures, it is obtained that pressure gradients are estimated with an average absolute percent error of 10.86% by using the developed model.

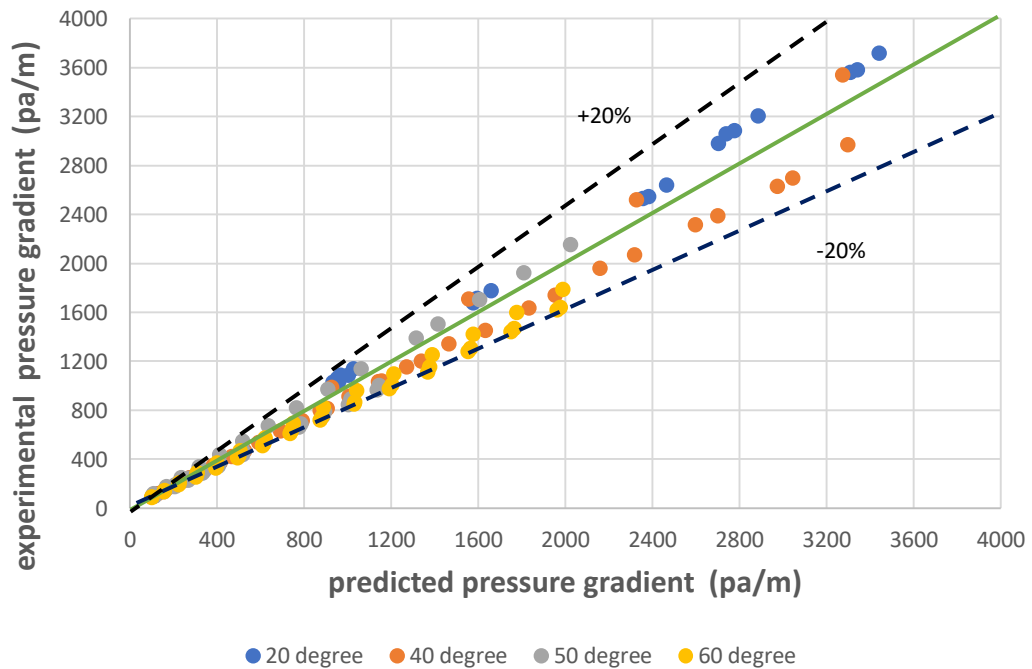


**Figure 5.46** Measured and predicted pressure gradient comparisons for low pressure gradient values and for all fluid temperatures

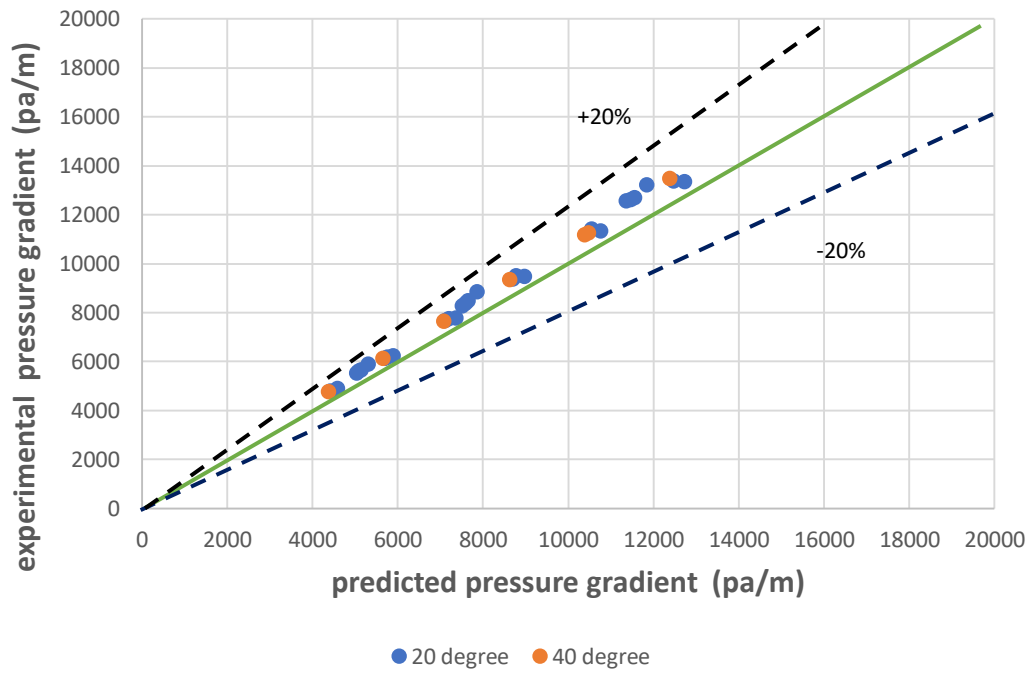


**Figure 5.47** Measured and predicted pressure gradient comparisons for high pressure gradient values and for all fluid temperatures

## 6.CONCLUSIONS

In this thesis, for various flowrates and pipe diameters, fully turbulent flows of Newtonian fluids through rough pipes for room and different fluid temperature conditions and non-Newtonian fluids through rough pipes for room temperature condition are numerically and experimentally investigated. The experimental study is conducted in the Flow Loop of Civil Engineering Department at İzmir Kâtip Çelebi University. Newtonian fluid flow experiments are performed with water. For the non-Newtonian fluid flow experiments, three different non-Newtonian fluids with different concentrations and viscous characteristics are prepared in the laboratory. During the experiments, pressure gradients, flowrates, and fluid temperatures are recorded.

A dimensional analysis is performed to understand the effective parameters of the friction factor. Under the guidance of experimentally obtained results, in order to estimate frictional pressure losses, new friction factor equations are developed for Newtonian and non-Newtonian fluid flows for the stated circumstances.

Moreover, a user-friendly mathematical model is developed for Newtonian fluid flows in rough pipes for room and different fluid temperature conditions. For this purpose, Reynolds averaging is applied and the Navier-Stokes equations in cylindrical coordinates are decomposed. The closure problem that appeared in turbulence modeling is solved by adopting the mixing length theory.

The calculation procedure is performed in Matlab software by developing a code to solve the Navier-Stokes equation with fluid temperature effects based on finite difference techniques. In order to estimate the turbulent boundary layer on rough surfaces, the damping function proposed by Krogstad [70] is used.

The developed friction factor equations and the mathematical model are validated with experimental results and with the available literature as well.

The findings of this study are presented as follows.

1. Comparing the experimental friction factor values with Colebrook [18] friction factor values showed that roughness height of the pipes vary significantly with pipe diameter. Different roughness heights are obtained for each galvanized pipe that are used in the experimental study. Commercially, the roughness heights of the galvanized pipes have constant values as 0.15 mm but they are found to be different while the diameters of the pipes vary. The obtained roughness values are 0.052 mm, 0.06 mm, 0.07 mm and 0.12 mm for pipes with the diameter of 40 mm, 50 mm, 80 mm, and 90 mm, respectively, and friction factor investigations are performed based on this finding.
2. The developed friction factor for fully turbulent flows of Newtonian fluids through rough pipes with various fluid temperatures is presented as the function of Reynolds Number, Prandtl Number, and also relative roughness. It is experimentally obtained that, if other parameters are conserved constant, while the relative roughness and Prandtl Number have direct proportion with friction factor, the Reynolds number has inverse proportion with friction factor. In addition, since the Prandtl Number and the fluid temperature have inverse proportion, the friction factor decreases while the fluid temperature increases.
3. The experimental results, explicit equations of Blasius [5] and Taler [10] for smooth pipes, and implicit equation of Colebrook [18] for rough pipes are compared with the equation which is proposed for the Newtonian fluid flow case. Results of the comparisons indicate that with the proposed friction factor equation for Newtonian fluid flow a reasonable accuracy is obtained with the experimental data at various fluid temperatures and explicit equations. It is seen that the performance of the Colebrook equation slightly better than the proposed equation. On the other hand, in order to show the

performance of the proposed friction factor equation at high temperatures, data obtained from the experiments at 40 °C are compared with the proposed friction factor equation and Colebrook equation. Colebrook equation does not contain fluid temperature effects and it can be clearly seen that at high temperatures, proposed friction factor equation presents better performance than the Colebrook equation. Colebrook equation overestimates the friction factors. Additionally, results present that frictional pressure losses are accurately estimated using the new friction factor equation.

4. Based on the experimental results, significant influences of roughness and temperature on the friction factor for turbulent flow through rough pipes are obtained. Pipes that are used in engineering applications have roughnesses and they have usages in areas where temperature matters such as geothermal energy. For this reason, when selecting pumps that affect the operational costs and capabilities of piping systems, pipe roughness must be correctly determined and the effects of fluid temperature on pressure losses must be taken into account.
5. In this study, all rheological models of non-Newtonian fluid flows are investigated. Two different fluids with the different type of polymer characteristics (high and low viscous) and with different weights of polymers are precisely prepared in the laboratory. According to the performed rheological analyses in this study, it is obtained that Herschel-Bulkley model (consists of both Bingham Plastic and Power-Law models) accurately represents the rheological behavior of the concentrated CMC (carboxymethyl cellulose) polymeric solutions used in this study.
6. Reed and Pilehvari [52] presented an equation to calculate the friction factor for Herschel-Bulkley fluids in rough pipes but it has not been validated with experimental data yet. In this Ph.D. thesis, experimental investigation of turbulent flow of yield-pseudoplastic fluids in rough pipes is performed for the first time in the literature.

7. A new explicit friction factor equation for Herschel-Bulkley fluid flows in rough pipes is proposed based on the experimental data. The proposed explicit friction factor equation is a function of generalized Reynolds Number and relative roughness. In order to analyze the accuracy of the proposed friction factor correlation, the proposed friction factor correlation is compared with experimental data and other correlations of Herschel-Bulkley fluid presented in the literature. For the turbulent flows of Herschel-Bulkley fluids in rough pipes, a good concordance between experimental data and the proposed correlation is obtained. Also, the proposed correlation surpasses Reed and Pilehvari [52] correlation.
  
8. A mathematical model for the fully turbulent flow of Newtonian fluid with different fluid temperatures is also developed. In order to do it, experimentally studied pipe flow is modeled by using finite difference techniques. For this purpose, Reynolds averaging method is applied to the Navier-Stokes equations in cylindrical coordinates to decompose them. In order to solve the closure problem which is appeared during the turbulence modeling process, mixing length theory is used. All computational work is performed in Matlab software by developing a user-friendly code. The results which are obtained from the model are validated with experimental results. Satisfactory agreement is achieved for all pipe diameters, roughness values, and fluid temperature conditions which makes the developed model can be used to predict pressure losses of fully developed turbulent flow of Newtonian fluids with different fluid temperatures through rough pipes with reasonable accuracy.



## REFERENCES

1. Weisbach, J. (1845). Lehrbuch der Ingenieur- und Maschinen-Mechanik, Vol. 1. Theoretische Mechanik, Vieweg und Sohn, Braunschweig
2. Darcy, H. (1857). Recherches expérimentales relatives au mouvement de l'eau dans les tuyaux, Mallet-Bachelier, Paris
3. Hagen, G. (1839). Über die Bewegung des Wassers in engen zylindrischen Röhren, Pogg. Ann., 46, 423-442
4. Poiseuille, J. L. (1841). Recherches expérimentales sur le mouvement des liquides dans les tubes de très-petits diamètres, Comptes Rendus, Académie des Sciences, Paris 12, 112
5. Blasius, H. (1913). Das Ähnlichkeitsgesetz bei Reibungsvorgängen in Flüssigkeiten, Forschungs-Arbeit des Ingenieur-Wesens 131
6. Drew, T. B., Koo, R. C., McAdams, W. H. (1932). The friction factor for clean round pipes, Trans. AIChE 1932, 28, 56
7. Prandtl, L. (1949). Führer durch die Strömungslehre. F. Vieweg & S, Braunschweig
8. Filonienko, G. K. (1954). Friction factor for turbulent pipe flow, Teploenergetika 1.4 (1954): 40-44
9. Allen, R. W. and Eckert, E. R. G. (1964). Friction and heat-transfer measurements to turbulent pipe flow of water ( $Pr = 7$  and  $8$ ) at uniform wall heat flux, J. Heat Transfer 86, 301-310 (1964)
10. Taler, D. (2016). Determining velocity and friction factor for turbulent flow in smooth tubes, International Journal of Thermal Sciences 105 (2016): 109-122
11. Mises, R. (1914). Elemente der technischen Hydrodynamik, Teubner, Leipzig, 1914
12. Schiller, L. (1923). über den Strömungswiderstand von Rohren verschiedenen Querschnitts und Rauigkeitsgrades, Z. Angew. Math. Mech., Vol. 3, p.2, 1923

13. Hopf, L. (1923). Die Messung der hydraulischen Rauigkeit, Z. Angew. Math. Mech., Vol. 3, pp. 329-339, 1923
14. Fromm, K. (1923). Strömungswiderstand in rauhen Rohren, Z. Angew. Math. Mech., Vol. 3, pp. 339-358, 1923
15. Fritsch, W. (1928). Einfluss der Wandrauigkeit auf die turbulente Geschwindigkeitsverteilung in Rinnen, Z. Angew. Math. Mech., Vol. 8, pp. 199-216, 1928
16. Kármán, Th. von. (1930). Mechanische Aehnlichkeit und Turbulenz, Proc. Third International Congress for Applied Mechanics, C. W. Oseen and W. Weibull eds., Stockholm. Vol. 1, 79-93
17. Nikuradse, J. (1933). Strömungsgesetze in rauhen Rohren, Forschungs-Arbeit des Ingenieur-Wesens 361
18. Colebrook, C. F. (1939). Turbulent flow in pipes with particular reference to the transition region between the smooth and rough pipe laws, J. Instit. Civil Eng., pp. 133–155, 1939
19. Moody, L. F. (1944). Friction factors for pipe flow, Trans. ASME, 66:671-678
20. Moody, L.F. (1947). An approximate formula for pipe friction factors, Transactions of the ASME, Vol. 69, pp. 1005-1006, 1947
21. (Altshul) Алтшуль, А.Д. (1952). Обобщенная формула сопротивления трубопроводов, Гидравлические строительство, No. 6, 1952
22. Wood, D.J. (1966). An explicit friction factor relationship, Civil Engineering, Vol. 36, No. 12, pp. 60-61, 1966
23. Powe, R. E. and Townes, H. W. (1973). Turbulence structure for fully developed flow in rough pipes, J. Fluids Eng., pp. 255-261, 1973
24. Eck, B. (1973). Technische Stromungslehre, New York: Springer; 1973
25. Swamee, PK., Jain, AK. (1976). Explicit equation for pipe flow problems, J Hydr Div ASCE 1976;102:657–64
26. Churchill, SW. (1977). Friction factor equation spans all fluid-flow ranges, Chem. Eng. 84: p. 91–92
27. Cebeci, T. and Chang, K.C. (1978). A general method for calculating momentum and heat transfer in laminar and turbulent duct flows, Num. Heat Transfer 1, 39-68, 1978

28. Cebeci, T. and Chang, K.C. (1978). Calculation of incompressible rough-wall boundary-layer flows, *AIAA J.* 16, 730-735, 1978
29. Chen, N.H. (1979). An explicit equation for friction factor in pipes, *Ind. Eng. Chem. Fundam.* 18 (3), 296–297
30. Round, G.F. (1980). An explicit approximation for the friction factor-Reynolds number relation for rough and smooth pipes, *Can. J. Chem. Eng.* 58 (1), 122–123
31. Barr, D.I.H. (1981). Solutions of the Colebrook–White function for resistance to uniform turbulent flow, *Proc. Inst. Civil. Eng.* 71 (2), 529–536
32. Zigrang, D.J., Sylvester N.D. (1982). Explicit approximations to the Colebrook’s friction factor, *AIChE J* 1982;28(3):514–5
33. Haaland, S.E. (1983). Simple and Explicit formulas for friction factor in turbulent pipe flow, *J Fluid Eng, ASME* 1983;105(1):89–90
34. Serghides, T.K. (1989). Estimate friction factor accurately, *Chem Eng* 1984;91:63–4
35. Tsal, R. J. (1989). Altshul-Tsal friction factor equation, *Heating, Piping and Air Conditioning*, No. 8, pp. 30-45, 1989
36. Manadilli, G. (1997). Replace implicit equations with signomial functions, *Chem Eng* 1997;104(8):129–32
37. Pimentel, L. C. G., Cotta, R. M. and Kakac, S. (1999). Fully developed turbulent flow in ducts with symmetric and asymmetric rough walls, *Chem. Eng. J.*, Vol. 74, pp. 147–153, 1999
38. Romeo, E., Royo, C., Monzón, A. (2002). Improved explicit equations for estimation of the friction factor in rough and smooth pipes, *J Chem Eng* 2002;86(3):369–74
39. Sonnad J.R., Goudar C.T. (2006). Turbulent flow friction factor calculation using a mathematically exact alternative to the Colebrook-White equation, *J Hydr Eng ASCE* 2006;132(8):863–7
40. Shockling M.A., Allen J.J., Smits A.J. (2006). Roughness effects in turbulent pipe flow, *J Fluid Mech* 564:267 – 285
41. Buzzelli, D. (2008). Calculating friction in one step, *Mach Des*, 80, 54–55
42. Cheng, Nian-Sheng (2008). Formulas for Friction Factor in Transitional Regimes, *Journal of Hydraulic Engineering.* 134 (9): 1357–1362

43. Avci, A., Karagoz, I. (2009). A novel explicit equation for friction factor in smooth and rough pipes, *Journal of Fluids Engineering* 131.6 (2009)
44. Papaevangelou, G., Evangelide, C., Tzimopoulos, C. A. (2010). New explicit relation for friction coefficient in the Darcy-Weisbach equation, In: *Proceedings of the Tenth Conference on Protection and Restoration of the Environment*. Corfu, Greece, PRE 10 July 6-09, 166; 2010: p. 1–7
45. Brkic, D. (2011). An explicit approximation of the Colebrook equation for fluid flow friction factor, *Petrol Sci Technol* 2011;29(15):1596–602
46. Fang, X., Xua, Y., Zhou, Z. (2011). New correlations of single-phase friction factor for turbulent pipe flow and evaluation of existing single-phase friction factor correlations, *Nucl Eng Des* 2011;241:897–902
47. Ghanbari, A., Farshad, F., Rieke, H.H. (2011). Newly developed friction factor correlation for pipe flow and flow assurance, *J Chem Eng Mat Sci* 2011;2:83–6
48. Bellos, Vasilis., Nalbantis, Ioannis., Tsakiris, George. (2018). Friction Modeling of Flood Flow Simulations, *Journal of Hydraulic Engineering*. 144 (12): 04018073
49. Genic, S., Arandjelovic, I., Kolendic, P., Jaric, M., Budimir, N., Genic, V. (2011). A review of explicit approximations of Colebrook's equation, *FME Trans.* 39 (2011) 67–71
50. Metzner, A.B. and Reed, J.C. (1955). Flow of non-Newtonian Fluids Correlation of the Laminar, Transition and Turbulent Flow Regions, *AIChE J.*, 1, No. 4, 434 (1955)
51. Dodge, D.W., Metzner A.B. (1959). Turbulent Flow of Non-Newtonian Systems, *AIChE Journal*. 1959;2:189-204
52. Reed, T.D., Pilehvari, A. (1993). A New Model for Laminar, Transitional, and Turbulent Flow of Drilling Muds, Paper SPE 25456, presented at the 1993 SPE/IADC Drilling Conference Oklahoma City, OK, USA, 21-23 March, 3-6 October
53. Melton, L.L. and Malone, W.T. (1964). Fluid Mechanics Research and Engineering Application in non-Newtonian Fluid Systems, *Soc. Pet. Eng. J.* 4, 56 (1964)
54. Lord, D.L. Hulsey, B.W., and Melton, L.L. (1967). General Turbulent Pipe Flow Scale-Up Correlation for Rheologically Complex Fluid, *Soc. Pet. Eng. J.*, 252 (1967)

55. Shah, S.N. (1984). Correlations Predict Friction Pressures of Fracturing Gels, Oil and Gas J. 92 (Jan. 16, 1984)
56. Szilas, A.P., Bobok, E., Navratil, L. (1981). Determination of turbulent pressure loss of non-Newtonian oil flow in rough pipes, Rheol. Acta. 1981;20: 487-496
57. Heywood, N. I., and D. C. H. Cheng. (1984). Comparison of Methods for Predicting Head Loss in Turbulent Pipe Flow of Non-Newtonian Fluids, Transactions of the Institute of Measurement and Control, vol. 6, no. 1, Jan. 1984, pp. 33–45
58. Garcia, Edgardo J., and James F. Steffe. (1986). Comparison of Friction Factor Equations for non-Newtonian Fluids in Pipe Flow, Journal of Food Process Engineering 9.2 (1986): 93-120
59. Khan, M. M. K. (1992). Friction factor and flow characterisation of non-Newtonian fluids, 11th Australian Fluid Mechanics Conference. 1992
60. Hemeida, Adel M. (1993). Effect of wall roughness in turbulent pipe flow of a pseudoplastic crude oil: An evaluation of pipeline field data, Journal of Petroleum Science and Engineering 10.2 (1993): 163-170
61. Kawase, Y., Shenoy, A.V., Wakabayashi, K. (1994). Friction and heat and mass transfer for turbulent pseudoplastic non -Newtonian fluid flows in rough pipes, Canadian Journal of Chemical Engineering. 1994;72: 798 -804
62. Langelandsvik, L.I., Kungel, G.J., Smits, A.J. (2008). Flow in a commercial steel pipe, J. Fluid Mech. 595 (2008) 323–339.
63. Avci A., Karagoz I. (2019). A new explicit friction factor formula for laminar, transtion and turbulent flows in smooth and rough pipes, European Journal of Mechanics/B Fluids, 2019, 78, 182-187
64. Dosunmu, I. T., and Shah, S. N. (2013). Evaluation of friction factor correlations and equivalent diameter definitions for pipe and annular flow of non-Newtonian fluids, Journal of Petroleum Science and Engineering, 109, 80–86
65. Dosunmu, I. T., and Shah, S. N. (2014). Turbulent flow behaviour of surfactant solutions in straight pipes, J. Pet. Sci. Eng. 124 (2014) 323-330
66. Diogo, A.F., and Vilela, F.A. (2014). Head losses and friction factors of steady turbulent flows in plastic pipes, Urban Water Journal, 11:5, 414-425
67. Boussinesq, J. (1877). Essai sur la théorie des eaux courantes, Mémoires présentés par divers savants à l'Académie des Sciences 23 (1): 1-680

68. Prandtl, L. (1925). *Z. angew, Math. Mech.* 5 (1): 136–139
69. van Driest, E. R. (1956). On Turbulent Flow Near a Wall, *J. Aeronautical Sci.*, Nov. 1956, pp 1007-1011
70. Krogstad, P.-A. (1989). Tenth Australasian Fluid Mechanics Conference, University of Melbourne, 11-15 December 1989, 13C-2, 13.25-13.28
71. Munson B.R., Okiishi T.H., Huebsch W.W., Rothmayer A.P. *Fundamentals of Fluid Mechanics*. 7th ed. John Wiley & Sons, 2013.
72. Kell, G. S. (1975). Density, thermal expansivity, and compressibility of liquid water from 0. deg. to 150. deg.. correlations and tables for atmospheric pressure and saturation reviewed and expressed on 1968 temperature scale. *Journal of Chemical and Engineering Data*, 20(1), 97-105.
73. Sorgun M., Muftuoglu T.D. (2020). A new friction factor formula for single phase liquid flow through geothermal pipelines, *Geothermics*. 2020;88:101901. ANSYS CFX 8.0, Tutorial, Section Laminar to Turbulent Flow.

# CURRICULUM VITAE

## PERSONAL INFORMATION

Surname, Name Müftüoğlu, Tevfik Denizhan  
Nationality Turkish (Republic of Turkey)  
Date and Place of Birth 02 July 1992, Muğla / Turkey  
Marital Status Single  
Phone +90 554 381 45 95  
E-mail td.muftuoglu@gmail.com



## EDUCATION

Degree	Institution	Year of Graduation
M.Sc.	İzmir Katip Çelebi University, Turkey (Civil Engineering)	2016
B.Sc.	Manisa Celal Bayar University, Turkey (Civil Engineering)	2014
	Politechnika Krakowska, Poland (Civil Engineering) Erasmus Exchange Programme	2014

## ACADEMIC ACTIVITIES

**Muftuoglu, T.D.** (2021). “Experimental Investigation of Newtonian and non-Newtonian Fluid Flows in Rough Pipes and Modeling Using Computational Fluid Dynamics”. Izmir Katip Celebi University. (Ph.D. Thesis, supported by Izmir Katip Celebi University, Scientific Research Project Coordinatorship under grant no 2018-TDR-FEBE-0042)

**Muftuoglu, T.D.** (2016). “Fuzzy Logic Modelling of Sediment Transport in Annulus”. Izmir Katip Celebi University. (M.Sc. Thesis)

Sorgun, M., **Muftuoglu, T.D.** (2020). “A New Friction Factor Formula for Single Phase Liquid Flow through Geothermal Pipelines”. Geothermics, Volume 88, November 2020, 101901. (Article)

Sorgun, M., **Muftuoglu, T.D.**, Ulker, E. (2018). “Fuzzy Logic Modelling of Liquid-Solid Two-Phase Flow in Horizontal and Inclined Wellbores”. International Journal of Oil, Gas and Coal Technology, 2018 Vol.19 No.4, pp.438 – 448. (Article)

Sorgun, M., **Muftuoglu, T.D.** (2019). “A Friction Factor Correlation for Turbulent Flow in Rough Pipes Under Various Temperature Conditions”. 1st International Symposium on Innovations in Civil Engineering and Technology (ICIVILTECH 2019). 23-25 Oct 2019, Afyonkarahisar / TURKEY. (Conference)

**Muftuoglu, T.D.**, Sorgun, M., Ulker, E. (2019). “Pressure Loss Estimation of Turbulent Newtonian Fluid in Rough Pipes under Various Temperature Conditions”. International Civil Engineering and Architecture Conference (ICEARC19). 17-20 Apr 2019, Trabzon / TURKEY. (Conference)

Ozdemir, A., Alaybeyoglu, A., Balbal, K.F., **Muftuoglu, T.D.** (2016). “Fuzzy Logic Based Door Lock-Release Control System for Metro Systems”. International Conference on Research in Education and Science (ICRES2016), May 19-22, Bodrum / TURKEY. (Conference)

**Muftuoglu, T.D.**, Sorgun, M., Ulker, E. (2015). “A Fuzzy Model To Estimate Cuttings Bed Thickness in Horizontal and Inclined Wellbores”. International Conference on Advances in Applied and Computational Mechanics (ACM-2015), 5-7 Aug 2015, Izmir / TURKEY. (Conference)

## **TECHNICAL SKILLS AND COMPUTER KNOWLEDGE**

Matlab, Ansys, Autocad, Idecad, Sap2000, Microsoft Office, Web Design

## **LANGUAGE**

Turkish (Native)

English (Fluent)

Russian (Intermediate)

Polish (Beginner)



